International Journal of Computer Vision 64(1), 31–67, 2005

Local Shape from Mirror Reflections

SILVIO SAVARESE, MIN CHEN AND PIETRO PERONA
California Institute of Technology, Mail Stop 136-93, Pasadena, CA 91125, USA
savarese@vision.caltech.edu
perona@vision.caltech.edu
minchencm@yahoo.com

Received May 3, 2004; Revised February 2, 2005; Accepted February 2, 2005

First online version published in April, 2005

Abstract. We study the problem of recovering the 3D shape of an unknown smooth specular surface from a single image. The surface reflects a calibrated pattern onto the image plane of a calibrated camera. The pattern is such that points are available in the image where position, orientations, and local scale may be measured (e.g. checkerboard). We first explore the differential relationship between the local geometry of the surface around the point of reflection and the local geometry in the image. We then study the inverse problem and give necessary and sufficient conditions for recovering surface position and shape. We prove that surface position and shape up to third order can be derived as a function of local position, orientation and local scale measurements in the image when two orientations are available at the same point (e.g. a corner). Information equivalent to scale and orientation measurements can be also extracted from the reflection of a planar scene patch of arbitrary geometry, provided that the reflections of (at least) 3 distinctive points may be identified. We validate our theoretical results with both numerical simulations and experiments with real surfaces.

1. Introduction and Motivation

Estimating the 3D shape of physical objects is one of most useful functions of vision. Texture, shading, contour, stereoscopy, motion parallax and active projection of structured lighting are the most frequently studied cues for recovering 3D shape. These cues, however, are often inadequate for recovering the shape of shiny reflective objects, such as a silver plate, a glass goblet or a well-washed automobile, since it is not possible to observe their surfaces directly, rather only what they reflect.

Yet, the ability of recovering the shape of specular or highly reflective surfaces is valuable in many applications such as industrial metrology of polished metallic and plastic parts, medical imaging of moist or gelatinous tissues, digital archival of artworks and heritage objects, remote sensing of liquid surfaces, and diagnostic of space metallic structures.

Although specular surfaces are difficult to measure with traditional techniques, specular reflections present an additional cue that potentially may be exploited for shape recovery. A curved mirror produces 'distorted' images of the surrounding world (see Fig. 1(a)). For example, the image of a straight line reflected by a curved mirror is, in general, a curve. It is clear that such distortions are systematically related to the shape of the surface. Is it possible to invert this map, and recover the shape of the mirror from its reflected images?

The general 'inverse mirror' problem is clearly under-constrained: by opportunely manipulating the surrounding world, we may produce a great variety of

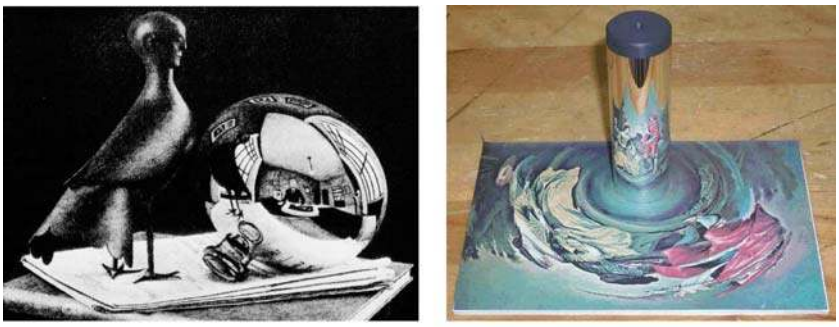

(a) (b)

Figure 1. (a) A scene reflected off a specular surface—M.C. Escher, *Still Life with Spherical Mirror*, 1934. (b) Anamorphic image.

images from any curved mirror surface, as illustrated by the anamorphic images that were popular during the Renaissance (see Fig. 1(b)). This inverse problem may become tractable under the assumption that the structure of the scene is known.

1.1. Proposed Approach and Summary of the Results

In this study we assume that both the camera (modelled as a perspective camera) and the scene are calibrated. We ignore the contribution of other visual cues such as contours, shading and texture and we focus on the geometry relating a scene and its corresponding reflected image. We use this relationship to estimate the local shape of the mirror surface.

We start from the observation that the mapping from a scene line to its reflected curve in the camera image plane (due to mirror reflection) changes "orientation" and "curvature" of the scene line as well as "stretches" its length, modifying the local scale of the scene line. See Fig. 2. We first analyze this map and derive analytical expressions for the local geometry in the image (namely, first- and second-order derivatives of the reflected image curve at any given point) as a function of the position and shape of the mirror surface. We then generalize our results to a planar scene of arbitrary texture and describe the mapping between a local planar scene patch to the corresponding reflected patch in the image plane as a function of the local parameters of the mirror surface. Finally, we explore the inverse problem in three settings.

First, we show that by exploiting position and orientation measurements of (at least) three reflected curves intersecting at an examined point, it is possible to recover the local geometry up to first order (second order up to one free parameter). An example is shown in Fig. 6. Second, we show that by exploiting local position, orientation and local scale measurements of (at least) two reflected curves intersecting at a point, the surface geometry at such a point can be recovered up to third-order. An example is shown in Fig. 12. Third, we demonstrate that scale and orientation measurements may be also extracted from the reflection of a planar scene patch of arbitrary geometry. We prove that local surface shape can be estimated if locations of (at least) 3 arbitrary points are available within a neighborhood of the reflected scene patch. These results are summarized in Table 1.

1.2. Previous Work and Our Contribution

Previous authors have used highlights as a cue to infer information about the geometry of a specular surface. Koenderink and van Doorn (1980) qualitatively described how pattern of specularities change under viewer motion. This analysis was extended by Blake et al. to stereoscopic vision (Blake and Brelstaff, 1988; Blake, 1985). Additionally, Zisserman et al. (1989) investigated what geometrical information can be obtained by tracking the motion of specularities. Other approaches were based on the idea of modelling specular reflections with reflectance maps (Healey and Binford, 1988) or introduce them in the context of photometric stereo (Ikeuchi, 1981). Oren and Nayar (1997) performed an analysis on classification of real and virtual features, and developed an algorithm recovering the 3D surface profiles traveled by virtual features. Zheng and Murata (2000) developed a system where a rotating specular object is reconstructed by

Table 1. Summary of the results.

	Surface quantities up to 3rd order					
Measurements	Point	Normal	2nd order param.	3rd order param.	DOF	Pointer
Point position	s	s	a, b, c	e, f, g, h	8	Section 2.1
Point position + 2 orientations	s	s	r	e, f, g, h	6	Section 5.2
Point position + 3 orientations	✓	✓	r	e, f, g, h	5	Section 5.3.1
						Section 5.3.4
Point position + 3 orientations + 4 curvatures	✓	✓	r	r	1	Section 5.3.7
Point position + 2 orientations + 2 scales	✓	✓	✓	✓	0	Section 5.4.1
						Section 5.4.2

The first column shows different types of measurements available in the image plane. Each type of measurement enables the local reconstruction of the surface up to different degrees of freedom (which are shown in column 6). Columns 2–5 indicate the corresponding free parameters which cannot be estimated given that amount of measured information. The free parameters are s, a, b, c, e, f, g, h and will be introduced in the next sections. A check mark (✓) indicates that all parameters may be recovered. For example, (see third row) given the measurement of the position of one point and the orientations of 3 curves at that point, surface position and orientation can be fully recovered, curvature can be recovered up to one unknown (r), third surfaces parameters (e, f, g, h) can not be estimated at all. The last column gives a pointer to further details.

illuminating it by extended lights and then analyzing the motion of the highlight stripes. Halsead et al. (1996) proposed a reconstruction algorithm where a surface global model is fitted to a set of normals obtained by imaging a pattern of light reflected by specular surface. Their results were applied to interactive visualization of the cornea. Swaminathan et al. (2001) presented an in-depth analysis of caustics of catadioptric cameras with conic reflectors. The same authors (Swaminathan et al., 2004) gave insights on how to design the shape of mirrors in catadioptric imaging systems. Perard (2001) and Tarini et al. (2002) proposed a structured lighting technique for the iterative reconstruction of surface normal vectors and topography. Solem et al. (2003) formulated the problem in a variational framework, using an implicit level set representation of the surface. Wang et al. (2003) proposed a scanning system to recover fine-scale surface shape using a curved mirror to view multiple angles in a single image. Finally, Bonfort and Sturm (2003) presented a novel voxel-based approach in the spirit of multiple view (space carving) algorithms. The main limitations of these studies are the necessity of having (i) some knowledge on shape and position of the object; (ii) multiple images under different condition of the illuminant; (iii) dedicated hardware equipment.

Our method departs from previous work in several aspects. First, we work on the static monocular case and explore the amount of information available from a single image. As we will show in Section 6.2, with only one image we can calibrate the camera, the scene and recover information about an unknown specular shape (e.g. the car fender in Fig. 21). Second, our reconstruction scheme requires a simple setup and minimal hardware: a digital camera and a planar textured board. Finally, our analysis is local and differential rather than global and algebraic. For the first time we provide an explicit differential relationship between the local structure of a scene patch, its corresponding reflection in the image, and the local shape of the specular surface (up to third order). In this paper we gather and generalize our own work (Savarese and Perona, 2001, 2002; Savarese et al., 2002, 2004) in that we: (i) present a first and second order differential description of the mapping between the local scene patch and the corresponding reflection in the image; (ii) reframe our previous reconstruction schemes in a new formulation; (iii) study degenerate conditions of such a mapping; (iv) validate our theory with experiments on images of real surfaces.

1.3. Organization of the Paper

We formulate the problem and introduce the motivation in Section 2. In Section 3 we present the direct problem and analyze how the surface geometry affects the image measurements using a differential approach. In Section 4 we present several properties of the reflection mapping and discuss its degenerate conditions. In Section 5, we apply the analytical expressions derived in Section 3 to study the inverse problem and present a new technique to estimate surface position and shape

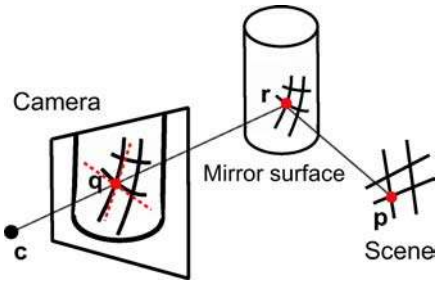

Figure 2. The setup.

from various image measurements. In Section 6, we describe a practical algorithm for surface local reconstruction and validate our theoretical results with both numerical simulations and experiments with real surfaces. We finally discuss our findings in Section 7 and propose a number of issues for future research.

2. Problem Formulation

Our geometric setup is depicted in Fig. 2. For now, we assume that a calibrated scene is composed of a planar pattern of intersecting lines. We will consider the general case of arbitrary planar scene in Section 5.4.5. The scene is reflected off an unknown smooth mirror surface and the reflection is observed by a calibrated camera. Our goal is to obtain local geometrical information of the mirror surface around **r** by analyzing the deformation produced upon the pattern of lines intersecting at point **p**.

In Section 2.1 we introduce the notation and study the simple case of a single known point reflected off the mirror surface. We show in Proposition 1 that given the measurement of the reflected point in the image, the orientation of the surface at the reflection point is known up to one distance parameter. In Section 2.2 we introduce a new reference system to give a simpler surface representation. In Section 2.3 we define the mapping between a scene line and the corresponding reflected image curve. We conclude the section by sketching out our proposed reconstruction scheme.

2.1. Notation and Basic Geometry of Specular Reflections

Points and vectors (i.e. difference of points) in $3D$ are denoted by a bold lower case letter[1] (e.g. $\mathbf{x} = [x\ y\ z]^T$). Tensors, matrices and $4D$ vectors are all denoted by a bold capital letter (e.g. $\mathbf{X}$). Let $\mathbf{c}$ be the center of projection of the camera. The image plane is positioned l distance units in front of $\mathbf{c}$, perpendicular to the view direction $\mathbf{v}$. Given a scene point $\mathbf{p}$, let $\mathbf{q}$ be the image of $\mathbf{p}$ observed on the image plane through a specular reflection on the mirror surface at $\mathbf{r}$ (see Fig. 3(a)). Since we assume that the camera and the scene pattern are calibrated, $\mathbf{p}$ and $\mathbf{q}$ are known, whereas $\mathbf{r}$ and the unit normal $\mathbf{n}_r$ to the surface at $\mathbf{r}$ are unknown. It follows from the perspective projection constraint that the point $\mathbf{r}$ must belong to the line defined by $\mathbf{c}$ and $\mathbf{q}$, resulting in the following relationship:

$$\mathbf{r} = \mathbf{c} + s\,\mathbf{d}, \tag{1}$$

where the unit vector $\mathbf{d} = (\mathbf{q} - \mathbf{c})/\parallel \mathbf{q} - \mathbf{c} \parallel$ is parallel to the line of sight, and $s = \parallel \mathbf{r} - \mathbf{c} \parallel$ is the distance from $\mathbf{c}$ to $\mathbf{r}$. With $\mathbf{c}$ fixed and $\mathbf{q}$ measured, the surface position at $\mathbf{r}$ is completely determined by a single

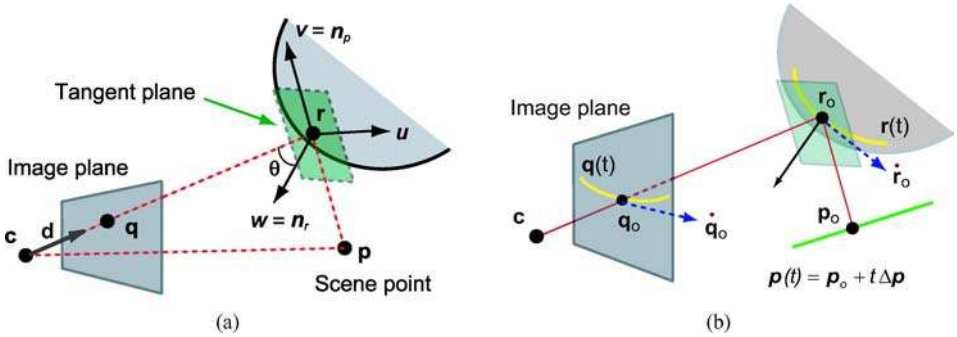

Figure 3. Geometry of specular reflections. (a) Notation and the *principal reference system* $[\mathbf{u}\,\mathbf{v}\,\mathbf{w}]$. (b) Given a fixed camera position $\mathbf{c}$, a mapping $t \in \mathbb{R}^0 \rightarrow \mathbf{r} \in \mathbb{R}^3$ defines a parameterized space curve $\mathbf{r}(t)$ lying on the mirror surface, which describes the position of the reflection point as t varies. Through a perspective projection, $\mathbf{r}(t)$ is mapped to another parameterized curve $\mathbf{q}(t)$ on the image plane.

distance parameter s. Furthermore, let us call the plane defined by $\mathbf{p}$, $\mathbf{r}$ and $\mathbf{c}$ the *principal plane*, let $\mathbf{n}_p$ be its unit normal vector and let θ denote the reflection angle at $\mathbf{r}$; then:

Proposition 1. *The unit normal vector $\mathbf{n}_r$ and the reflection angle θ are completely determined by the position parameter s.*

Proof: The geometry of our setup satisfies 2 basic constraints:

1. By the geometry of specular reflection, the incident vector $\mathbf{r}-\mathbf{p}$ and the reflected vector $\mathbf{r}-\mathbf{c}$ are coplanar with the normal vector $\mathbf{n}_r$ and the plane they define is the principal plane; namely,
$$\langle \mathbf{n}_r, \mathbf{n}_p \rangle = 0, \tag{2}$$
where $\langle , \rangle$ denotes the inner product of two vectors.
2. Furthermore, the angle between the incident vector and $\mathbf{n}_r$ must be equal to the angle between the reflected vector and $\mathbf{n}_r$. Namely,
$$\langle \mathbf{n}_r, \mathbf{d} \rangle = \left\langle \mathbf{n}_r, \frac{\mathbf{r}-\mathbf{p}}{\| \mathbf{r}-\mathbf{p} \|} \right\rangle, \tag{3}$$
which leads to
$$\left\langle \mathbf{n}_r, \mathbf{d} - \frac{\mathbf{r}-\mathbf{p}}{\| \mathbf{r}-\mathbf{p} \|} \right\rangle = 0. \tag{4}$$

By combining Eqs. (2) and (4), we can express $\mathbf{n}_r$ as a function of s (up to a sign) as follows:

$$\begin{aligned} \mathbf{n}_r &= \left(\mathbf{d} - \frac{\mathbf{r}-\mathbf{p}}{\| \mathbf{r}-\mathbf{p} \|} \right) \times \mathbf{n}_p \\ &= \frac{\mathbf{p}-\mathbf{c}-(s - \| \mathbf{p}-\mathbf{c}-s\,\mathbf{d} \|)\,\mathbf{d}}{\| \mathbf{p}-\mathbf{c}-s\,\mathbf{d} \|} \times \mathbf{n}_p. \end{aligned} \tag{5}$$

Similarly, the reflection angle θ can be parameterized by s as well by noting that

$$\cos 2\theta = 2\cos^2\theta - 1 = \left\langle \mathbf{d}, \frac{\mathbf{r}-\mathbf{p}}{\| \mathbf{r}-\mathbf{p} \|} \right\rangle,$$

which yields

$$\cos\theta = \frac{\sqrt{2}}{2} \sqrt{\frac{s - \langle \mathbf{d}, \mathbf{p}-\mathbf{c} \rangle}{\| \mathbf{c}+s\mathbf{d}-\mathbf{p} \|} + 1}. \tag{6}$$

□

2.2. *Reference System and Surface Representation*

Following Blake (1985), we now introduce a new reference system to give a simpler surface representation and a more compact relationship between higher order local surface parameters and the remaining geometrical quantities. We call this new reference system the *principal reference system* [**u** **v** **w**]. The principal reference system is centered at $\mathbf{r}$ and $\mathbf{w} = \mathbf{n}_r$, $\mathbf{v} = \mathbf{n}_p$, and $\mathbf{u} = \mathbf{v} \times \mathbf{w}$. Given an arbitrary point $\mathbf{a}$ represented in a reference system [**x** **y** **z**] centered in $\mathbf{c}$, its corresponding coordinates $\mathbf{a}'$ in [**u** **v** **w**] can be obtained by a transformation $\mathbf{a}' = \mathbf{R}^{\mathrm{T}}(\mathbf{a}-\mathbf{r})$, where $\mathbf{R} = [\mathbf{n}_p \times \mathbf{n}_r \ \mathbf{n}_p \ \mathbf{n}_r]$. Proposition 1 implies that this transformation is a function of the unknown parameter s. Therefore, the choice of principal reference system does not introduce any other unknown variables. From now on we will work in this principal reference system unless otherwise stated.

In the principal reference system, the normal of the surface at the origin is $\mathbf{w}$ and the tangent plane to the surface at the origin is the plane defined by $\mathbf{u}$ and $\mathbf{v}$; thus the surface around $\mathbf{r}$ can be written in the *special Monge form* (Cipolla and Giblin, 2000), yielding

$$\begin{aligned} w = {} & \frac{1}{2!}(a\,u^2 + 2c\,uv + b\,v^2) \\ & + \frac{1}{3!}(e\,u^3 + 3f\,u^2 v + 3g\,uv^2 + h\,v^3) + \cdots, \end{aligned} \tag{7}$$

where u, v, w are the coordinates of the special Monge form in the principal reference system; a, b, c and e, f, g, h are the second-order and third-order surface parameters around $\mathbf{r}$, respectively. Accordingly, we refer to the distance parameter s as the first-order surface parameter since it determines the position and normal of the surface. Our goal is to recover these surface parameters around $\mathbf{r}$ using quantities that are known or measurable. Note that $\mathbf{c}$, $\mathbf{q}$, $\mathbf{p}$ are known by assuming calibrated camera and scene.

2.3. *Differential Approach*

Let $\mathbf{p}_0 (= [\mathbf{p}_{0u} \ \mathbf{p}_{0v} \ \mathbf{p}_{0w}]^{\mathrm{T}})$ denote a scene point in 3D space. A line $\mathbf{p}$ passing through $\mathbf{p}_0$ may be described in a parametric form:

$$\mathbf{p}(t) = \mathbf{p}_0 + t\,\delta\mathbf{p} \tag{8}$$

where t is a parameter and $\delta\mathbf{p} = [\delta\mathbf{p}_u \ \delta\mathbf{p}_v \ \delta\mathbf{p}_w]^{\mathrm{T}}$ is the orientation vector of the line. Given a fixed camera

position $\mathbf{c}$, a mapping $t \in \mathbb{R}^0 \rightarrow \mathbf{r} \in \mathbb{R}^3$ defines a parameterized space curve $\mathbf{r}(t)$ lying on the mirror surface, which describes the position of the reflection point as t varies. See Fig. 3(b). Consequently, through a perspective projection, $\mathbf{r}(t)$ is mapped to another parameterized curve $\mathbf{q}(t)$ on the image plane. We denote the first-order derivatives (tangent vector) of $\mathbf{r}(t)$ and $\mathbf{q}(t)$ respectively by $\dot{\mathbf{r}}$ and $\dot{\mathbf{q}}$, and denote their second-order derivatives respectively by $\ddot{\mathbf{r}}$ and $\ddot{\mathbf{q}}$. When $t = t_0 = 0$, we denote $\mathbf{r}(t_0)$ by $\mathbf{r}_0$, which is the reflection point of $\mathbf{p}_0$ on the mirror surface and can be set as the origin of the principal reference system. Accordingly, the values of $\dot{\mathbf{r}}$, $\dot{\mathbf{q}}$, $\ddot{\mathbf{r}}$ and $\ddot{\mathbf{q}}$ evaluated at t_0 are denoted by $\dot{\mathbf{r}}_0$, $\dot{\mathbf{q}}_0$, $\ddot{\mathbf{r}}_0$ and $\ddot{\mathbf{q}}_0$. Throughout this paper, if there is no further explanation, we always assume that we evaluate $\dot{\mathbf{r}}$, $\dot{\mathbf{q}}$, $\ddot{\mathbf{r}}$ and $\ddot{\mathbf{q}}$ at t_0, and omit the subscript 0 to make the notation easier on the eye. Furthermore, we denote as κ^q the curvature $\kappa^q(t)$ of the image plane curve $\mathbf{q}(t)$ evaluated at t_0.

Our approach is to perform differential analysis around the point of intersection $\mathbf{r}_0$ of two or more scene lines. Specifically, we derive analytical expressions for the first- and second-order derivatives of deformed image curves at $\mathbf{q}_0$, in terms of surface parameters up to the third order (s, a, b, c, e, f, g, h) (see Section 3). By comparing these analytical formulas with their corresponding local measurements in the image, we impose a set of constraints on the unknown surface parameters. The resulting constraint system allows us to recover the mirror surface locally around the reflection point $\mathbf{r}_0$ up to the third order accuracy (see Section 5).

3. Direct Problem

Given a mirror surface, the problem of finding the point $\mathbf{r}$ on the surface where the ray is reflected from the scene point $\mathbf{p}$ to the observer $\mathbf{c}$ (see Fig. 2) can be traced back to Ptolemy's *Optics* in about AD 150. For a spherical mirror, this problem is known as *Alhazen's Problem* after the Arab scholar Ibn al-Haytham, who wrote an extensive account of it almost 1000 years ago. For historical pointers see (Smith, 1992; Dörrie, 1989). Neumann (1998) proved that the reflection point can not be found by ruler and compass methods of classical geometry. Thus, even for simple convex shapes, such as a sphere, it is very difficult to find $\mathbf{r}$ analytically.

In this section we assume that the reflection point $\mathbf{r}$ is known and study how the geometry of a specular surface determines its reflective behavior on a pattern line $\mathbf{p}(t)$ through $\mathbf{p}_0$ and consequently affects image plane measurements of $\mathbf{q}(t)$. Specifically, we carry out a differential analysis on the fundamental relationship between the image measurements such as $\dot{\mathbf{q}}_0$, $\ddot{\mathbf{q}}_0$, κ^q and and the first-, second- and third-order surface parameters of the mirror surface around the reflection point.

Table 2. Dependency between image measurements and local surface parameters. The last column points to the most meaningful equations.

Image derivatives at $\mathbf{q}_0$	Local surface parameters at $\mathbf{r}_0$	Equations
First order derivative of $\mathbf{q}(t)$ (i.e. $\dot{\mathbf{q}}_0$)	Distance s, tangent plane, curvature (i.e. a, b, c)	Eqs. (9) and (29)
Second order derivative of $\mathbf{q}(t)$ (i.e. $\ddot{\mathbf{q}}_0$)	Distance s, tangent plane, curvature (i.e. a, b, c), third order parameters (i.e. e, f, g, h)	Eqs. (38) and (53)

The main results of this analysis are summarized in Table 2: (i) first order derivative of the image curve $\mathbf{q}(t)$ at $\mathbf{q}_0$ (namely, $\dot{\mathbf{q}}_0$) is a function of the first and second order parameters of the surface at $\mathbf{r}_0$ (namely, distance s, tangent plane orientation and curvature parameters a, b, c); (ii) second order derivative of the image curve $\mathbf{q}(t)$ at $\mathbf{q}_0$ (namely, $\ddot{\mathbf{q}}_0$) is a function of the first, second and third order parameters of the surface at $\mathbf{r}_0$ (namely, s, a, b, c, e, f, g, h); in particular, $\ddot{\mathbf{q}}_0$ depends linearly on e, f, g, h.

In Section 3.1, we study the first order differential behavior of $\mathbf{r}(t)$ around t_0 . Proposition 2 expresses the relationship among $\dot{\mathbf{r}}_0$ (i.e. the first-order derivative of the reflected curve $\mathbf{r}(t)$ at $\mathbf{r}_0$), the surface shape up to second order (i.e. s, a, b, c) and the scene line geometry. Proposition 4 relates $\dot{\mathbf{r}}_0$ to $\dot{\mathbf{q}}_0$. By combining these two propositions we demonstrate the first row of Table 2.

Then, in Section 3.2 we study the second order differential behavior of $\mathbf{r}(t)$ around t_0. Proposition 5 expresses the relationship among $\ddot{\mathbf{r}}_0$ (i.e. the second-order derivative of the reflected curve $\mathbf{r}(t)$ at $\mathbf{r}_0$), surface shape up to third order (i.e. s, a, b, c, e, f, g, h) and the scene line geometry. Proposition 6 relates $\ddot{\mathbf{r}}_0$ to $\ddot{\mathbf{q}}_0$. By combining these two propositions we demonstrate the second row of Table 2.

3.1. First Order Analysis

3.1.1. First-order Derivative of $\mathbf{r}(t)$**.** In this section we study the first order differential behavior of $\mathbf{r}(t)$ around t_0.

Proposition 2. *The first-order derivative of the surface curve* $\mathbf{r}(t)$ *at* t_0 (*namely, the tangent vector* $\dot{\mathbf{r}}_0$ *of* $\mathbf{r}(t)$ *at* $\mathbf{r}_0$) *is a function of the first-order surface parameter* s *and second-order surface parameters* (a, b, c). *Specifically,* $\dot{\mathbf{r}}_0$ *may be expressed as*

$$\dot{\mathbf{r}}_0 = \begin{bmatrix} \dot{u} \\ \dot{v} \\ \dot{w} \end{bmatrix} = -\frac{1}{\Delta} \begin{bmatrix} J_v - 2b\cos\theta & 2c\cos\theta & 0 \\ 2c\cos\theta & J_u - 2a\cos\theta & 0 \\ 0 & 0 & \Delta \end{bmatrix} \begin{bmatrix} B_u \\ B_v \\ 0 \end{bmatrix}, \tag{9}$$

where

$$B_u = \frac{(\delta\mathbf{p})_w \cos\theta \sin\theta - (\delta\mathbf{p})_u \cos^2\theta}{\| \mathbf{p}_0 \|}, \; B_v = -\frac{(\delta\mathbf{p})_v}{\| \mathbf{p}_0 \|}, \tag{10}$$

$$J_v = \frac{s + \| \mathbf{p}_0 \|}{s \| \mathbf{p}_0 \|} = \frac{1}{s} + \frac{1}{\| \mathbf{p}_0 \|}, \; J_u = J_v \cos^2\theta, \tag{11}$$

$$\Delta = (J_u - 2a\cos\theta)(J_v - 2b\cos\theta) - 4c^2\cos^2\theta. \tag{12}$$

Proof: The Fermat principle (Born and Wolf, 1965) stipulates that the reflection point $\mathbf{r}$ must be located on the mirror surface in such a way that locally minimizes the length of the specular path from the scene point $\mathbf{p}$ to the camera $\mathbf{c}$. Thus, the reflection point $\mathbf{r}$ can be found by solving a constrained optimization problem, that is:

$$\begin{aligned} &\text{minimize} \quad \| \mathbf{r} - \mathbf{p} \| + \| \mathbf{r} - \mathbf{c} \| \\ &\text{subject to} \quad g(\mathbf{r}) = 0, \end{aligned} \tag{13}$$

where $g(u, v, w) = 0$ denotes the implicit function of the mirror surface, which can be obtained from its Monge form (7) as:

$$\begin{aligned} &g(u, v, w) \\ &= w - \frac{1}{2!}(a\,u^2 + 2c\,uv + b\,v^2) \\ &- \frac{1}{3!}(e\,u^3 + 3f\,u^2 v + 3g\,uv^2 + h\,v^3) + \cdots = 0. \end{aligned} \tag{14}$$

By applying the Lagrange Multiplier Theorem, as demonstrated by Chen and Arvo (2000), we obtain

$$\begin{cases} \mathbf{x}_r(\mathbf{r}) + \mathbf{x}_i(\mathbf{r}, t) + \lambda \nabla g(\mathbf{r}) = \mathbf{0} \\ g(\mathbf{r}) = 0 \end{cases}, \tag{15}$$

where we have used $\mathbf{x}_i$ and $\mathbf{x}_r$ to denote the incident direction (depending on both $\mathbf{r}$ and t) and reflection direction (depending on $\mathbf{r}$), which are defined respectively as

$$\mathbf{x}_i = \frac{\mathbf{r} - \mathbf{p}(t)}{\| \mathbf{r} - \mathbf{p}(t) \|}, \tag{16}$$

$$\mathbf{x}_r = \frac{\mathbf{r} - \mathbf{c}}{\| \mathbf{r} - \mathbf{c} \|}. \tag{17}$$

Notice that $\mathbf{x}_r$ has already been introduced as $\mathbf{d}$ in Eq. (1). Here we emphasize the dependence on $\mathbf{r}$. Eq. (15) is a non-linear system of 4 equations in 5 unknowns (t, $\mathbf{r}$ and λ) and obviously $(0, \mathbf{r}_0, 2\cos\theta_0)^2$is one of its solutions. We refer to it as *Fermat equation* and denote it by $\mathbf{F}(t, \mathbf{r}, \lambda) = \mathbf{0}$, where each component of $\mathbf{F} = [F_1\ F_2\ F_3\ F_4]$ captures the left-hand side of one of the equations in (15).

We take advantage of Implicit Function Theorem to study the differential behavior of $\mathbf{r}(t)$ around t_0. The theorem states that if $(t_0, \mathbf{r}_0, \lambda_0)$ is a solution of $\mathbf{F}(t, \mathbf{r}, \lambda) = 0$ and the Jacobian

$$\Delta = \det\left[\frac{\partial \mathbf{F}(t, \mathbf{r}, \lambda)}{\partial(\mathbf{r}, \lambda)} \right]\Bigg|_{t=t_0} \neq 0, \tag{18}$$

the smooth mapping function $\mathbf{r}(t)$ exists around the neighborhood of $\mathbf{r}_0$. Furthermore, we may compute the derivative of $\mathbf{r}(t)$ with respect to t by differentiating $\mathbf{F}$ with respect to t. By chain rule, we obtain:

$$\mathbf{B}(t, \mathbf{r}, \lambda) = -\mathbf{J}(t, \mathbf{r}, \lambda)\,\mathbf{S}(t), \tag{19}$$

where

$$\mathbf{B}(t, \mathbf{r}, \lambda) = \frac{\partial \mathbf{F}(t, \mathbf{r}, \lambda)}{\partial t}, \quad \mathbf{J}(t, \mathbf{r}, \lambda) = \frac{\partial \mathbf{F}(t, \mathbf{r}, \lambda)}{\partial(\mathbf{r}, \lambda)},$$
$$\mathbf{S}(t) = [\dot{u}(t)\ \dot{v}(t)\ \dot{w}(t)\ \dot{\lambda}(t)]^T = [\dot{\mathbf{r}}(t)\ \dot{\lambda}(t)]^T.$$

We may express $\mathbf{B}$ and $\mathbf{J}$ as follows:

$$\mathbf{B} = \begin{bmatrix} \mathbf{B}_{31} \\ 0 \end{bmatrix}, \quad \mathbf{J} = \begin{bmatrix} \mathbf{J}_{33} & \nabla g(\mathbf{r}) \\ (\nabla g(\mathbf{r}))^{\mathrm{T}} & 0 \end{bmatrix}, \tag{20}$$

where the sub-matrices $\mathbf{B}_{31}$ and $\mathbf{J}_{33}$ (the subscript denotes the matrix dimension) are defined as

$$\mathbf{B}_{31} = -\frac{(\mathbf{I} - \mathbf{x}_i \mathbf{x}_i{}^{\mathrm{T}})\delta\mathbf{p}}{\| \mathbf{r} - \mathbf{p}(t) \|},$$
$$\mathbf{J}_{33} = \frac{(\mathbf{I} - \mathbf{x}_i \mathbf{x}_i{}^{\mathrm{T}})}{\| \mathbf{r} - \mathbf{p}(t) \|} + \frac{(\mathbf{I} - \mathbf{x}_r \mathbf{x}_r{}^{\mathrm{T}})}{\| \mathbf{r} - \mathbf{c} \|} + \lambda \mathbf{H}_g. \quad (21)$$

Here, g denotes the implicit definition of the surface and ∇g, $\mathbf{H}_g$ are respectively the gradient vector and the Hessian matrix of g. It follows from Eq. (14) that

$$\nabla g = \begin{bmatrix} -a\,u - c\,v - \frac{1}{2}e\,u^2 - f\,uv - \frac{1}{2}g\,v^2 + \cdots \\ -c\,u - b\,v - \frac{1}{2}f\,u^2 - g\,uv - \frac{1}{2}h\,v^2 + \cdots \\ 1 \end{bmatrix},$$

$$\mathbf{H}_g = \begin{bmatrix} -a - e\,u - f\,v + \cdots & -c - f\,u - g\,v + \cdots & 0 \\ -c - f\,u - g\,v + \cdots & -b - g\,u - h\,v + \cdots & 0 \\ 0 & 0 & 0 \end{bmatrix}. \quad (22)$$

In order to compute $\dot{\mathbf{r}}(t)$ at $\mathbf{r}_0$, we need to evaluate $\mathbf{B}$, $\mathbf{J}$ at $t = t_0$ (and thus, at $\mathbf{p} = \mathbf{p}_0$, $\mathbf{r} = \mathbf{r}_0$ and $\lambda = \lambda_0 = 2\cos\theta_0$). At that end, we note that, since we work in the principal reference system, $\mathbf{x}_r$ and $\mathbf{x}_i$ may be expressed in terms of the reflection angle θ:

$$\mathbf{x}_i = (\sin\theta, 0, -\cos\theta)^{\mathrm{T}}, \quad \mathbf{x}_r = (-\sin\theta, 0, -\cos\theta)^{\mathrm{T}}.$$

Thus, we may expand Eq. (19) as follows:

$$\begin{bmatrix} B_u \\ B_v \\ B_w \\ 0 \end{bmatrix} = -\begin{bmatrix} J_u - 2a\cos\theta & -2c\cos\theta & J_w & 0 \\ -2c\cos\theta & J_v - 2b\cos\theta & 0 & 0 \\ J_w & 0 & J_v \sin^2\theta & 1 \\ 0 & 0 & 1 & 0 \end{bmatrix} \times \begin{bmatrix} \dot{u}(0) \\ \dot{v}(0) \\ \dot{w}(0) \\ \dot{\lambda}(0) \end{bmatrix}, \quad (23)$$

where $\cos\theta$ is given by Eq. (6), $\sin^2\theta = 1 - \cos^2\theta$; B_u, B_v, J_u and J_v are defined in Proposition 2; B_w and J_w are defined as follows:

$$B_w = \frac{(\delta\mathbf{p})_u \cos\theta \sin\theta - (\delta\mathbf{p})_w \sin^2\theta}{\| \mathbf{p}_0 \|}, \quad (24)$$
$$J_w = \frac{\| \mathbf{p}_0 \| - s}{s \| \mathbf{p}_0 \|} \sin\theta\cos\theta \quad (25)$$

It follows from the last row of Eq. (23) that $\dot{w}(0) = 0$. Consequently,

$$\begin{bmatrix} B_u \\ B_v \\ B_w \end{bmatrix} = -\begin{bmatrix} J_u - 2a\cos\theta & -2c\cos\theta & 0 \\ -2c\cos\theta & J_v - 2b\cos\theta & 0 \\ J_w & 0 & 1 \end{bmatrix} \times \begin{bmatrix} \dot{u}(0) \\ \dot{v}(0) \\ \dot{\lambda}(0) \end{bmatrix}. \quad (26)$$

By inverting the matrix in Eq. (26), we obtain the first-order derivative of the surface curve $\mathbf{r}(t)$ at $\mathbf{r}_0$ (i.e.,t_0) and the proposition is proved. The determinant of the matrix in Eq. (26) (i.e., $\Delta = (J_u - 2a\cos\theta)(J_v - 2b\cos\theta) - 4c^2\cos^2\theta$) is equal to the Jacobian in Eq. (18). □

Proposition 2 tells us that $\dot{\mathbf{r}}_0$ is *not* function of the third or higher order parameters of the surface around the reflection point. A similar relationship was derived by Zisserman et al. (1989) in the dual context of a moving observer. Note that Proposition 2 holds under the condition of $\Delta \neq 0$ in Eq. (18), which guarantees that the mapping $\mathbf{r}(t)$ is unique in the neighborhood of $(t_0, \mathbf{r}_0, \lambda_0)$. From now on we shall always assume that $\Delta \neq 0$. This assumption is reasonable as we shall see in more details in Section 4.1.

If we call ϕ the angle between $\dot{\mathbf{r}}$ and $\mathbf{u}$ axis, the orientation of the tangent vector of $\mathbf{r}(t)$ at $\mathbf{r}_0$ within the tangent plane may be expressed as

$$\tan\phi = \frac{\dot{v}}{\dot{u}} = \frac{(J_u - 2a\cos\theta)B_v + 2cB_u\cos\theta}{(J_v - 2b\cos\theta)B_u + 2cB_v\cos\theta}. \quad (27)$$

3.1.2. Relationship Between $\dot{\mathbf{r}}$ *and* $\dot{\mathbf{q}}$.

Proposition 3. *The direction of the tangent vector* $\dot{\mathbf{r}}$ *is directly related to the direction of the tangent vector* $\dot{\mathbf{q}}$ *by the following relationship* (*up to a sign*)

$$\frac{\dot{\mathbf{r}}}{\| \dot{\mathbf{r}} \|} = \frac{\mathbf{n}_r \times (\mathbf{c}/\| \mathbf{c} \| \times \dot{\mathbf{q}}/\| \dot{\mathbf{q}} \|)}{\| \mathbf{n}_r \times (\mathbf{c}/\| \mathbf{c} \| \times \dot{\mathbf{q}}/\| \dot{\mathbf{q}} \|) \|}. \quad (28)$$

Proof: It is not difficult to show that $\dot{\mathbf{q}}$ is proportional to the perspective projection of $\dot{\mathbf{r}}$ into the image plane. Thus the plane defined by $\mathbf{c}$ and $\dot{\mathbf{q}}$ contains $\dot{\mathbf{r}}$. Let $\mathbf{n}_t$ denote the normal vector of this plane, then we have $\langle \mathbf{n}_t, \dot{\mathbf{r}} \rangle = 0$. Since $\langle \mathbf{n}_r, \dot{\mathbf{r}} \rangle = 0$, we have $\frac{\dot{\mathbf{r}}}{\|\dot{\mathbf{r}}\|} = \frac{\mathbf{n}_t \times \mathbf{n}_r}{\|\mathbf{n}_t \times \mathbf{n}_r\|}$ up to a sign, which gives rise to Eq. (28). □

More generally,

Proposition 4. *Let* $\mathbf{r}(t)$ *be the surface curve and* $\mathbf{q}(t)$ *be its camera image. Then respective tangent vectors are linearly related*:

$$\dot{\mathbf{q}} = \mathbf{T}\,\dot{\mathbf{r}} \tag{29}$$

where $\mathbf{T}$ *is a* 3×3 *matrix function of the camera parameters,* $\mathbf{r}_0$ *and* $\mathbf{q}_0$. *Specifically, the matrix* $\mathbf{T}$ *is defined as follows*:

$$\mathbf{T} = \frac{l}{s\,\langle \mathbf{d}, \mathbf{v} \rangle}\left[\mathbf{I} - \frac{\mathbf{d}\mathbf{v}^{\mathrm{T}}}{\langle \mathbf{d}, \mathbf{v} \rangle}\right]. \tag{30}$$

where $\mathbf{d} = (\mathbf{q} - \mathbf{c})/\,\|\,\mathbf{q} - \mathbf{c}\,\|$, $s = \|\,\mathbf{r} - \mathbf{c}\,\|$, $\mathbf{v}$ *is the view direction and* l *is the distance from* $\mathbf{c}$ *of the image plane along* $\mathbf{v}$.

Proof: Letting $\gamma(t) = \|\,\mathbf{q}(t) - \mathbf{c}\,\| \,/\, \|\,\mathbf{r}(t) - \mathbf{c}\,\|$ be the ratio between the distance from $\mathbf{c}$ to $\mathbf{q}(t)$ and that from $\mathbf{c}$ to $\mathbf{r}(t)$. We may express the image plane curve $\mathbf{q}(t)$ as follows:

$$\mathbf{q}(t) - \mathbf{c} = \gamma(t)(\mathbf{r}(t) - \mathbf{c}). \tag{31}$$

Thus, $\mathbf{q}(t)$ satisfies

$$\langle \mathbf{q}(t) - \mathbf{c}, \mathbf{v} \rangle = l,$$

which can be expressed in terms of γ using Eq. (31), yielding

$$\gamma(t)\,\langle \mathbf{r}(t) - \mathbf{c}, \mathbf{v} \rangle = l. \tag{32}$$

Differentiating Eq. (32) with respect to t, we have

$$\dot{\gamma}\,\langle \mathbf{r} - \mathbf{c}, \mathbf{v} \rangle + \gamma\,\langle \dot{\mathbf{r}}, \mathbf{v} \rangle = 0. \tag{33}$$

We may then solve for γ from Eqs. (32) and (1) and $\dot{\gamma}$ from Eq. (33), obtaining

$$\gamma = \frac{l}{\langle \mathbf{r}(t) - \mathbf{c}, \mathbf{v} \rangle} = \frac{l}{s\,\langle \mathbf{d}, \mathbf{v} \rangle}, \tag{34}$$

$$\dot{\gamma} = -\frac{l\,\langle \dot{\mathbf{r}}, \mathbf{v} \rangle}{s^2\,\langle \mathbf{d}, \mathbf{v} \rangle^2}. \tag{35}$$

Note that γ and $\dot{\gamma}$ are both evaluated at $t = t_0$. Using Eqs. (34) and (35), we can differentiate Eq. (31) with respect to t and compute $\dot{\mathbf{q}}$ as follows:

$$\dot{\mathbf{q}} = \gamma\dot{\mathbf{r}} + s\dot{\gamma}\mathbf{d}, \tag{36}$$

$$= \frac{l}{s\,\langle \mathbf{d}, \mathbf{v} \rangle}\left[\mathbf{I} - \frac{\mathbf{d}\mathbf{v}^{\mathrm{T}}}{\langle \mathbf{d}, \mathbf{v} \rangle}\right]\dot{\mathbf{r}} = \mathbf{T}\,\dot{\mathbf{r}}, \tag{37}$$

□

3.2. *Second Order Analysis*

***3.2.1. Second-order Derivative of* $\mathbf{r}(t)$.** In this section we study the second order differential behavior of $\mathbf{r}(t)$ around $t = t_0$.

Proposition 5. *The second-order derivative of the surface curve* $\mathbf{r}(t)$ *at* $\mathbf{r}_0$ *(i.e.,* t_0*) is a function of the first-order surface parameter* s, *second-order surface parameters* a, b, c *and third-order surface parameters* e, f, g, h. *Particularly, it depends linearly on the third-order surface parameters* e, f, g, h. *Specifically,* $\ddot{\mathbf{r}}$ *may be expressed as*

$$\ddot{\mathbf{r}} = \ddot{\mathbf{r}}_1 + \ddot{\mathbf{r}}_2 = \begin{bmatrix} \ddot{u}_1 \\ \ddot{v}_1 \\ \ddot{w}_1 \end{bmatrix} + \begin{bmatrix} \ddot{u}_2 \\ \ddot{v}_2 \\ 0 \end{bmatrix} \tag{38}$$

where the first term is

$$\begin{bmatrix} \ddot{u}_1 \\ \ddot{v}_1 \end{bmatrix} = -\frac{1}{\Delta}\begin{bmatrix} J_v - 2b\cos\theta & 2c\cos\theta \\ 2c\cos\theta & J_u - 2a\cos\theta \end{bmatrix} \times \begin{bmatrix} D_1 + J_w\ddot{w} \\ D_2 \end{bmatrix} \tag{39}$$

$$\ddot{w}_1 = -a\dot{u}^2 - 2c\dot{u}\dot{v} - b\dot{v}^2, \tag{40}$$

and D_1, D_2 (*which are both functions of* $\dot{u}$ *and* $\dot{v}$) *are derived in the proof; the second term is*

$$\begin{bmatrix} \ddot{u}_2 \\ \ddot{v}_2 \end{bmatrix} = \frac{2\cos\theta}{\Delta}\begin{bmatrix} J_v - 2b\cos\theta & 2c\cos\theta \\ 2c\cos\theta & J_u - 2a\cos\theta \end{bmatrix} \times \begin{bmatrix} \dot{u}^2 & 2\dot{u}\dot{v} & \dot{v}^2 & 0 \\ 0 & \dot{u}^2 & 2\dot{u}\dot{v} & \dot{v}^2 \end{bmatrix}\begin{bmatrix} e \\ f \\ g \\ h \end{bmatrix}. \tag{41}$$

In both terms, the quantities J_u, J_v, Δ are defined in Proposition 2.

Proof: By differentiating Eq. (19) with respect to t, we have

$$\frac{d\mathbf{B}(t,\mathbf{r},\lambda)}{dt} = -\frac{d\mathbf{J}(t,\mathbf{r},\lambda)}{dt}\mathbf{S} - \mathbf{J}\frac{d\mathbf{S}(t)}{dt}, \quad (42)$$

where

$$\frac{d\mathbf{S}}{dt} = [\ddot{\mathbf{r}}(t) \;\; \ddot{\lambda}(t)]^{\mathrm{T}} = [\ddot{u}(t) \;\; \ddot{v}(t) \;\; \ddot{w}(t) \;\; \ddot{\lambda}(t)]^{\mathrm{T}}$$

Since our goal is to compute $\ddot{\mathbf{r}}$, we calculate the components $d\mathbf{B}/dt$ and $d\mathbf{J}/dt$ in Eq. (42). Note that we should think of $(\mathbf{r}, \lambda)$ as a function of t (i.e., $\mathbf{r}(t)$ which is guaranteed to exist from our first order analysis) while calculating these derivatives. This is indicated by notation d/dt instead of $\partial/\partial t$. These expressions are derived for a general t, and will be evaluated at the specular path through $\mathbf{p}_0$, that is, $t = 0$. In this derivation, we will use the identities:

$$\mathbf{N}_r = \mathbf{I} - \mathbf{x}_r\mathbf{x}_r{}^{\mathrm{T}} = \begin{bmatrix} \cos^2\theta & 0 & -\sin\theta\cos\theta \\ 0 & 1 & 0 \\ -\sin\theta\cos\theta & 0 & \sin^2\theta \end{bmatrix},$$

$$\mathbf{N}_i = \mathbf{I} - \mathbf{x}_i\mathbf{x}_i{}^{\mathrm{T}} = \begin{bmatrix} \cos^2\theta & 0 & \sin\theta\cos\theta \\ 0 & 1 & 0 \\ \sin\theta\cos\theta & 0 & \sin^2\theta \end{bmatrix}$$

$$\frac{\partial \| \mathbf{r} - \mathbf{p}(t) \|}{\partial t} = -\mathbf{x}_r{}^{\mathrm{T}}\delta\mathbf{p}, \quad \frac{\partial \mathbf{x}_r}{\partial t} = -\frac{\mathbf{N}_r}{\| \mathbf{r} - \mathbf{p}(t) \|}\delta\mathbf{p},$$

$$\frac{\partial \| \mathbf{r} - \mathbf{p}(t) \|}{\partial \mathbf{r}} = \mathbf{x}_r{}^{\mathrm{T}}, \quad \frac{\partial \mathbf{x}_r}{\partial \mathbf{r}} = \frac{\mathbf{N}_r}{\| \mathbf{r} - \mathbf{p}(t) \|},$$

$$\frac{\partial \mathbf{N}_r}{\partial t} = \frac{\mathbf{N}_r\delta\mathbf{p}\mathbf{x}_r{}^{\mathrm{T}} + \mathbf{x}_r\delta\mathbf{p}^{\mathrm{T}}\mathbf{N}_r}{\| \mathbf{r} - \mathbf{p}(t) \|},$$

$$\frac{\partial(\mathbf{N}_r\delta\mathbf{p})}{\partial \mathbf{r}} = -\frac{\mathbf{N}_r\mathbf{x}_r{}^{\mathrm{T}}\delta\mathbf{p} + \mathbf{x}_r\delta\mathbf{p}^{\mathrm{T}}\mathbf{N}_r}{\| \mathbf{r} - \mathbf{p}(t) \|}$$

We start by differentiating $\mathbf{B}$ and obtain:

$$\frac{\partial \mathbf{B}_{31}}{\partial t} = -\mathbf{A}\delta\mathbf{p}, \quad \frac{\partial \mathbf{B}_{31}}{\partial \mathbf{r}} = \mathbf{A},$$

where the matrix factor $\mathbf{A}$ is defined as

$$\mathbf{A} = \frac{\mathbf{N}_r\mathbf{x}_r{}^{\mathrm{T}}\delta\mathbf{p} + \mathbf{N}_r\delta\mathbf{p}\mathbf{x}_r{}^{\mathrm{T}} + \mathbf{x}_r\delta\mathbf{p}^{\mathrm{T}}\mathbf{N}_r}{\| \mathbf{r} - \mathbf{p}(t) \|^2}$$

Consequently, we obtain from the chain rule

$$\begin{aligned} \frac{d\mathbf{B}(t,\mathbf{r},\lambda)}{dt} &= \frac{\partial \mathbf{B}}{\partial t} + \frac{\partial \mathbf{B}}{\partial(\mathbf{r},\lambda)} \cdot \mathbf{S} \\ &= \begin{bmatrix} -\mathbf{A}\delta\mathbf{p} \\ 0 \end{bmatrix} + \begin{bmatrix} \mathbf{A} & 0 \\ 0 & 0 \end{bmatrix} \begin{bmatrix} \dot{\mathbf{r}}(t) \\ \dot{\lambda}(t) \end{bmatrix} \\ &= \begin{bmatrix} \mathbf{A}(\dot{\mathbf{r}}(t) - \delta\mathbf{p}) \\ 0 \end{bmatrix}. \end{aligned} \quad (43)$$

Similarly, we may compute $d\mathbf{J}/dt$ through $\partial\mathbf{J}/\partial t$ and $\partial\mathbf{J}/\partial(\mathbf{r},\lambda)$ as follows:

$$\begin{aligned} \frac{\partial \mathbf{J}}{\partial t} &= \begin{bmatrix} \frac{\partial \mathbf{J}_{33}}{\partial t} & 0 \\ 0 & 0 \end{bmatrix} = \begin{bmatrix} \frac{\partial \mathbf{N}r/\| \mathbf{r}-\mathbf{p}(t) \|}{\partial t} & 0 \\ 0 & 0 \end{bmatrix} \\ &= \begin{bmatrix} \mathbf{A} & 0 \\ 0 & 0 \end{bmatrix}. \end{aligned}$$

The computation of $\partial\mathbf{J}/\partial(\mathbf{r},\lambda)$ becomes a little more complicated, since the result will be a third order tensor, which, after being multiplied by $\mathbf{S}$, returns a matrix. This third order tensor can be computed by calculating the differential matrix associated with each column of $\mathbf{J}$. Let

$$\mathbf{e}_1 = (1,0,0)^{\mathrm{T}}, \quad \mathbf{e}_2 = (0,1,0)^{\mathrm{T}}, \quad \mathbf{e}_3 = (0,0,1)^{\mathrm{T}}.$$

and define $\mathbf{V}^j$ the jth column of a matrix $\mathbf{V}$. Using Eq. (21), we have

$$\mathbf{J}_{33}^j = \frac{\mathbf{N}_r^j}{\| \mathbf{r} - \mathbf{p}(t) \|} + \frac{\mathbf{N}_i^j}{\| \mathbf{r} - \mathbf{c} \|} + \lambda\mathbf{H}_g^j$$

Differentiating the first two components of $\mathbf{J}_{33}^j$, we have

$$\begin{aligned} \mathbf{C}_r^j &= \frac{\partial(\mathbf{N}_r^j)/\| \mathbf{r} - \mathbf{p}(t) \|}{\partial \mathbf{r}} \\ &= -\frac{\mathbf{N}_r\mathbf{x}_r{}^{\mathrm{T}}\mathbf{e}_j + \mathbf{N}_r\mathbf{e}_j\mathbf{x}_r{}^{\mathrm{T}} + \mathbf{x}_r\mathbf{e}_j{}^{\mathrm{T}}\mathbf{N}_r}{\| \mathbf{r} - \mathbf{p}(t) \|^2}, \\ \mathbf{C}_i^j &= \frac{\partial(\mathbf{N}_i^j)/\| \mathbf{r} - \mathbf{c} \|}{\partial \mathbf{r}} \\ &= -\frac{\mathbf{N}_i\mathbf{x}_i{}^{\mathrm{T}}\mathbf{e}_j + \mathbf{N}_i\mathbf{e}_j\mathbf{x}_i{}^{\mathrm{T}} + \mathbf{x}_i\mathbf{e}_j{}^{\mathrm{T}}\mathbf{N}_i}{\| \mathbf{r} - \mathbf{c} \|^2}. \end{aligned}$$

Furthermore, it follows from Eq. (22) that

$$\mathbf{C}_h^1 = \frac{\partial \mathbf{H}_g^1}{\partial \mathbf{r}} = \begin{bmatrix} -e & -f & 0 \\ -f & -g & 0 \\ 0 & 0 & 0 \end{bmatrix},$$
$$\mathbf{C}_h^2 = \frac{\partial \mathbf{H}_g^2}{\partial \mathbf{r}} = \begin{bmatrix} -f & -g & 0 \\ -g & -h & 0 \\ 0 & 0 & 0 \end{bmatrix}, \tag{44}$$
$$\mathbf{C}_h^3 = \frac{\partial \mathbf{H}_g^3}{\partial \mathbf{r}} = \mathbf{0}.$$

Consequently, we can compute

$$\frac{\partial \mathbf{J}_{33}^j}{\partial(\mathbf{r}, \lambda)} = \begin{bmatrix} \mathbf{C}_r^j + \mathbf{C}_i^j + \mathbf{C}_h^j & \mathbf{H}_g^j \end{bmatrix}_{34}.$$

Moreover, we have

$$\frac{\partial(\nabla g)}{\partial(\mathbf{r}, \lambda)} = \begin{bmatrix} \mathbf{H}_g & 0 \end{bmatrix}_{34}.$$

Define

$$\begin{aligned} \mathbf{C} &= \begin{bmatrix} \left(\mathbf{C}_r^1 + \mathbf{C}_i^1\right)\dot{\mathbf{r}}(t) + \mathbf{H}_g^1\dot{\lambda}(t) & \left(\mathbf{C}_r^2 + \mathbf{C}_i^2\right)\dot{\mathbf{r}}(t) \\ + \mathbf{H}_g^2\dot{\lambda}(t) & \left(\mathbf{C}_r^3 + \mathbf{C}_i^3\right)\dot{\mathbf{r}}(t) + \mathbf{H}_g^3\dot{\lambda}(t) \end{bmatrix}_{33}, \\ \mathbf{C}' &= \lambda \begin{bmatrix} \mathbf{C}_h^1\dot{\mathbf{r}}(t) & \mathbf{C}_h^2\dot{\mathbf{r}}(t) & \mathbf{C}_h^3\dot{\mathbf{r}}(t) \end{bmatrix} \\ &= \lambda \begin{bmatrix} -e\dot{u}(0) - f\dot{v}(0) & -f\dot{u}(0) - g\dot{v}(0) & 0 \\ -f\dot{u}(0) - g\dot{v}(0) & -g\dot{u}(0) - h\dot{v}(0) & 0 \\ 0 & 0 & 0 \end{bmatrix}. \end{aligned}$$

It follows from the chain rule that

$$\begin{aligned} \frac{d\mathbf{J}(t, \mathbf{r}, \lambda)}{dt} &= \begin{bmatrix} \mathbf{A} & 0 \\ 0 & 0 \end{bmatrix} + \begin{bmatrix} \mathbf{C} + \mathbf{C}' & \mathbf{H}_g\dot{\mathbf{r}}(t) \\ \left(\mathbf{H}_g\dot{\mathbf{r}}(t)\right)^{\mathrm{T}} & 0 \end{bmatrix} \\ &= \begin{bmatrix} \mathbf{A} + \mathbf{C} + \mathbf{C}' & \mathbf{H}_g\dot{\mathbf{r}}(t) \\ \left(\mathbf{H}_g\dot{\mathbf{r}}(t)\right)^{\mathrm{T}} & 0 \end{bmatrix} \end{aligned} \tag{45}$$

Finally, by substituting Eqs. (43) and (45) into Eq. (42), we obtain

$$\begin{bmatrix} \mathbf{A}(\dot{\mathbf{r}}(t) - \delta\mathbf{p}) \\ 0 \end{bmatrix} = -\begin{bmatrix} \mathbf{A} + \mathbf{C} + \mathbf{C}' & \mathbf{H}_g\dot{\mathbf{r}}(t) \\ \left(\mathbf{H}_g\dot{\mathbf{r}}(t)\right)^{\mathrm{T}} & 0 \end{bmatrix} \times \begin{bmatrix} \dot{\mathbf{r}}(t) \\ \dot{\lambda}(t) \end{bmatrix} - \begin{bmatrix} \mathbf{J}_{33} & \nabla g(\mathbf{r}) \\ (\nabla g(\mathbf{r}))^{\mathrm{T}} & 0 \end{bmatrix} \begin{bmatrix} \ddot{\mathbf{r}}(t) \\ \ddot{\lambda}(t) \end{bmatrix},$$

which may be expressed as

$$\mathbf{D} = -\begin{bmatrix} \mathbf{J}_{33} & \nabla g(\mathbf{r}) \\ (\nabla g(\mathbf{r}))^{\mathrm{T}} & 0 \end{bmatrix} \begin{bmatrix} \ddot{\mathbf{r}}(t) \\ \ddot{\lambda}(t) \end{bmatrix}, \tag{46}$$

where $\mathbf{D}$ is defined as

$$\begin{aligned} \mathbf{D} &= \begin{bmatrix} \mathbf{A}(\dot{\mathbf{r}}(t) - \delta\mathbf{p}) \\ 0 \end{bmatrix} + \begin{bmatrix} \mathbf{A} + \mathbf{C} + \mathbf{C}' & \mathbf{H}_g\dot{\mathbf{r}}(t) \\ \left(\mathbf{H}_g\dot{\mathbf{r}}(t)\right)^{\mathrm{T}} & 0 \end{bmatrix} \\ &\quad \times \begin{bmatrix} \dot{\mathbf{r}}(t) \\ \dot{\lambda}(t) \end{bmatrix} \\ &= \begin{bmatrix} \mathbf{A}(\dot{\mathbf{r}}(t) - \delta\mathbf{p}) + (\mathbf{A} + \mathbf{C} + \dot{\lambda}(t)\mathbf{H}_g)\dot{\mathbf{r}}(t) \\ (\mathbf{H}_g\dot{\mathbf{r}}(t))^{\mathrm{T}}\dot{\mathbf{r}}(t) \end{bmatrix} \\ &\quad + \begin{bmatrix} \mathbf{C}'\dot{\mathbf{r}}(t) \\ 0 \end{bmatrix} \\ &= \mathbf{D}_1 + \mathbf{D}_2. \end{aligned} \tag{47}$$

Here we have defined

$$\mathbf{D}_1 = \begin{bmatrix} \mathbf{A}(\dot{\mathbf{r}}(t) - \delta\mathbf{p}) + (\mathbf{A} + \mathbf{C} + \dot{\lambda}(t)\mathbf{H}_g)\dot{\mathbf{r}}(t) \\ (\mathbf{H}_g\dot{\mathbf{r}}(t))^{\mathrm{T}}\dot{\mathbf{r}}(t) \end{bmatrix} \tag{48}$$

and

$$\mathbf{D}_2 = \begin{bmatrix} \mathbf{C}'\dot{\mathbf{r}}(t) \\ 0 \end{bmatrix}. \tag{49}$$

Notice that the third-order surface parameters e, f, g, h (of the Monge form, see Eq. (7)) only appear in the second term $\mathbf{D}_2$. From the last row of Eq. (46), we obtain an expression in the second order parameters a, b, c of the Monge form:

$$a\dot{u}^2(t) + 2c\dot{u}(t)\dot{v}(t) + b\dot{v}^2(t) - \ddot{w}(t) = 0,$$

which yields

$$\ddot{w}(0) = a\dot{u}^2(0) + 2c\dot{u}(0)\dot{v}(0) + b\dot{v}^2(0). \tag{50}$$

In addition, we can solve for $\ddot{u}(0)$ and $\ddot{v}(0)$ from the first two rows of Eq. (46). Specifically,

$$\begin{bmatrix} D_1 + D_1' + J_w\ddot{w}(0) \\ D_2 + D_2' \end{bmatrix} = -\begin{bmatrix} J_u - 2a\cos\theta & -2c\cos\theta \\ -2c\cos\theta & J_v - 2b\cos\theta \end{bmatrix} \begin{bmatrix} \ddot{u}(0) \\ \ddot{v}(0) \end{bmatrix},$$

where D_1, D_2 and D_1', D_2' denote the first two rows of $\mathbf{D}_1$ and $\mathbf{D}_2$ respectively. In particular, suppose that D_3 denotes the third row of $\mathbf{D}_1$, it follows from Eq. (48) that

$$\begin{bmatrix} D_1 & D_2 & D_3 \end{bmatrix}^{\mathrm{T}} = (2\mathbf{A} + \mathbf{C} + \dot{\lambda}(t)\mathbf{H}_g)\dot{\mathbf{r}}(t) - \mathbf{A}\delta\mathbf{p}, \tag{51}$$

and

$$\begin{bmatrix} D_1' \\ D_2' \end{bmatrix} = -2\cos\theta \begin{bmatrix} \dot{u}^2 & 2\dot{u}\dot{v} & \dot{v}^2 & 0 \\ 0 & \dot{u}^2 & 2\dot{u}\dot{v} & \dot{v}^2 \end{bmatrix} \begin{bmatrix} e \\ f \\ g \\ h \end{bmatrix}. \tag{52}$$

Consequently,

$$\begin{bmatrix} \ddot{u}(0) \\ \ddot{v}(0) \end{bmatrix} = -\frac{1}{\Delta} \begin{bmatrix} J_v - 2b\cos\theta & 2c\cos\theta \\ 2c\cos\theta & J_u - 2a\cos\theta \end{bmatrix} \times \begin{bmatrix} D_1 + D_1' + J_w\ddot{w}(0) \\ D_2 + D_2' \end{bmatrix}.$$

Hence, by combining with Eq. (50) the proposition is proven. □

Note that Eq. (40) expresses Meusnier's Theorem (see (Carmo, 1976)). Additionally, note that the second term of Eq. (38) depends linearly on the third-order surface parameters; finally, when the third-order terms of the Monge form of the mirror surface are equal to zero, $\mathbf{C}_h^j = 0$ for $j = 1, 2, 3$ and the second term of Eq. (38) is zero. This leads to a special case in surface reconstruction as we shall see in Section 5.1.

3.2.2. Relationship between $\dot{\mathbf{r}}$, $\ddot{\mathbf{r}}$ *and* $\ddot{\mathbf{q}}$.

Proposition 6. *Let* $\mathbf{r}(t)$ *be the surface curve and* $\mathbf{q}(t)$ *its camera image. Then,* $\ddot{\mathbf{r}}$ *and* $\ddot{\mathbf{q}}$ *are linearly related*:

$$\ddot{\mathbf{q}} = \mathbf{T}\left[\ddot{\mathbf{r}} - \alpha\dot{\mathbf{r}}\right], \tag{53}$$

where the 3×3 *matrix* $\mathbf{T}$ *and the scalar* α *are functions of the camera parameters,* $\mathbf{r}_0$, $\mathbf{q}_0$ *and* $\dot{\mathbf{r}}$. *Specifically,* $\mathbf{T}$ *is defined in Eq*. (30) *and* α *as follows*:

$$\alpha = \frac{2}{s\,\langle \mathbf{d}, \mathbf{v}\rangle}\,\langle \dot{\mathbf{r}}, \mathbf{v}\rangle\,. \tag{54}$$

Proof: To relate the second-order derivative of $\mathbf{r}(t)$ to that of its image plane projection $\mathbf{q}(t)$, we differentiate Eq. (36) with respect to t, obtaining

$$\ddot{\mathbf{q}} = \gamma\,\ddot{\mathbf{r}} + 2\dot{\gamma}\,\dot{\mathbf{r}} + \ddot{\gamma}\,s\,\mathbf{d} \tag{55}$$

where $\gamma, \dot{\gamma}$ are defined in Eqs. (34) and (35), and $\ddot{\gamma}$ may be computed from further differentiating Eq. (33), yielding

$$\ddot{\gamma} = -\frac{2\dot{\gamma}\,\langle \dot{\mathbf{r}}, \mathbf{v}\rangle + \gamma\,\langle \ddot{\mathbf{r}}, \mathbf{v}\rangle}{s\,\langle \mathbf{d}, \mathbf{v}\rangle} \tag{56}$$

Thus we obtain an analytical expression for $\ddot{\mathbf{q}}$ by substituting into Eq. (55), that is

$$\begin{aligned} \ddot{\mathbf{q}} &= \gamma\left(\ddot{\mathbf{r}} - \frac{\langle \ddot{\mathbf{r}}, \mathbf{v}\rangle}{\langle \mathbf{d}, \mathbf{v}\rangle}\mathbf{d}\right) + 2\dot{\gamma}\left(\dot{\mathbf{r}} - \frac{\langle \dot{\mathbf{r}}, \mathbf{v}\rangle}{\langle \mathbf{d}, \mathbf{v}\rangle}\mathbf{d}\right) \\ &= \mathbf{T}\left[\ddot{\mathbf{r}} - \frac{2}{s\,\langle \mathbf{d}, \mathbf{v}\rangle}\,\langle \dot{\mathbf{r}}, \mathbf{v}\rangle\,\dot{\mathbf{r}}\right] = \mathbf{T}\left[\ddot{\mathbf{r}} - \alpha\dot{\mathbf{r}}\right]. \end{aligned} \tag{57}$$

□

In accordance with the decomposition of $\ddot{\mathbf{r}}$ in Eq. (38), we may also divide $\ddot{\mathbf{q}}$ into two terms

$$\ddot{\mathbf{q}} = \ddot{\mathbf{q}}_1 + \ddot{\mathbf{q}}_2, \tag{58}$$

where

$$\ddot{\mathbf{q}}_1 = \mathbf{T}\left[\ddot{\mathbf{r}}_1 - \frac{2}{s\,\langle \mathbf{d}, \mathbf{v}\rangle}\,\langle \dot{\mathbf{r}}, \mathbf{v}\rangle\,\dot{\mathbf{r}}\right], \quad \ddot{\mathbf{q}}_2 = \mathbf{T}\,\ddot{\mathbf{r}}_2. \tag{59}$$

Notice that third-order surface parameters e, f, g, h only appear in the second term $\ddot{\mathbf{q}}_2$.

3.2.3. Relationship between $\dot{\mathbf{r}}$, $\ddot{\mathbf{r}}$ *and* κ^q.

Proposition 7. *The curvature* κ^q *of* $\mathbf{q}(t)$ *at* $\mathbf{q}_0$ *may be expressed as*:

$$\kappa^q = \frac{s\,\langle \mathbf{d}, \mathbf{v}\rangle^3}{l} \times \frac{\langle \ddot{\mathbf{r}}, \mathbf{v}\rangle\,[\dot{\mathbf{r}}, \mathbf{v}, \mathbf{d}] - \langle \dot{\mathbf{r}}, \mathbf{v}\rangle\,[\ddot{\mathbf{r}}, \mathbf{v}, \mathbf{d}] + \langle \mathbf{d}, \mathbf{v}\rangle\,[\ddot{\mathbf{r}}, \mathbf{v}, \dot{\mathbf{r}}]}{\left(\|\,\dot{\mathbf{r}}\,\|^2\,\langle \mathbf{d}, \mathbf{v}\rangle^2 + \langle \dot{\mathbf{r}}, \mathbf{v}\rangle^2 - 2\,\langle \dot{\mathbf{r}}, \mathbf{v}\rangle\,\langle \dot{\mathbf{r}}, \mathbf{d}\rangle\,\langle \mathbf{d}, \mathbf{v}\rangle\right)^{3/2}}. \tag{60}$$

Proof: For a planar curve $\mathbf{q}(t)$, its curvature and geodesic curvature are equivalent. Thus, from differential geometry (Cipolla and Giblin, 2000) [Eq. (2.26), p.37]

$$\kappa^q = \frac{\langle \ddot{\mathbf{q}}, \mathbf{n}^q \rangle}{\| \dot{\mathbf{q}} \|^2}. \tag{61}$$

where $\mathbf{n}^q = \mathbf{v} \times \frac{\dot{\mathbf{q}}}{\| \dot{\mathbf{q}} \|}$. By taking the scalar product with $\mathbf{n}^q$ on both sides of Eq. (55), we have

$$\left\langle \ddot{\mathbf{q}}, \mathbf{n}^q \right\rangle = \gamma \left\langle \ddot{\mathbf{r}}, \mathbf{n}^q \right\rangle + 2\dot{\gamma} \left\langle \dot{\mathbf{r}}, \mathbf{n}^q \right\rangle + \ddot{\gamma} s \left\langle \mathbf{d}, \mathbf{n}^q \right\rangle. \tag{62}$$

By using Eq. (36), we may express the three dot products in Eq. (62) as follows:

$$\left\langle \ddot{\mathbf{r}}, \mathbf{n}^q \right\rangle = \frac{1}{\| \dot{\mathbf{q}} \|} \left(\gamma \left[\ddot{\mathbf{r}},\ \mathbf{v},\ \dot{\mathbf{r}} \right] + s\dot{\gamma} \left[\ddot{\mathbf{r}},\ \mathbf{v},\ \mathbf{d} \right] \right), \tag{63}$$

$$\left\langle \dot{\mathbf{r}}, \mathbf{n}^q \right\rangle = \frac{s\dot{\gamma}}{\| \dot{\mathbf{q}} \|} \left[\dot{\mathbf{r}},\ \mathbf{d},\ \mathbf{v} \right], \tag{64}$$

$$\left\langle \mathbf{d}, \mathbf{n}^q \right\rangle = \frac{\gamma}{\| \dot{\mathbf{q}} \|} \left[\mathbf{d},\ \mathbf{v},\ \dot{\mathbf{r}} \right]. \tag{65}$$

In the equations above, $[A,\ B,\ C]$ denotes the triple scalar product of three vectors. Substituting Eqs. (63)–(65) into Eq. (61) and then simplifying the result using Eqs. (34), (35) and (56), we obtain

$$\begin{aligned} \kappa^q &= \frac{1}{\| \dot{\mathbf{q}} \|^3} (s(\ddot{\gamma}\gamma - 2\dot{\gamma}^2) \left[\mathbf{d},\ \mathbf{v},\ \dot{\mathbf{r}} \right] \\ &\quad + \gamma^2 \left[\ddot{\mathbf{r}},\ \mathbf{v},\ \dot{\mathbf{r}} \right] + s\gamma\dot{\gamma} \left[\ddot{\mathbf{r}},\ \mathbf{v},\ \mathbf{d} \right]) \\ &= \frac{l^2}{s^2 \langle \mathbf{d}, \mathbf{v} \rangle^3 \| \dot{\mathbf{q}} \|^3} (\langle \ddot{\mathbf{r}}, \mathbf{v} \rangle \left[\dot{\mathbf{r}},\ \mathbf{v}, \mathbf{d} \right] \\ &\quad - \langle \dot{\mathbf{r}}, \mathbf{v} \rangle \left[\ddot{\mathbf{r}},\ \mathbf{v},\ \mathbf{d} \right] + \langle \mathbf{d}, \mathbf{v} \rangle \left[\ddot{\mathbf{r}},\ \mathbf{v},\ \dot{\mathbf{r}} \right]), \end{aligned} \tag{66}$$

where we have used the fact that $[\mathbf{d},\ \mathbf{v},\ \dot{\mathbf{r}}] = -[\dot{\mathbf{r}},\ \mathbf{v},\ \mathbf{d}]$, and the identity

$$s(\ddot{\gamma}\gamma - 2\dot{\gamma}^2) = -\frac{l^2 \langle \ddot{\mathbf{r}}, \mathbf{v} \rangle}{s^2 \langle \mathbf{d}, \mathbf{v} \rangle^3}.$$

Furthermore, it follows from Eq. (36) that

$$\begin{aligned} \| \dot{\mathbf{q}} \|^2 &= \langle \dot{\mathbf{q}}, \dot{\mathbf{q}} \rangle = \langle \gamma\dot{\mathbf{r}} + s\dot{\gamma}\mathbf{d}, \gamma\dot{\mathbf{r}} + s\dot{\gamma}\mathbf{d} \rangle \\ &= \gamma^2 \| \dot{\mathbf{r}} \|^2 + s^2\dot{\gamma}^2 + 2s\gamma\dot{\gamma} \langle \mathbf{d}, \dot{\mathbf{r}} \rangle \\ &= \gamma^2 \| \dot{\mathbf{r}} \|^2 + \gamma^2 \frac{\langle \dot{\mathbf{r}}, \mathbf{v} \rangle^2}{\langle \mathbf{d}, \mathbf{v} \rangle^2} - 2\gamma^2 \frac{\langle \dot{\mathbf{r}}, \mathbf{v} \rangle \langle \mathbf{d}, \dot{\mathbf{r}} \rangle}{\langle \mathbf{d}, \mathbf{v} \rangle} \\ &= \frac{\gamma^2}{\langle \mathbf{d}, \mathbf{v} \rangle^2} (\| \dot{\mathbf{r}} \|^2 \langle \mathbf{d}, \mathbf{v} \rangle^2 + \langle \dot{\mathbf{r}}, \mathbf{v} \rangle^2 \\ &\quad - 2 \langle \dot{\mathbf{r}}, \mathbf{v} \rangle \langle \dot{\mathbf{r}}, \mathbf{d} \rangle \langle \mathbf{d}, \mathbf{v} \rangle). \end{aligned}$$

Therefore, we obtain

$$\begin{aligned} \| \dot{\mathbf{q}} \| = \frac{l}{s \langle \mathbf{d}, \mathbf{v} \rangle^2} &(\| \dot{\mathbf{r}} \|^2 \langle \mathbf{d}, \mathbf{v} \rangle^2 + \langle \dot{\mathbf{r}}, \mathbf{v} \rangle^2 \\ &- 2 \langle \dot{\mathbf{r}}, \mathbf{v} \rangle \langle \dot{\mathbf{r}}, \mathbf{d} \rangle \langle \mathbf{d}, \mathbf{v} \rangle)^{1/2}. \end{aligned} \tag{67}$$

By combining Eqs. (67) and (66), we find the final expression (60) for κ^q. □

Proposition 8. *κ^q depends linearly on the third-order surface parameters.*

Proof: $\dot{\mathbf{r}}$ in Eq. (9) and $\ddot{\mathbf{r}}_1$ in Eq. (38) are independent of the third-order surface parameters, and only the second term $\ddot{\mathbf{r}}_2$ in Eq. (38) of $\ddot{\mathbf{r}}$ depends linearly on $e,\ f,\ g,\ h$. Thus, the proposition follows from Eq. (60). □

4. Properties of the Reflection Mapping

In this section we present several properties attached to first order derivative of the mapping $\mathbf{r}(t)$ when more than one line passes through the same reflection point. Such properties will be used in Section 5 when we study the inverse problem and we show how to recover surface position and shape from various type of image measurements. We start by introducing in Section 4.1 the concept of geometrical configuration as a geometrical structure defined by a scene, an observer and the mirror surface. We say that the geometrical structure is *singular* if the mapping $\mathbf{r}(t)$ is not differentiable at the reflection point and *degenerate* if distinct coplanar scene lines are mapped into the same tangent direction after reflection. Then, we study in Section 4.2 and Section 4.3 the rank of the mapping when N distinct orientations of $\dot{\mathbf{r}}$ are considered (for both degenerate and non-degenerate configurations).

4.1. Geometrical Configurations

Let us assume a scene composed of N coplanar lines $\mathbf{p}_1,\ \mathbf{p}_2,\ \ldots\ \mathbf{p}_N$ through a point $\mathbf{p}_0$.[3] As discussed in section 3, each scene line $\mathbf{p}_i$ is mapped into a reflected curve $\mathbf{r}_i(t)$ on the mirror surface and an image curve $\mathbf{q}_i(t)$ observed on the image plane, with their tangent

vectors at t_0 denoted by $\dot{\mathbf{r}}_i$ and $\dot{\mathbf{q}}_i$ respectively. Let ϕ_i be the angle between $\dot{\mathbf{r}}_i$ and the $\mathbf{u}$ axis at $\mathbf{r}_0$, and let ψ_i be the angle between $\dot{\mathbf{q}}_i$ and horizontal axis in the image plane at $\mathbf{q}_0$. It then follows from Eq. (27) that the tangent direction $\tan\phi_i$ of $\mathbf{r}_i(t)$ can be computed by

$$\tan\phi_i = \frac{(J_u - 2a\cos\theta)B_{v_i} + 2cB_{u_i}\cos\theta}{(J_v - 2b\cos\theta)B_{u_i} + 2cB_{v_i}\cos\theta}. \quad (68)$$

The corresponding tangent direction $\tan\psi_i$ of $\mathbf{q}_i(t)$ in the image plane can be related to $\tan\phi_i$ by means of Proposition 4.

Definition 1. We call a *geometrical configuration* $\wp = \wp(\mathbf{c}, \mathbf{p}_0, \mathbf{p}_1, \mathbf{p}_2, \ldots \mathbf{p}_n\ \mathbf{r}_0, \mathbf{n}_r, a, b, c)$ a geometrical structure where $\mathbf{p}_0$ is a a scene point, $\mathbf{c}$ is an observer, $\mathbf{r}_0$ is the corresponding reflected point on a mirror surface S, $\mathbf{n}_r$ is the normal of S at $\mathbf{r}_0$, the quantities a, b, c are the second-order parameters of S around $\mathbf{r}_0$ in the principal reference system and $\mathbf{p}_1, \mathbf{p}_2, \ldots, \mathbf{p}_n$ are n coplanar distinct scene lines passing through $\mathbf{p}_0$.

4.1.1. Singular Configurations.

Definition 2. We call a geometrical configuration *singular* if the condition (18) for the existence of the mapping $\mathbf{r}(t)$ around the neighborhood of $\mathbf{r}_0$ is not satisfied (i.e. if the Jacobian $\Delta = 0$).

Notice that if $\Delta = 0$ the mapping $\mathbf{r}_i(t)$ is not differentiable at t_0. An example of singular geometrical configuration is shown in Fig. 4.

Proposition 9. *A geometrical configuration $\wp$ is singular if and only if the condition*

$$c^2 = \left(\frac{J_u}{2\cos\theta} - a\right)\left(\frac{J_v}{2\cos\theta} - b\right) \quad (69)$$

holds.

Proof: from Proposition 2, condition (69) holds if and only if $\Delta = 0$. □

Proposition 10. *If the surface is a convex paraboloid in the neighborhood of the reflection point, then the corresponding geometrical configuration is non-singular.*

Proof: If the surface is a convex paraboloid in the neighborhood of the reflection point, the second order parameters a, b and c satisfy:

$$\begin{cases} a < 0; \quad b < 0 \\ c^2 < ab \end{cases} \quad (70)$$

Let us assume by contradiction that the geometrical configuration is singular. Since $J_u, J_v > 0$ and the

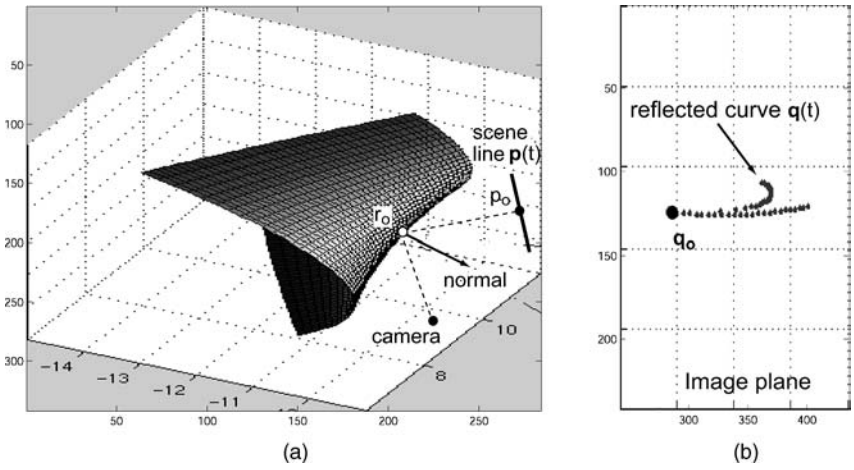

Figure 4. Example of singular geometrical configuration: (a) A line $\mathbf{p}(t)$ passing through $\mathbf{p}_0$ is reflected off a paraboloid mirror and observed by a camera. The curvature of the paraboloid at $\mathbf{r}_0$ is such that the corresponding geometrical configuration is singular. (b) The reflected image curve is shown. Notice the discontinuity of mapping $\mathbf{q}(t)$ at $\mathbf{q}_0$.

reflection angle $\theta < \pi/2$

$$c^2 < ab < \left(\frac{J_u}{2\cos\theta} - a\right)\left(\frac{J_v}{2\cos\theta} - b\right) \quad (71)$$

which contradicts Eq. (69) □

4.1.2. Degenerate Configurations.

Definition 3. We call a geometrical configuration *degenerate* if for any i, $j (i \neq j)$, we have $\phi_i = \phi_j$.

Proposition 11. *A geometrical configuration $\wp$ is degenerate if and only if the scene lines $\mathbf{p}_1, \mathbf{p}_2, \ldots \mathbf{p}_n$ define a plane passing through $\mathbf{p}_0$ and $\mathbf{r}_0$.*

Proof: We divide the proof in two steps: (1) we prove that for any i, $j (i \neq j)$, $\phi_i = \phi_j$ if and only if $\frac{B_{u_i}}{B_{v_i}} = \frac{B_{u_j}}{B_{v_j}}$; (2) we prove that $\frac{B_{u_i}}{B_{v_i}} = \frac{B_{u_j}}{B_{v_j}} = k$ if and only if $\mathbf{p}_i, \mathbf{p}_j$ define a plane passing through $\mathbf{p}_0$ and $\mathbf{r}_0$.

1. ($\leftarrow$) Suppose $B_{u_i}/B_{v_i} = B_{u_j}/B_{v_j} = k$, it follows from Eq. (68) that

$$\tan\phi_i = \tan\phi_j = \frac{(J_u - 2a\cos\theta)k + 2c\cos\theta}{(J_v - 2b\cos\theta) + 2kc\cos\theta}. \quad (72)$$

   ($\rightarrow$) From Eq. (68):

$$\frac{B_{u_i}}{B_{v_i}} = \frac{(J_u - 2a\cos\theta) + 2c\tan\phi_i\cos\theta}{(J_v - 2b\cos\theta)\tan\phi_i + 2c\cos\theta}. \quad (73)$$

   Then $B_{u_i}/B_{v_i} = B_{u_j}/B_{v_j}$ follows immediately from $\phi_i = \phi_j$.
2. It follows from Eq. (10) that if $k = \infty$ (or equivalently, $B_{v_i} = B_{v_j} = 0$), $\mathbf{p}_i$ and $\mathbf{p}_j$ belong to the principal plane which passes through $\mathbf{p}_0$ and $\mathbf{r}_0$. If $k \neq \infty$, we have

$$\begin{aligned}\frac{B_{u_i}}{B_{v_i}} = \frac{B_{u_j}}{B_{v_j}} = k \;&\Leftrightarrow \frac{(\delta\mathbf{p}_i)_w\sin\theta - (\delta\mathbf{p}_i)_u\cos\theta}{(\delta\mathbf{p}_i)_v} \\ &= \frac{(\delta\mathbf{p}_j)_w\sin\theta - (\delta\mathbf{p}_j)_u\cos\theta}{(\delta\mathbf{p}_j)_v} = \frac{-k}{\cos\theta} \;\Leftrightarrow \tan\theta \\ &= \frac{(\delta\mathbf{p}_i)_u(\delta\mathbf{p}_j)_v - (\delta\mathbf{p}_j)_u(\delta\mathbf{p}_i)_v}{(\delta\mathbf{p}_i)_w(\delta\mathbf{p}_j)_v - (\delta\mathbf{p}_j)_w(\delta\mathbf{p}_i)_v} = -\frac{(\mathbf{n_s})_w}{(\mathbf{n_s})_u}\end{aligned}$$

   where $\mathbf{n_s} = [(\mathbf{n_s})_u\ (\mathbf{n_s})_v\ (\mathbf{n_s})_w]^{\mathrm{T}}$ is the normal vector of the plane formed by the scene lines $\mathbf{p}_i$ and $\mathbf{p}_j$. $(\mathbf{n_s})_w = -\tan\theta(\mathbf{n_s})_u$ implies that $\mathbf{n_s}$ must be orthogonal to $\mathbf{p}_0 - \mathbf{r}_0$ (see Fig. 5 for details). By construction, the plane defined by $\mathbf{p}_i$ and $\mathbf{p}_j$ passes through $\mathbf{p}_0$.

□

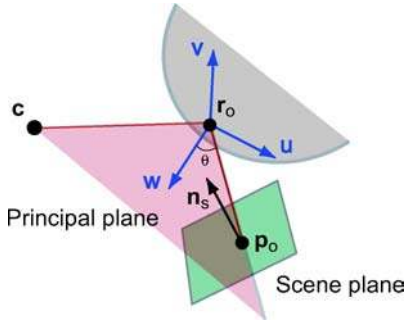

Figure 5. Sketch of the proof of Proposition 11 (step 2): Condition $(\mathbf{n_s})_w = -\tan\theta(\mathbf{n_s})_u$ is equivalent to have the scene lines contained in a plane which also contains $\mathbf{p}_0 - \mathbf{r}_0$. In principal reference system $[\mathbf{u}\ \mathbf{v}\ \mathbf{w}]$, $\mathbf{n_s} = ((\mathbf{n_s})_u, (\mathbf{n_s})_v, (\mathbf{n_s})_w)$, and the unit vector $(\mathbf{p}_0) - \mathbf{r}_0)/\parallel \mathbf{p}_0 - \mathbf{r}_0 \parallel$ has coordinate $(\sin\theta, \cos\theta, 0)$. Thus, $(\mathbf{n_s})_w = -\tan\theta(\mathbf{n_s})_u$ implies that $\langle \mathbf{p}_0 - \mathbf{r}_0, \mathbf{n_s}\rangle = 0$, that is, $\mathbf{n_s}$ is perpendicular to $\mathbf{p}_0 - \mathbf{r}_0$. Since $\mathbf{n_s}$ is the normal vector of the plane containing all scene lines (i.e., the *scene plane* indicated in the figure), $\mathbf{p}_0 - \mathbf{r}_0$ must be co-planar with these scene lines.

Notice that in the special case where $\mathbf{p}_i, \mathbf{p}_j$ belongs to the principal plane (hence, $k = \infty$), we have from Eq. (68) that

$$\tan\phi_i = \tan\phi_j = \frac{2c\cos\theta}{(J_v - 2b\cos\theta)}. \quad (74)$$

As we shall see in Section 5, if a geometrical configuration is degenerate, the reconstruction of the surface around $\mathbf{r}_0$ is not feasible. In particular, having two or more scene lines contained in the principal plane leads to inaccurate reconstruction results (see Section 5.3.3 or Fig. 17 for details).

4.2. The Rank Theorem

In this section we study the rank of the mapping when N distinct coplanar scene lines are considered (for both degenerate and non-degenerate configurations). We show that if the configuration is degenerate, the rank of the mapping is 1, whereas if the configuration is non-degenerate, the rank of the mapping is 2. We group these properties under the name of *Rank Theorem*.

By considering n ($n \geq 3$) distinct coplanar scene lines intersecting at $\mathbf{p}_0$, we may obtain a linear system

about the 3 parameters a, b, c. In fact, let

$$\begin{aligned}\alpha &= J_u - 2a\cos\theta,\\ \beta &= J_v - 2b\cos\theta,\\ \gamma &= 2c\cos\theta,\end{aligned}$$

then Eq. (68) can be represented as

$$\begin{bmatrix} B_{v_i} & -B_{u_i}\tan\phi_i & B_{u_i} - B_{v_i}\tan\phi_i \end{bmatrix}\begin{bmatrix}\alpha\\ \beta\\ \gamma\end{bmatrix} = 0,$$

denoted by

$$\mathbf{H}_n\,\mathbf{g} = 0, \tag{75}$$

where

$$\mathbf{g} = [J_u - 2a\cos\theta \quad J_v - 2b\cos\theta \;\; 2c\cos\theta]^{\mathrm{T}} \tag{76}$$

and $\mathbf{H}_n$ is a $n \times 3$ matrix defined as

$$\mathbf{H}_n = \begin{bmatrix} B_{v_1} & -B_{u_1}\tan\phi_1 & B_{u_1} - B_{v_1}\tan\phi_1\\ B_{v_2} & -B_{u_2}\tan\phi_2 & B_{u_2} - B_{v_2}\tan\phi_2\\ \vdots & \vdots & \vdots\\ B_{v_n} & -B_{u_n}\tan\phi_n & B_{u_n} - B_{v_n}\tan\phi_n \end{bmatrix}, \tag{77}$$

In the following we show some properties of $Rank(\mathbf{H}_n)$.

Proposition 12. *Given a non-singular geometrical configuration $\wp$, the $Rank(\mathbf{H}_n)$ is always different from zero.*

Proof: Suppose by contradiction that $Rank(\mathbf{H}_n) = 0$. Then, each entry of $\mathbf{H}_n$ is zero. Hence, $B_{v_i} = B_{u_i} = 0$ for $\forall i$. Thus, all scene lines lie in the principal plane formed by $\mathbf{c}, \mathbf{r}_0, \mathbf{p}_0$ and satisfy the constraint $(\delta\mathbf{p}_i)_w \cos\theta\sin\theta = (\delta\mathbf{p}_i)_u\cos^2\theta$, namely $(\delta\mathbf{p}_i)_u/(\delta\mathbf{p}_i)_w = \tan\theta$. As a result, each scene line is oriented along the incident vector $\mathbf{r}_0 - \mathbf{p}_0$, contradicting the underlying assumption of n distinct scene lines (see Definition 1). □

Proposition 13. *Given a non-singular geometrical configuration $\wp$, $Rank(\mathbf{H}_n) = 1$ for $n \geq 3$, if and only if $\wp$ is degenerate.*

Proof: We denote the row vectors of $\mathbf{H}_n$ by $\mathbf{h}_1, \mathbf{h}_2, \ldots, \mathbf{h}_n$.

1. ($\rightarrow$) If $Rank(\mathbf{H}_n) = 1$, any 2 rows $\mathbf{h}_i$ and $\mathbf{h}_j$ of $\mathbf{H}_n$ are linearly dependent, namely there exists a scalar $\alpha \neq 0$ such that $\mathbf{h}_j = \alpha\mathbf{h}_i$. Thus,

$$B_{v_j} = \alpha\, B_{v_i}, \tag{1}$$
$$B_{u_j}\tan\phi_j = \alpha\, B_{u_i}\tan\phi_i, \tag{2}$$
$$B_{u_j} - B_{v_j}\tan\phi_j = \alpha B_{u_i} - \alpha B_{v_i}\tan\phi_i, \tag{3}$$

   Substituting (1) and (2) into (3), yields the following equations:

$$\begin{aligned}(\tan\phi_i - \tan\phi_j)(B_{u_i} - B_{v_i}\tan\phi_j) = 0\\ (\tan\phi_i - \tan\phi_j)(B_{u_j} + B_{v_j}\tan\phi_i) = 0\end{aligned}$$

   which is satisfied when either $\phi_i = \phi_j$ or $\tan\phi_i = -B_{u_j}/B_{v_j}$ and $\tan\phi_j = B_{u_i}/B_{v_i}$. If $\phi_i = \phi_j$, it follows from Proposition 11 (see proof, step 2) that $\mathbf{p}_i$ and $\mathbf{p}_j$ defines a plane passing through $\mathbf{p}_0$ and $\mathbf{r}_0$. Since the scene lines are coplanar from Definition 1, it follows immediately that all the scene lines fall in this same plane passing through $\mathbf{r}_0$, which leads to a degenerate configuration according to Proposition 11. In fact, if there exists a pair of rows $\mathbf{h}_i$ and $\mathbf{h}_j$ such that $\phi_i = \phi_j$, $\wp$ is degenerate. If $\tan\phi_i = -B_{u_j}/B_{v_j}$ and $\tan\phi_j = B_{u_i}/B_{v_i}$, by considering another pair of rows $\mathbf{h}_i$ and $\mathbf{h}_k$ and following the similar derivations, we may obtain another pair of constraints, that is, $\tan\phi_i = -B_{u_k}/B_{v_k}$ and $\tan\phi_k = B_{u_i}/B_{v_i}$. Therefore, we have $\phi_j = \phi_k$, again leading to a degenerate configuration due to the reason mentioned above.
2. ($\leftarrow$) If the geometrical configuration is degenerate, then according to Definition 3 and Proposition 11 (see proof, step 1) , $\exists k$, such that $\forall i, j$, $B_{u_i}/B_{v_i} = B_{u_j}/B_{v_j} = k$. It follows that $\mathbf{h}_j = \mathbf{h}_i\; k\; B_{u_j}/B_{v_i}$. Thus, $Rank(\mathbf{H}_n) = 1$, since $Rank(\mathbf{H}_n) \neq 0$ is guaranteed by Proposition 12.

□

Proposition 14. *Given a non-singular geometrical configuration $\wp$, $Rank(\mathbf{H}_n) = 2$ for $n \geq 3$, if and only if $\wp$ is non-degenerate.*

Proof: We denote the row vectors of $\mathbf{H}_n$ by $\mathbf{h}_1, \mathbf{h}_2, \ldots, \mathbf{h}_n$.

1. ($\leftarrow$) Since the row rank and the column rank of a matrix are equal, $Rank(\mathbf{H}_n)$ can only have values of 0, 1, 2, 3. It follows immediately from Propositions 12 and 13 that $Rank(\mathbf{H}_n) = 2$ or $Rank(\mathbf{H}_n) = 3$. If $Rank(\mathbf{H}_n) = 3$, then there exists three independent row vectors among $\mathbf{h}_1, \mathbf{h}_2, \ldots, \mathbf{h}_n$. Without loss of generality, we assumes that they are $\mathbf{h}_1, \mathbf{h}_2, \mathbf{h}_3$. It then follows from Eq. (75) that

$$\begin{bmatrix} B_{v_1} & -B_{u_1}\tan\phi_1 & B_{u_1} - B_{v_1}\tan\phi_1 \\ B_{v_2} & -B_{u_2}\tan\phi_2 & B_{u_2} - B_{v_2}\tan\phi_2 \\ B_{v_3} & -B_{u_3}\tan\phi_3 & B_{u_3} - B_{v_3}\tan\phi_3 \end{bmatrix} \begin{bmatrix} \alpha \\ \beta \\ \gamma \end{bmatrix} = \mathbf{0},$$

   which leads to a zero solution, that is, $\alpha = \beta = \gamma = 0$. Consequently, according to Proposition 9, $\wp$ is singular, contradictory to the assumption.
2. ($\rightarrow$) Proof by contradiction. If $\wp$ is degenerate, $Rank(\mathbf{H}_n) = 1$ by means of Proposition 13.

□

We combine Propositions 12–14 under the name of *Rank Theorem*.

4.3. The Generalized Rank Theorem for Arbitrary Tangent Directions

The rank of matrix $\mathbf{H}_n$ is obviously related to the values of $\phi_1, \phi_2, \ldots, \phi_n$. Such values are in turn function of the measurements since they are the projection of the measurements into the surface tangent plane at $\mathbf{r}_0$. What happens if $\phi_1, \phi_2, \ldots, \phi_n$ are arbitrary (i.e. uncorrelated to the measurements)? How does the rank of $\mathbf{H}_n$ change? Does it still depend on whether the geometrical configuration is degenerate or not? In this section we address these questions. We show that if the configuration is degenerate, the rank of $\mathbf{H}_n$ is 2, whereas if the configuration is non-degenerate, the rank of $\mathbf{H}_n$ is 3. We group these properties under the name of *Generalized Rank Theorem*. We shall use these results in Section 5.

As discussed in Section 2, we refer to parameter s (namely, the distance between $\mathbf{c}$ and actual reflecting point $\mathbf{r}_0$) as the first-order surface parameter which determines the position $\mathbf{r}_0$ and normal $\mathbf{n}_r$ of the surface (by means of Eq. (1) and (5)). Thus, as the first order parameter s varies, a family of geometrical configurations $\wp(s)$ can be defined (here $\mathbf{c}$, $\mathbf{p}_0$ $\mathbf{p}_1$, $\mathbf{p}_2$, $\ldots$ $\mathbf{p}_n$, a, b, c are fixed).

Let $\Psi^{\mathbf{m}} = [\psi_1^m, \psi_2^m, \ldots, \psi_n^m]$ denote the set of tangent directions measured at $\mathbf{q}_0$ for the image curves $\mathbf{q}_1$, $\mathbf{q}_2$, $\ldots$, $\mathbf{q}_n$ (images of the n scene lines $\mathbf{p}_1, \mathbf{p}_2, \ldots \mathbf{p}_n$ intersecting at $\mathbf{p}_0$) for a geometrical configuration $\wp(s)$. Let $\hat{\Psi}$ denote an arbitrary set of tangent directions $[\hat{\psi}_1, \hat{\psi}_2, \ldots, \hat{\psi}_n]$ at $\mathbf{q}_0$.

Definition 4. We say that the set of directions $\hat{\Psi}$ is *compatible* with a geometrical configuration at s if $\wp(s)$ yields a set of measurements $\Psi^{\mathbf{m}}$ equal to $\hat{\Psi}$. Otherwise, $\hat{\Psi}$ is *not compatible* with $\wp(s)$.

Let $[\hat{\phi}_1, \hat{\phi}_2, \ldots, \hat{\phi}_n]$ denote the projection of $\hat{\Psi}$ into the surface tangent plane at $\mathbf{r}_0$. Thus, we may define a matrix $\hat{\mathbf{H}}_n$ with a similar form as $\mathbf{H}_n$ in Eq. (77), that is,

$$\hat{\mathbf{H}}_n = \begin{bmatrix} B_{v_1} & -B_{u_1}\tan\hat{\phi}_1 & B_{u_1} - B_{v_1}\tan\hat{\phi}_1 \\ B_{v_2} & -B_{u_2}\tan\hat{\phi}_2 & B_{u_2} - B_{v_2}\tan\hat{\phi}_2 \\ \vdots & \vdots & \vdots \\ B_{v_n} & -B_{u_n}\tan\hat{\phi}_n & B_{u_n} - B_{v_n}\tan\hat{\phi}_n \end{bmatrix}. \tag{78}$$

Obviously, if $\hat{\Psi} = \Psi^{\mathbf{m}}$, then $\hat{\mathbf{H}}_n = \mathbf{H}_n$. In the following, we shall study the rank property of $\hat{\mathbf{H}}_n$.

Proposition 15. *Consider a geometrical configuration $\wp(s)$, an arbitrary set of tangent directions $\hat{\Psi} = [\hat{\psi}_1, \hat{\psi}_2, \ldots, \hat{\psi}_n]$ and its corresponding projections $[\hat{\phi}_1, \hat{\phi}_2, \ldots, \hat{\phi}_n]$ on the tangent plane. Assume that tangent orientations are distinct; i.e., $\forall i, j (i \neq j)$, $\hat{\phi}_i \neq \hat{\phi}_j$; Then $Rank(\hat{\mathbf{H}}_n) \geq 2$.*

Proof: We want to prove that $Rank(\hat{\mathbf{H}}_n)$ can be neither 0 nor 1 by contradiction.

1. If $Rank(\hat{\mathbf{H}}_n) = 0$, all scene lines $\mathbf{p}_1, \ldots, \mathbf{p}_N$ are aligned, which contradicts Definition 1.
2. If $Rank(\hat{\mathbf{H}}_n) = 1$, using a proof similar to that of Proposition 13, one can show that the hypothesis of distinct tangent orientations is violated.

□

Proposition 16. *Consider a geometrical configuration $\wp(s)$, an arbitrary set of tangent directions $\hat{\Psi} = [\hat{\psi}_1, \hat{\psi}_2, \ldots, \hat{\psi}_n]$ and its corresponding projections $[\hat{\phi}_1, \hat{\phi}_2, \ldots, \hat{\phi}_n]$ on the tangent plane. Assume that tangent orientations are distinct; i.e., $\forall i, j (i \neq j)$, $\hat{\phi}_i \neq \hat{\phi}_j$. Additionally, assume that $\hat{\Psi}$ is* not *compatible with $\wp(s)$. Then, $Rank(\hat{\mathbf{H}}_n) = 2$ if and only if $\wp(s)$ is degenerate.*

Proof:

1. ($\leftarrow$) We want to show that if $\wp(s)$ is degenerate then $Rank(\hat{\mathbf{H}}_n) = 2$. It follows from Definition 3 and Proposition 11 (see proof, step 1) that $\exists k$, $B_{u_i} = kB_{v_i}$ $\forall i \neq j$. If $k \neq \infty$, we may express $\hat{\mathbf{H}}_n$ as follows:

$$\hat{\mathbf{H}}_n = \hat{\mathbf{H}}_n^1 \hat{\mathbf{H}}_n^2 = \begin{bmatrix} B_{u_1} & 0 & \dots & 0 \\ 0 & B_{u_2} & \dots & 0 \\ & \vdots & & \\ 0 & 0 & \dots & B_{u_n} \end{bmatrix} \times \begin{bmatrix} \frac{1}{k} & -\tan\hat{\phi}_1 & 1 - \frac{1}{k}\tan\hat{\phi}_1 \\ \frac{1}{k} & -\tan\hat{\phi}_2 & 1 - \frac{1}{k}\tan\hat{\phi}_2 \\ & \vdots & \\ \frac{1}{k} & -\tan\hat{\phi}_n & 1 - \frac{1}{k}\tan\hat{\phi}_n \end{bmatrix}$$

Hence, $Rank(\hat{\mathbf{H}}_n) = Rank(\hat{\mathbf{H}}_n^1 \hat{\mathbf{H}}_n^2) \leq \min(Rank(\hat{\mathbf{H}}_n^1), Rank(\hat{\mathbf{H}}_n^2))$. Since the third column of $\hat{\mathbf{H}}_n^2$ can be expressed as a linear combination of the first two, $Rank(\hat{\mathbf{H}}_n^2) \leq 2$, and thus $Rank(\hat{\mathbf{H}}_n) \leq 2$. On the other hands, we have $Rank(\hat{\mathbf{H}}_n) \geq 2$ from Proposition 15. Therefore, $Rank(\hat{\mathbf{H}}_n) = 2$. Furthermore, if $k = \infty$,

$$\hat{\mathbf{H}}_n = \hat{\mathbf{H}}_n^1 \hat{\mathbf{H}}_n^2 = \begin{bmatrix} B_{u_1} & 0 & B_{u_1}\tan\hat{\phi}_1 \\ B_{u_2} & 0 & B_{u_2}\tan\hat{\phi}_2 \\ & \vdots & \\ B_{u_n} & 0 & B_{u_n}\tan\hat{\phi}_n \end{bmatrix}$$

which leads again to $Rank(\hat{\mathbf{H}}_n) = 2$.

2. ($\rightarrow$) We want to show that if $Rank(\hat{\mathbf{H}}_n) = 2$ then $\wp(s)$ is degenerate. Assume by contradiction that $\wp(s)$ is non-degenerate. Consider the system $\hat{\mathbf{H}}_n \mathbf{g} = 0$ in Eq. (75). Since $Rank(\hat{\mathbf{H}}_n) = 2$, vector $\mathbf{g}$ is perpendicular to the plane spanned by any two rows of $\hat{\mathbf{H}}_n$. That is, $\mathbf{g} = r\,\mathbf{h}$, where r is an scalar parameter and $\mathbf{h} = [h_1 \;\; h_2 \;\; h_3]^{\mathrm{T}} = \mathbf{h}_k \times \mathbf{h}_j$, where $\mathbf{h}_k, \mathbf{h}_j$ are the kth and jth rows of $\mathbf{H}$ associated with 2 arbitrary lines $\mathbf{p}_k$ and $\mathbf{p}_j$. Since $\mathbf{g} = [J_u - 2a\cos\theta \;\; J_v - 2b\cos\theta \;\; 2c\cos\theta]^{\mathrm{T}}$, we have found a family of values for a, b, c and a corresponding family of non-degenerate geometrical configurations $\wp(s, a, b, c)$ which are parameterized by r and yield the set of tangent orientations $\hat{\Psi}$, contradicting the non-compatibility assumption.

□

Table 3. Rank property of $\hat{\mathbf{H}}_n$ for arbitrary tangent directions.

$Rank(\hat{\mathbf{H}}_n)$	$\wp(s)$ deg.	$\wp(s)$ non-deg.	Pointer
$\hat{\Psi}$ compatible with $\wp(s)$	1	2	Proposition 13
			Proposition 14
$\hat{\Psi}$ not compatible with $\wp(s)$	2	3	Proposition 16
			Proposition 17

Proposition 17. *Consider a geometrical configuration $\wp(s)$, an arbitrary set of tangent directions $\hat{\Psi} = [\hat{\psi}_1, \hat{\psi}_2, \dots, \hat{\psi}_n]$ and its corresponding projections $[\hat{\phi}_1, \hat{\phi}_2, \dots, \hat{\phi}_n]$ on the image plane. Assume that tangent orientations are distinct; i.e., $\forall i, j (i \neq j)$, $\hat{\phi}_i \neq \hat{\phi}_j$. Additionally, assume that $\hat{\Psi}$ is not compatible with $\wp(s)$. Then, $Rank(\hat{\mathbf{H}}_n) = 3$ if and only if $\wp(s)$ is non-degenerate.*

Proof:

1. ($\leftarrow$) By contradiction, assume that $Rank(\hat{\mathbf{H}}_n) \neq 3$. By Proposition 15 $Rank(\hat{\mathbf{H}}_n) \geq 2$ and since $Rank(\hat{\mathbf{H}}_n) \leq 3$, $Rank(\hat{\mathbf{H}}_n) = 2$. It then follows from Proposition 16 that $\wp(s)$ must be degenerate, contradicting to our assumption.
2. ($\rightarrow$) By contradiction, assume that $\wp$ is degenerate. It follows from Proposition 16 that $Rank(\hat{\mathbf{H}}_n) = 2$, contradicting to the assumption $Rank(\hat{\mathbf{H}}_n) = 3$.

□

We combine Propositions 15–17 under the name of *Generalized Rank Theorem*.

To sum up, we have listed the results obtained in this section in Table 3.

5. The Inverse Problem

5.1. Inverse Problem

In this section we study the inverse problem and apply the analytical formulas derived in Section 3 to reconstruct the geometry of a mirror surface by measuring its deforming effects on a scene planar grid. We start by showing in Section 5.2 that if the measurements

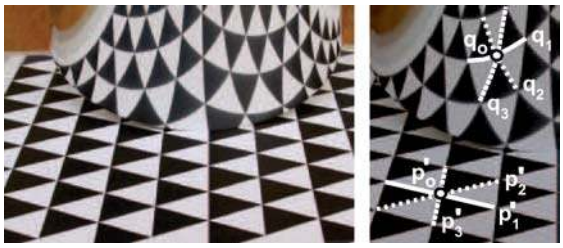

Figure 6. Data gathered from the image. In this example the measurements are the orientations of the reflected curves $\mathbf{q}_1$, $\mathbf{q}_2$ and $\mathbf{q}_3$ evaluated at the intersecting point $\mathbf{q}_0$ and the position of $\mathbf{q}_0$ in the image plane.

of orientation and position of (at least) two reflected curves are available, the parameters describing local shape of the surface can be reduced. Then, we demonstrate in Sections 5.3 and 5.4 that by exploiting different types of image measurements and by assuming that the scene is calibrated, we may recover the shape of the mirror surface to different accuracy. We take advantage of the results proven in Section 4 to study degenerate solutions and ambiguities of the reconstruction problem.

We present two reconstruction algorithms. The first algorithm (call it A1) assumes that the orientation of at least 3 lines are available at the same intersection point (see Fig. 6). The algorithm estimates surface position and orientation at the reflection point. Surface curvature and the third order surface parameters can only be recovered up to a free parameter. Surface curvature can be fully estimated only when the third order surface parameters are negligible.

The second algorithm (call it A2) assumes that orientation and scale of at least 2 lines are available at the same intersection point (see Fig. 12). Scale information measures the "velocity" along the line in the image, assuming known velocity along the line in the scene. The algorithm estimates surface position and surface orientation at the reflection point; additionally, it estimates surface curvature and the third order surface parameters in closed-form. These results are summarized in Table 4.

Finally, in Section 5.4.5 we show that the hypothesis on the structure of the scene (i.e. scene composed of a grid of intersecting lines) is not necessary. We demonstrate that scale and orientation measurements may be also extracted from the reflection of a planar scene patch of arbitrary geometry. We prove that local surface shape can be estimated if the location of at least 3 arbitrary points is available within a neighborhood of the reflected scene patch.

Table 4. Comparison of the two algorithms.

Algorithm	Measurements	Estimated surface quantities
A1	point $\mathbf{q}_0$ + orientation of 3 lines through $\mathbf{q}_0$	distance, tangent plane at $\mathbf{r}_0$
A2	point $\mathbf{q}_0$ + orientation & scale of 2 lines through $\mathbf{q}_0$	distance, tangent plane, curvature and 3rd order parameters at $\mathbf{r}_0$

For clarity, throughout this section, we indicate the quantities measured in the image plane with the superscript m and the quantities associated with different scene lines with a subscript. For example the measurement of the first-order derivative of the ith curve $\mathbf{q}_i(t)$ in the image plane is indicated by $\dot{\mathbf{q}}_i^m$.

5.2. Parameter Reduction

In this section we show that if the measurements of the orientation of (at least) two reflected curves and the position of the point of intersection are available, the parameters describing the surface position, orientation and curvature (i.e. s, a, b, c) can be reduced from 4 to 2.

As discussed in Section 2, we refer to parameter s as the distance between $\mathbf{c}$ and actual reflecting point $\mathbf{r}_0$. Denote by $\Psi^{\mathbf{m}} = [\psi_1^m, \psi_2^m, \ldots \psi_n^m]$ the set of tangent directions measured at $\mathbf{q}_0$ for the image curves $\mathbf{q}_1, \mathbf{q}_2, \ldots, \mathbf{q}_n$ (images of the n scene lines $\mathbf{p}_1, \mathbf{p}_2, \ldots \mathbf{p}_n$ intersecting at $\mathbf{p}_0$). We may construct the $n \times 3$ matrix $\mathbf{H}$ and the vector $\mathbf{g}$ in Eq. (75) from measurements ($\Psi^{\mathbf{m}}$ and $\mathbf{q}_o^m$) and known geometrical quantities from calibration. Notice that in Eq. (75) measurements and second surfaces parameters are separated. In fact, tangent measurements are contained in $\mathbf{H}$ only and second order surface parameters (a, b, c) are contained in $\mathbf{g}$ only. Both $\mathbf{H}$ and $\mathbf{g}$ are function of s.

Proposition 14 suggests that given a non-singular geometrical configuration, the vector $\mathbf{g}$ in Eq. (76) is perpendicular to the plane spanned by any two rows of $\mathbf{H}$. That is, $\mathbf{g} = r\,\mathbf{h}$, where r is an unknown scalar parameter and $\mathbf{h} = [h_1 \;\; h_2 \;\; h_3]^{\mathrm{T}} = \mathbf{h}_k \times \mathbf{h}_j$. Here $\mathbf{h}_k, \mathbf{h}_j$ are the kth and jth rows of $\mathbf{H}$ associated with 2 arbitrary lines $\mathbf{p}_k$ and $\mathbf{p}_j$. As a result, only two lines suffice to univocally constrain a, b, c as a function of

r and s, that is

$$\begin{cases} a = \dfrac{J_u}{2\cos\theta} - r\dfrac{h_1}{2\cos\theta} \\ b = \dfrac{J_v}{2\cos\theta} - r\dfrac{h_2}{2\cos\theta} \\ c = r\dfrac{h_3}{2\cos\theta} \end{cases}, \tag{79}$$

which reduces the total number of unknowns from 8 (s, a, b, c, e, f, g, h) to 6 (s, r, e, f, g, h). Note that r appears as a free parameter.

5.3. Image Measurements: Curve Orientations

In Section 5.3.1 we show that by measuring position and tangent orientations of the reflection images of (at least) three scene lines intersecting at a point $\mathbf{p}_0$, we are able to recover the geometry of a mirror surface up to first order (position and normal). In Section 5.3.2 we give an explicit reconstruction algorithm which may be summarized in 8 steps. In Section 5.3.3 we discuss the possibility of having multiple solutions (*first order parameter ambiguity*) and degenerate solutions. In Section 5.3.4 we show that the second-order surface parameters can only be recovered up to one free parameter r and we refer to it as *second order parameter ambiguity*. In Section 5.3.5 we present explicit solutions for the second-order surface parameters for two special surfaces: the sphere and the cylinder. In Section 5.3.6 we attack the general case. We show that if the curvature of (at least) one reflected curve at $\mathbf{q}_0$ is available, the second order parameter ambiguity can be resolved and r can be derived in closed form solution. This derivation requires the assumption that third-order surface parameters e, f, g, h are negligible in the neighborhood of $\mathbf{r}_0$. Additionally, we prove (see Proposition 19) that the image curvature at $\mathbf{q}_0$ depends linearly asymptotically on r and that the slope of such a function does not depend on the third order surface parameters. Proposition 19 may be used to estimate the second order parameters in close form. Finally, we apply these results in Section 5.3.7 where we give expressions to constrain the third order surface parameter e, f, g, h. We show that if the measurements of (at least) 4 reflected image curvatures at $\mathbf{q}_0$ are available, then e, f, g, h can be estimated up to r. We refer to it as *third order parameter ambiguity*.

5.3.1. Recovering the First Order Parameters—The First Order Ambiguity. By constructing the $n \times 3$ matrix $\mathbf{H}$ in Eq. (77) from measurements ($\Psi^{\mathbf{m}}$ and $\mathbf{q}_o^m$) and known geometrical quantities, we obtain $\det(\mathbf{H}^{\mathrm{T}}\mathbf{H})$ as a parametric function of s. Consider n scene lines ($n \geq 3$) and denote by s^* the actual distance between $\mathbf{c}$ and unknown reflecting point $\mathbf{r}_0$. Since $Rank(\mathbf{H}) = Rank(\mathbf{H}^{\mathrm{T}}\mathbf{H})$, Proposition 14 suggests a necessary condition for s^*. Namely, $\det(\mathbf{H}^{\mathrm{T}}\mathbf{H})$ must vanish at s^*. If $\det(\mathbf{H}^{\mathrm{T}}\mathbf{H}) = 0$ has a single root, then we find s^* univocally. However, there might exist some values of $s \neq s^*$ such that $\det(\mathbf{H}^{\mathrm{T}}\mathbf{H}) = 0$. Considering a geometrical configuration $\wp(s)$ attached to s (see Section 4.3), $\det(\mathbf{H}^{\mathrm{T}}\mathbf{H})$ may become zero in two cases according to Table 4:

1. $\wp(s)$ is *non-degenerate* and the set of measurements $\Psi^{\mathbf{m}}$ is *compatible* with $\wp(s)$ (i.e., $Rank(\mathbf{H}) = 2$). We call such s as *ghost solution*.
2. $\wp(s)$ is *degenerate* (i.e., $Rank(\mathbf{H}) \leq 2$).

Therefore, we have the following proposition:

Proposition 18. *Given a matrix* $\mathbf{H}$ *formed by the observations* $\Psi^{\mathbf{m}}$ *and parameterized by* s, $\det(\mathbf{H}^{\mathrm{T}}\mathbf{H})$ *vanishes at* s *if and only if* s *is*: (i) *the actual distance* s^*, (ii) *a ghost solution,* iii) *attached to a degenerate geometrical configuration.*

In other words, a ghost solution s is a zero of the function $\det(\mathbf{H}^{\mathrm{T}}\mathbf{H})$ and arises when a non degenerate geometrical configuration $\wp(s)$ yields reflected lines with orientations coincident with those measured in the image plane. This leads to the following ambiguity: any mirror surface whose location and shape is determined by a ghost solution would generate exactly the same measurements $\Psi^{\mathbf{m}}$ as the ones generated by the actual mirror surface (attached to actual solution s^*). We call this ambiguity *the first order ambiguity*.

5.3.2. Reconstruction Algorithm. To obtain three orientations at each examined point, we can adopt a pattern composed of a tessellation of black and white equilateral triangles. Edges of the pattern grids act as a triplet of intersecting lines and corners serve as mark points. As indicated in the example in Fig. 6, the triplet of lines $\mathbf{p}'_1$, $\mathbf{p}'_2$, $\mathbf{p}'_3$ intersecting at $\mathbf{p}_0$ are reflected to $\mathbf{q}_1$, $\mathbf{q}_2$ and $\mathbf{q}_3$, respectively. Notice that $\mathbf{p}'_1$, $\mathbf{p}'_2$, $\mathbf{p}'_3$ are the images of the scene lines $\mathbf{p}_1$, $\mathbf{p}_2$, $\mathbf{p}_3$. Given a scene

Table 5. Algorithm A1.

1. Select a checkerboard intersection point and the its corresponding reflected point (e.g. points $\mathbf{p}'_0$ and $\mathbf{q}_0$ in Fig. 6).
2. Select a triplet of lines from the checkerboard pattern (e.g. image lines $\mathbf{p}'_1$, $\mathbf{p}'_2$, $\mathbf{p}'_3$) and corresponding reflected triplet of curves (e.g. $\mathbf{q}_1$, $\mathbf{q}_2$ and $\mathbf{q}_3$).
3. Compute the position of $\mathbf{p}_0$ and directions $\delta\mathbf{p}_1$, $\delta\mathbf{p}_2$, $\delta\mathbf{p}_3$ of $\mathbf{p}_1$ $\mathbf{p}_2$, $\mathbf{p}_3$ respectively at $\mathbf{p}_0$ by interpolating B-splines through each of $\mathbf{p}'_1$, $\mathbf{p}'_2$, $\mathbf{p}'_3$ and by numerical differentiation at $\mathbf{p}'_0$.
4. Estimate the position of $\mathbf{q}_0$ and directions $\tan\phi_1^m$, $\tan\phi_2^m$, $\tan\phi_3^m$ of $\mathbf{q}_1$, $\mathbf{q}_2$ and $\mathbf{q}_3$ respectively at $\mathbf{q}_0$ from B-spline numerical differentiation.
5. Compute matrix $\mathbf{H}$ (Eq. (77)) from $\mathbf{p}_0$, $\mathbf{q}_0$, $\delta\mathbf{p}_1$, $\delta\mathbf{p}_2$, $\delta\mathbf{p}_3$, $\tan\phi_1^m$, $\tan\phi_2^m$, $\tan\phi_3^m$.
6. Recover the distance s from $\det(\mathbf{H}^T\mathbf{H})$ (up to ghost solutions).
7. Recover the reflection point $\mathbf{r}_0$ on the mirror surface and the surface normal vector at $\mathbf{r}_0$ by Eq. (1) and Eq. (5), respectively.
8. Recover curvature parameters a, b, c by Eq. (79) up to one unknown parameter.

line $\mathbf{p}_i$, we may accurately measure the orientation of its reflected image curve $\mathbf{q}_i$ at $\mathbf{q}_0$ using B-spline interpolation. In fact, by constructing a B-spline that interpolates image points along the curve, the direction of $\dot{\mathbf{q}}$ (i.e.,$\tan\phi$) can be calculated by numerically differentiating the resulting B-spline. Using these numerical estimates, our reconstruction algorithm can be summarized in Table 5.

5.3.3. Numerical Simulations and Discussion. In order to validate our theoretical results, we simulated specular reflections in MatLab. Given a set of scene lines, a known surface and the observer, the program computes the corresponding reflected curves imaged by the observer. Thus, all of the geometrical quantities needed to form the matrix $\mathbf{H}$ can be numerically obtained.

Figure 7 shows the profile of $\det(\mathbf{H}^T\mathbf{H})$ as a function of s for an instance of geometrical configuration. The function $\det(\mathbf{H}^T\mathbf{H})$ vanishes at s^* (actual solution) and s' (degenerate geometrical configuration). According to Definition 3, we can analytically predict degenerate geometrical configurations by checking whether the value of s satisfies that $\forall i \neq j$, $\frac{B_{u_i}}{B_{v_i}} = \frac{B_{u_j}}{B_{v_j}}$. For instance, as in Fig. 7, since the surface point associated with s' belongs to the plane defined by the scene lines, we know from Proposition 11 that s' gives rise to a degenerate geometrical configuration and should be rejected. Additionally, empirical analysis with Matlab shows that the more one (or more) scene line approaches the principal plane, the lower is slope of $\det(\mathbf{H}^T\mathbf{H})$ at s^*. This in turn leads to a worse accuracy in estimating s^*. See for example the point highlighted with dashed circle in Fig. 17).

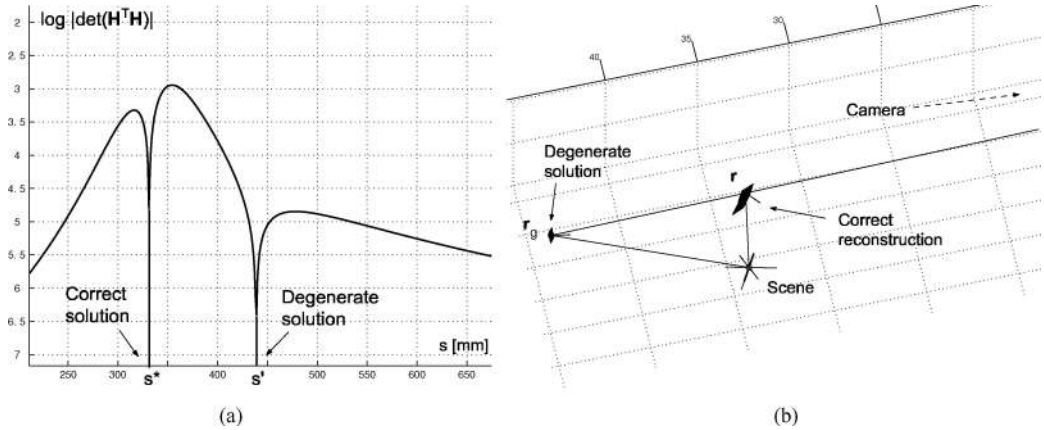

Figure 7. Multiple solutions for $\det(\mathbf{H}^T\mathbf{H})$. (a) Profile of $\det(\mathbf{H}^T\mathbf{H})$ as a function of s. The function $\det(\mathbf{H}^T\mathbf{H})$ vanishes at $s = s^*$ (actual solution) and at $s = s'$ (solution attached to a degenerate geometrical configuration). (b) The reconstructed point for $s = s^*$ is the real surface point $\mathbf{r}$; the reconstructed point for $s = s'$ is $\mathbf{r}_g$, which can be easily rejected as it belongs to the plane defined by the scene lines.

In this instance of simulation, no ghost solutions arise. In general, the existence of ghost solutions is more problematic for our reconstruction scheme because ghost solutions can not be ruled out analytically. Extensive numerical experiments with MatLab, however, show that ghost solutions are rather uncommon. Additionally, since the number of rows of $\mathbf{H}$ is equal to the number of scene lines, the greater is the number of scene lines, the lower is the probability that there exists a value of $s \neq s^*$ such that the set of measurements $\Psi^{\mathbf{m}}$ is compatible with $\wp(s)$. Finally, ghost solutions may be easily rejected if some form of prior global information on shape is available. Further work is needed in order to derive sufficient conditions to reject ghost solutions.

5.3.4. Recovering the Second Order Parameters—The Second Order Ambiguity. Once s is determined, we can recover the second-order surface parameters a, b, c as functions of one free parameter r from Eq. (79). As a consequence of Proposition 14, however, the free parameter r cannot be estimated from tangent orientations only. This leads to a fundamental ambiguity for the second order surface parameters as far as the image tangent orientations are concerned. We call this ambiguity *Second Order Ambiguity*. We can interpret the ambiguity as follows. Consider the family of geometrical configurations $\wp(r)$, where s is fixed and a, b, c are parameterized by r according to Eq. (79). Then, given an arbitrary scene line passing through $\mathbf{p}_0$, all the mirror surfaces attached to the family will produce reflected image curves with invariant tangent orientation. In Fig. 8 an example of Second Order Ambiguity is presented.

5.3.5. Recovering the Second Order Parameters—Two Special Cases. In the following we show how to resolve the Second Order Ambiguity and recover the parameter r under two special cases:

Sphere. If the mirror surface is a sphere with radius R, then the second order parameters satisfy $a = b$ and $c = 0$. By imposing $a = b$ to Eq. (79), we resolve the Second Order Ambiguity and obtain

$$r = \frac{J_u - J_v}{h_1 - h_2}, \tag{80}$$

and the radius of the sphere being

$$R = \frac{2(h_1 - h_2)\cos\theta}{J_v h_1 - J_u h_2} \tag{81}$$

Additionally, by imposing that $c = 0$, we have $r\, h_3 / \cos\theta = 0$. Since $\cos\theta \neq 0$ and $r \neq 0$ (otherwise the corresponding geometrical configuration would be degenerate), h_3 must be zero, namely:

$$-B_{v_i} B_{u_j} \tan\phi_j + B_{u_i} B_{v_j} \tan\phi_i = 0 \tag{82}$$

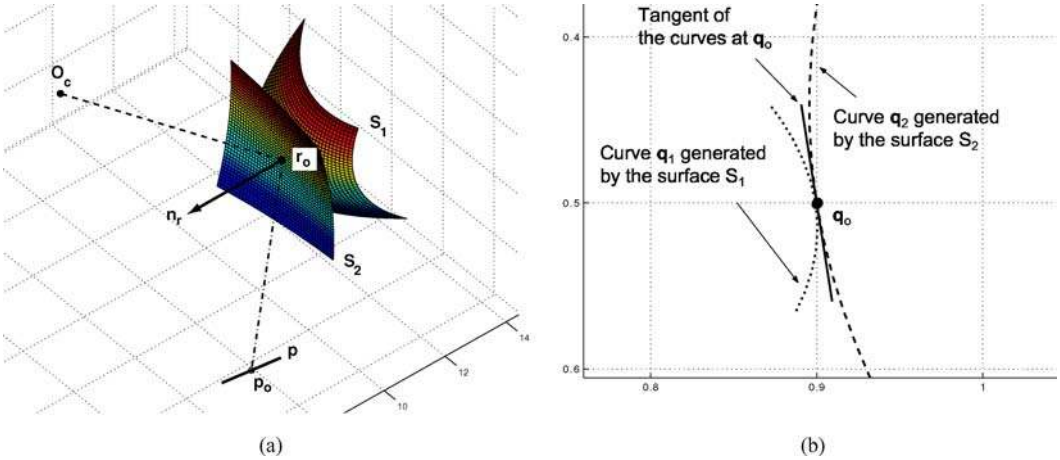

Figure 8. Example of Second Order Ambiguity. (a) Two mirror paraboloids S_1 and S_2 passing through $\mathbf{r}_0$, sharing the same orientation $\mathbf{n}_r$ at $\mathbf{r}_0$ and having the second order surface parameters defined by Eq. (79) for two arbitrary values r_1 and r_2 of r. In this example r_1 is chosen in order for S_1 to have elliptic curvature. r_2 is chosen in order for S_2 to have hyperbolic curvature. $\mathbf{p}$ is a scene line passing through $\mathbf{p}_0$. (b) $\mathbf{q}_1$ and $\mathbf{q}_2$ are the images of the reflected scene line $\mathbf{p}$ off the two mirrors S_1 and S_2, respectively. Notice that the tangents of the reflected curves at $\mathbf{q}_0$ are coincident as predicted by Eqs. (79) and (68). We call this property Second Order Ambiguity.

Notice that the quantity in Eq. (82) is the determinant of the 2×2 matrix obtained by taking the ith and jth rows and the first 2 columns of $\mathbf{H}$. Eq. (82) gives a necessary condition for the mirror surface to be locally described as a spherical paraboloid around the reflection point, that is, Eq. (82) holds for any pair of scene lines.

Cylinder. Let us consider the circular section (with radius R) of a cylinder. The surface can be locally described as a parabolic paraboloid following the relationship $c^2 = ab$ (see Cipolla and Giblin, 2000). Again from Eq. (79),

$$r = \frac{(J_v h_1 + J_u h_2) \pm \sqrt{(J_v h_1 + J_u h_2)^2 - 4\big(h_1 h_2 - h_3^2\big) J_u J_v}}{2\big(h_1 h_2 - h_3^2\big)} \tag{83}$$

It is not difficult to show that the radius of the circular section is $R = \frac{\cos^2 \xi}{2a}$, with $\xi = \arctan(b/a)$. The Second Order Ambiguity is solved up to a sign.

5.3.6. Recovering the Second Order Parameters-General Case. In order to reconstruct the second order parameters of a generic specular surface, we are required to determine the parameter r, which, from Proposition 14, can not be solved by using more scene lines. A straightforward approach to determine r is to apply our second order differential analysis and curvature measurement for additional constraints. Specifically, suppose that we can estimate the corresponding curvature κ_i^m of $\mathbf{q}_i(t)$ at $\mathbf{q}_0$, we may equate this image curvatures with its analytical expression κ_i^q derived in Eq. (60), yielding

$$\kappa_i^m = \kappa_i^q = \frac{s\,\langle \mathbf{d}, \mathbf{v}\rangle^3}{l} \times \frac{\langle \ddot{\mathbf{r}}_i, \mathbf{v}\rangle\,[\dot{\mathbf{r}}_i, \mathbf{v}, \mathbf{d}] - \langle \dot{\mathbf{r}}_i, \mathbf{v}\rangle\,[\ddot{\mathbf{r}}_i, \mathbf{v}, \mathbf{d}] + \langle \mathbf{d}, \mathbf{v}\rangle\,[\ddot{\mathbf{r}}_i, \mathbf{v}, \dot{\mathbf{r}}_i]}{\big(\|\,\dot{\mathbf{r}}_i\,\|^2\,\langle \mathbf{d}, \mathbf{v}\rangle^2 + \langle \dot{\mathbf{r}}_i, \mathbf{v}\rangle^2 - 2\,\langle \dot{\mathbf{r}}_i, \mathbf{v}\rangle\,\langle \dot{\mathbf{r}}_i, \mathbf{d}\rangle\,\langle \mathbf{d}, \mathbf{v}\rangle\big)^{3/2}} \tag{84}$$

Unfortunately, since $\ddot{\mathbf{r}}_i$ derived in Eq. (38) is dependent on not only $s, r(a, b, c)$, but also the third-order surface parameters e, f, g, h, the constraint (84) does not allow us to solve for r from curvature measurement κ_i^m. For a class of mirror surfaces whose third-order terms are negligible, however, we are able to recover the surface up to second-order accuracy using the constraint (84). As derived in Eq. (38), $\ddot{\mathbf{r}}_i$ can be divided into two parts: $\ddot{\mathbf{r}}_{i_1}$ and $\ddot{\mathbf{r}}_{i_2}$, where only the latter term depends on e, f, g, h. When $e, f, g, h \to 0$, $\ddot{\mathbf{r}}_i$ simplifies to $\ddot{\mathbf{r}}_{i_1}$, and the right-hand side of Eq. (84) becomes a function of s, r only. With s determined, we can estimate the free parameter r from the constraint (84) formed from the image curvature measurement of a single scene line. However, usage of 3 or more lines (combined with their corresponding curvature measurements) allows more robust estimation to reduce error from noise. For instance, we may estimate the parameter r by minimizing a mean curvature error function defined as follows:

$$E_\kappa(r) = \|\kappa^{\mathbf{m}} - \kappa^{\mathbf{q}}(\mathbf{r})\| \tag{85}$$

where $\kappa^{\mathbf{m}} = [\kappa_{\mathbf{1}}^{\mathbf{m}} \kappa_{\mathbf{2}}^{\mathbf{m}} \ldots \kappa_{\mathbf{n}}^{\mathbf{m}}]^{\mathbf{T}}$ and $\kappa^{\mathbf{q}} = [\kappa_{\mathbf{1}}^{\mathbf{q}} \kappa_{\mathbf{2}}^{\mathbf{q}} \ldots \kappa_{\mathbf{n}}^{\mathbf{q}}]^{\mathbf{T}}$. See Fig. 9.

We conclude this section by showing that for large values of r, there exists a linear relationship between image curvature and r. This property may used to estimate r in close form solution (rather that by least square minimization of Eq. (85)).

Proposition 19. *The image curvature κ for a scene line is asymptotically linearly dependent on the free parameter r.*

Proof: We first express $\dot{\mathbf{r}}$ in terms of the parameter r. Rewriting Eq. (79), we get

$$\begin{cases} r h_1 = J_u - 2a\cos\theta, \\ r h_2 = J_v - 2b\cos\theta, \\ r h_3 = 2c\cos\theta \end{cases} \tag{86}$$

Using Eq. (86), we can express Δ in Eq. (18) as

$$\Delta = r^2\big(h_1 h_2 - h_3^2\big). \tag{87}$$

It then follows from Eq. (9) that

$$\dot{\mathbf{r}} = -\frac{1}{r\big(h_1 h_2 - h_3^2\big)} \times \begin{bmatrix} h_2 & h_3 & 0 \\ h_3 & h_1 & 0 \\ 0 & 0 & r\big(h_1 h_2 - h_3^2\big) \end{bmatrix} \begin{bmatrix} B_u \\ B_v \\ 0 \end{bmatrix}. \tag{88}$$

As a result, we may express

$$\dot{\mathbf{r}} = \frac{1}{r}[q_1 \;\; q_2 \;\; 0], \tag{89}$$

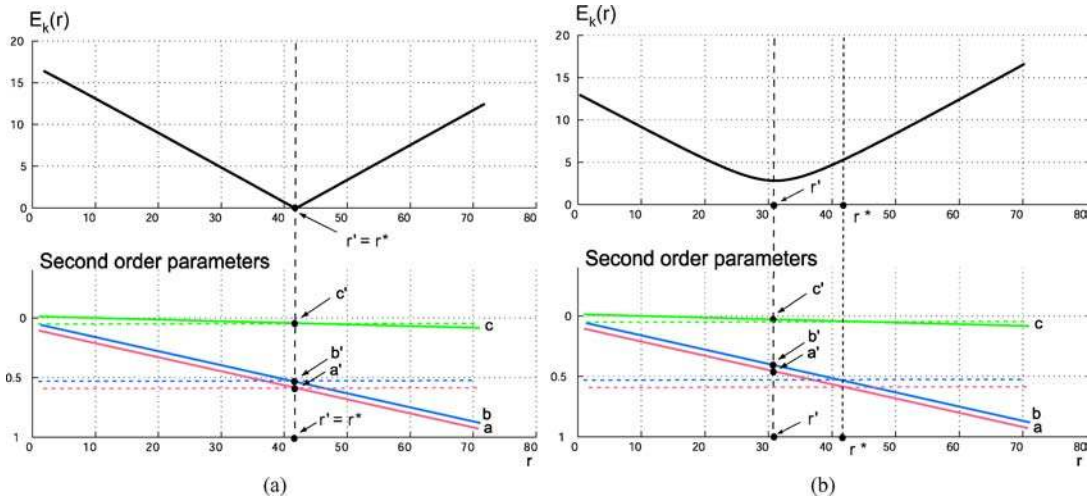

Figure 9. Example of reconstruction of r. (a) *Upper*: Mean curvature error function $E_\kappa(r)$ when the third order parameters are negligible. The estimated r is the value that minimizes $E_\kappa(r)$. Since the third order parameters are negligible, estimated (r') and actual (r^*) values of r are coincident. *Lower*: The 3 solid lines are the second order parameters of the surface as function of r (namely, $a(r)$, $b(r)$, $c(r)$). The dashed lines indicate the actual value of a, b, c. Solid and dashed lines intersect at $r' = r^*$. Thus, the estimated second order surface parameters (a', b', c') are calculated with no error. (b) *Upper*: Mean curvature error function $E_\kappa(r)$ when the third order parameters are not negligible. The estimated r is the value that minimizes $E_\kappa(r)$. Since the third order parameters are not negligible, r' and r^* are no necessarily coincident. *Lower*: The estimated second order surface parameters (a', b', c') are calculated at $r = r' \neq r^*$ and approximate the actual ones with non-zero error.

where q_1, q_2 are independent of r. Furthermore, we may express $\dot{\lambda}(0)$ in terms of r using Eq. (9), that is,

$$\dot{\lambda}(0) = \frac{J_w(h_2 B_u + h_3 B_v)}{r\big(h_1 h_2 - h_3^2\big)} - B_w = \frac{1}{r}\lambda_1 - B_w, \quad (90)$$

with λ_1 independent of r. We then express $\ddot{\mathbf{r}}$ in Eq. (39) and Eq. (41) in terms of r using Eqs. (86) and (89). That is,

$$\begin{aligned}\ddot{w}(0) &= \frac{1}{2r^2\cos\theta}\begin{bmatrix} q_1 & q_2 & 0\end{bmatrix} \\ &\quad\times\begin{bmatrix} J_u - rh_1 & rh_3 & 0 \\ rh_3 & J_v - rh_2 & 0 \\ 0 & 0 & 0\end{bmatrix}\begin{bmatrix} q_1 \\ q_2 \\ 0\end{bmatrix} \\ &= \frac{1}{2r^2\cos\theta}\big[\big(J_u q_1^2 + J_v q_2^2\big) \\ &\quad - r\big(h_1 q_1^2 - 2h_3 q_1 q_2 + h_2 q_2^2\big)\big] \\ &= \frac{1}{r^2}l_0 + \frac{1}{r}l_1 \end{aligned} \quad (91)$$

with l_0, l_1 as terms independent of r, and

$$\begin{bmatrix}\ddot{u}(0) \\ \ddot{v}(0)\end{bmatrix} = -\frac{1}{r\big(h_1 h_2 - h_3^2\big)}\begin{bmatrix} h_2 & h_3 \\ h_3 & h_1\end{bmatrix} \times \begin{bmatrix} D_1 + D_1' + J_w\ddot{w}(0) \\ D_2 + D_2'\end{bmatrix}. \quad (92)$$

Let's examine the dependence of D_1, D_2, D_1', D_2' on the parameter r. It follows from Eq. (47) that

$$\begin{aligned}&[D_1 \;\; D_2 \;\; D_3]^{\mathrm{T}} = -\mathbf{A}\delta\mathbf{p} + 2\mathbf{A}\,\dot{\mathbf{r}} + \dot{\mathbf{r}}^{\mathrm{T}}\tilde{\mathbf{C}}\,\dot{\mathbf{r}} + 2\dot{\lambda}(0)\mathbf{H}_g\dot{\mathbf{r}}), \\ &[D_1' \;\; D_2' \;\; D_3']^{\mathrm{T}} = \lambda\dot{\mathbf{r}}^{\mathrm{T}}\tilde{\mathbf{C}}'\,\dot{\mathbf{r}}\end{aligned} \quad (93)$$

where the tensors[4] $\tilde{\mathbf{C}}$ and $\tilde{\mathbf{C}}'$ are independent of r, derived from Eq. (47) as

$$\begin{aligned}\tilde{\mathbf{C}} &= \big[\mathbf{C}_r^1 + \mathbf{C}_i^1 \;\; \mathbf{C}_r^2 + \mathbf{C}_i^2 \;\; \mathbf{C}_r^3 + \mathbf{C}_i^3\big], \\ \tilde{\mathbf{C}}' &= \big[\mathbf{C}_h^1 \;\; \mathbf{C}_h^2 \;\; \mathbf{C}_h^3\big].\end{aligned}$$

Let $\mathbf{v}_i$ denote vectors independent of the parameter r. We may rewrite each term in Eq. (93) as

$$-\mathbf{A}\delta\mathbf{p} = \mathbf{v}_0, \quad 2\mathbf{A}\,\dot{\mathbf{r}} = \frac{1}{r}\mathbf{v}_1, \quad \dot{\mathbf{r}}^{\mathrm{T}}\tilde{\mathbf{C}}\,\dot{\mathbf{r}} = \frac{1}{r^2}\mathbf{v}_2,$$

$$\dot{\mathbf{r}}^{\mathrm{T}}\tilde{\mathbf{C}}'\,\dot{\mathbf{r}} = \frac{1}{r^2}\mathbf{v}_3,$$

$$\dot{\lambda}(0)\mathbf{H}_g\dot{\mathbf{r}} = -\frac{\lambda_1/r - B_w}{2r\cos\theta}\begin{bmatrix} J_u - rh_1 & rh_3 & 0 \\ rh_3 & J_v - rh_2 & 0 \\ 0 & 0 & 0\end{bmatrix}$$

$$\times \begin{bmatrix} q_1 \\ q_2 \\ 0 \end{bmatrix}$$

$$= \frac{1}{r^2}\mathbf{v}_4 + \frac{1}{r}\mathbf{v}_5 + \mathbf{v}_6.$$

Therefore, D_1, D_2, D'_1, D'_2 are linear combinations of $\{\frac{1}{r^2}, \frac{1}{r}, r^0\}$. It then follows from Eqs. (92) and (91) that $\ddot{\mathbf{r}}$ depends linearly on $\{\frac{1}{r^3}, \frac{1}{r^2}, \frac{1}{r}\}$. Consequently, it is obvious from Eq. (60) that the image curvature κ for a scene line depends linearly on $\{\frac{1}{r}, r^0, r^1\}$, or equivalently, κ depends asymptotically linearly on r. □

As a result, we may express the image curvature as

$$\kappa = \kappa_0 \frac{1}{r} + \kappa_1 + \kappa_2 r, \tag{94}$$

where expression for κ_0, κ_1 and κ_2 have been derived in the proof of Proposition 19. Third order surface parameters affect coefficients κ_0 and κ_1 only, which is confirmed by numerical simulation (see Fig. 10).

We can apply Eq. (94) to obtain an approximated closed form solution for r when the third order parameters are negligible and $r \gg 0$. If the image curvature measurements of $N (N \geq 1)$ lines are available:

$$r \simeq \frac{1}{N} \sum_{i}^{N} \frac{(\kappa)_i^m - (\kappa_1)_i}{(\kappa_2)_i} \tag{95}$$

where quantities attached to the ith curve are indicated with the subscript i. As a result, the second order surface parameters a, b, c can be estimated in closed form solution.

5.3.7. Recovering the Third Order Parameters. As discussed in Section 3.2.3, the image curvatures depend linearly on the third order surface parameters (see Proposition 8). Thus, curvature measurements can be further employed to constraint the third order surface parameters. In fact, suppose that $N \geq 4$ scene lines are considered and that the corresponding measurements of curvature are available in the image plane. We can derive from Eq. (60) the following system (in matrix form):

$$\kappa^{\mathbf{m}} = \mathbf{k} + \mathbf{K}\,[\mathbf{e}\ \ \mathbf{f}\ \ \mathbf{g}\ \ \mathbf{h}]^{\mathbf{T}} \tag{96}$$

where $\kappa^{\mathbf{m}} = [\kappa_{\mathbf{1}}^{\mathbf{m}} \kappa_{\mathbf{2}}^{\mathbf{m}} \ldots \kappa_{\mathbf{n}}^{\mathbf{m}}]^{\mathbf{T}}$ is the vector of measured curvatures, and the vector $\mathbf{k}$ and $N \times 4$ matrix $\mathbf{K}$ are function of r and may be derived from Eq. (60). Numerical analysis shows that $\mathbf{K}$ is in general non-singular. Thus, the third order surface parameters can be expressed as functions of the free parameter r.

One may wonder whether by adding (at least) a fifth additional curvature measurement, the free parameter r may be found. By adding (at least) a fifth additional curvature measurement, exploiting the asymptotic linearity of κ and the fact that κ_1 does not depend on r,

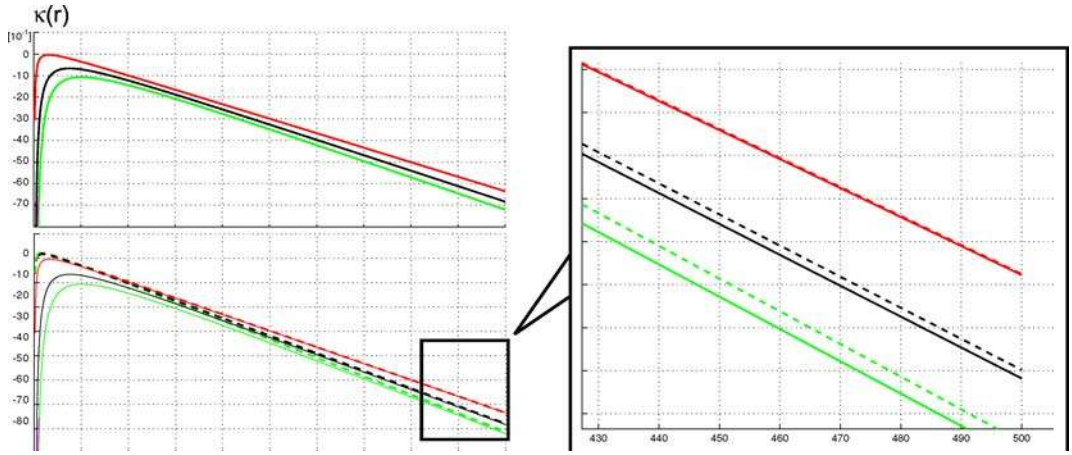

Figure 10. Numerical validation of Proposition 19. *Upper left panel*: Curvatures of 3 reflected image curves (depicted with different color codes) are plotted as functions of the parameter r when the third order parameters are not negligible. As stated by Proposition 19, the image curvature κ is asymptotically linearly dependent on the free parameter r. In the *lower left panel* the plots shown in the upper left panel are compared with those obtained when the third order surface parameters are negligible (dashed bold lines). Notice that the profiles (both asymptotically linear) have the same slope, as predicted by our theoretical analysis (see zoom-in box in the *right panel*).

we have

$$\kappa^{\mathbf{m}} \simeq \mathbf{k}' + \mathbf{K}' \, [\mathbf{e} \;\; \mathbf{f} \;\; \mathbf{g} \;\; \mathbf{h} \;\; \mathbf{r}]^{\mathbf{T}} \tag{97}$$

where vector $\mathbf{k}'$ and $N \times 5$ matrix $\mathbf{K}'$ can be derived from Eqs. (96) and (94); $N \geq 5$; $r \gg 0$. Numerical analysis shows that matrix $\mathbf{K}'$ is singular. Theoretical proof of this statement is postponed to future work. We speculate that the 5th (and additional) measurement would not carry independent information. As a result, likewise the second order surface parameters, the third order parameters would only be recovered up to the unknown r. We call this conjecture the *Third Order Ambiguity*. According to this conjecture, any mirror paraboloid passing through a point $\mathbf{r}_0$, sharing the same orientation $\mathbf{n}_r$ at $\mathbf{r}_0$ and having their second and third order surface parameters belonging to the family defined in Eqs. (79) and (96) respectively, would yield reflected image curves with invariant orientation and curvature at $\mathbf{q}_0$.

5.4. *Image Measurement: Orientations + Local Scale*

In this section we show that by measuring local position, orientation and local scale in the neighborhood of a reflected point $\mathbf{q}_0$, the local surface geometry can be recovered up to third-order accuracy. Local scale information indicates to which degree points along a reflected curve are deformed (stretched or compressed) by the specular surface. Orientation and local scale information may be captured by measuring the full first order derivative of the reflected curves $\mathbf{q}_1(t)$, $\mathbf{q}_2(t) \ldots$ $\mathbf{q}_n(t)$ at the point of intersection $\mathbf{q}_0$.

In Section 5.4.1 we show that by measuring the first order derivatives of at least two reflected curves at $\mathbf{q}_0$, it is possible to estimate surface position ($\mathbf{r}_0$) and surface orientation at $\mathbf{r}_0$. Additionally, the second order surface parameters (a, b, c) can be estimated in closed-form solution up to a sign. In Section 5.4.2 we show that by measuring the second order derivatives of at least two reflected curve at $\mathbf{q}_0$, the third surface parameters (e, f, g, h) can be estimated in closed-form solution. In Section 5.4.3 we show how to measure first and second derivatives of the reflected curves. Given these measurements, we present a reconstruction algorithm which may be summarized in 8 steps. In Section 5.4.4 we discuss to which extent the truncation error due to finite approximation of the measurements affects the reconstruction accuracy. Finally in Section 5.4.5 we show that the hypothesis on the structure of the scene (i.e. scene composed of a grid of intersecting lines) is, in fact, not necessary. Scale and orientation measurements can be also extracted from the reflection of a planar scene patch of arbitrary geometry. We show that local surface shape can be estimated if the location of at least 3 arbitrary points is available within a neighborhood of the reflected scene patch.

5.4.1. Recovering the First and Second Order Parameters. In Section 5.2 we showed that if we are able to measure the tangent directions ($\tan\phi_k$ and $\tan\phi_j$) for (at least) two image curves $\mathbf{q}_k(t)$ and $\mathbf{q}_j(t)$ at $\mathbf{q}_0$, the unknown parameters are reduced from s, a, b, c to r, s. We start our analysis from this result. By defining

$$\mathbf{V} = \frac{1}{h_1 h_2 - h_3^2} \begin{bmatrix} h_2 & h_3 \\ h_3 & h_1 \end{bmatrix}, \qquad \mathbf{B} = \begin{bmatrix} B_u \\ B_v \end{bmatrix}.$$

we may re-express $\dot{\mathbf{r}}$ in Eq. (88), as:

$$\dot{\mathbf{r}} = -\frac{1}{r} \begin{bmatrix} \mathbf{V}\,\mathbf{B} \\ 0 \end{bmatrix}. \tag{98}$$

Accordingly, it follows from Eq. (36) that the first-order derivative $\dot{\mathbf{q}}$ of the observed reflection curve in the image plane may be expressed in terms of the two unknowns r and s:

$$\dot{\mathbf{q}} = -\frac{1}{r} \mathbf{T} \begin{bmatrix} \mathbf{V}\,\mathbf{B} \\ 0 \end{bmatrix}, \tag{99}$$

where only the unknown s (not r) appears in $\mathbf{T}$, $\mathbf{V}$ and $\mathbf{B}$. Then we compute the L_2 norm of $\dot{\mathbf{q}}$ from Eq. (99) as:

$$\| \dot{\mathbf{q}} \|^2 = \langle \dot{\mathbf{q}}, \dot{\mathbf{q}} \rangle = \frac{1}{r^2} \begin{bmatrix} \mathbf{B}^{\mathrm{T}} \mathbf{V}^{\mathrm{T}} & 0 \end{bmatrix} \mathbf{T}^{\mathrm{T}} \mathbf{T} \begin{bmatrix} \mathbf{V}\mathbf{B} \\ 0 \end{bmatrix}. \tag{100}$$

Assume that we are able to estimate the first-order derivatives of $\mathbf{q}_k(t)$ and $\mathbf{q}_j(t)$ at $\mathbf{q}_0$ (see Section 5.4.3 for details). We denote them by $\dot{\mathbf{q}}_k^m$ and $\dot{\mathbf{q}}_j^m$ respectively. By taking the ratio $\|\dot{\mathbf{q}}_k^m\|^2 / \|\dot{\mathbf{q}}_j^m\|^2$, we have

$$\frac{\left\| \dot{\mathbf{q}}_k^m \right\|^2}{\left\| \dot{\mathbf{q}}_j^m \right\|^2} = \frac{[\,\mathbf{B}_k{}^{\mathrm{T}} \mathbf{V}^{\mathrm{T}} \; 0\,] \mathbf{T}^{\mathrm{T}} \mathbf{T} \begin{bmatrix} \mathbf{V}\mathbf{B}_k \\ 0 \end{bmatrix}}{[\,\mathbf{B}_j{}^{\mathrm{T}} \mathbf{V}^{\mathrm{T}} \quad 0\,] \mathbf{T}^{\mathrm{T}} \mathbf{T} \begin{bmatrix} \mathbf{V}\mathbf{B}_j \\ 0 \end{bmatrix}}, \tag{101}$$

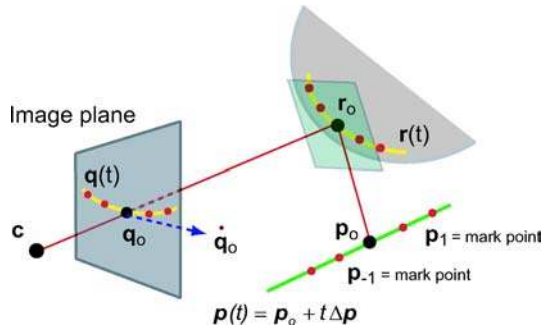

Figure 11. Mark points along the scene line $\mathbf{p}(t)$. To estimate the first-order and the second-order derivative of $\mathbf{q}(t)$ at $\mathbf{q}_0$, we may make use of the mark points $\mathbf{p}_0 = \mathbf{p}(t_0)$, $\mathbf{p}_{-1} = \mathbf{p}(t_{-1})$, $\mathbf{p}_1 = \mathbf{p}(t_1)$.

where the matrix $\mathbf{V}$ is expressed in terms of our tangent direction measurements $\tan\phi_k$ and $\tan\phi_j$. Notice that the matrix $\mathbf{T}$ defined in Eq. (30) does not depend on a particular line. Equation (101) imposes a constraint for us to solve for s. Equation (101) may have multiple solutions which we call *ghost solutions* as discussed in Section 5.3.1. Notice that the values of s for which the corresponding geometrical configuration is degenerate make the matrix V undefined. For those values of s Eq. (101) cannot be computed.

Once s is computed, we can derive the closed-form solution for r up to a sign from Eq. (100):

$$r^2 = \frac{[\,\mathbf{B}_k{}^{\mathrm{T}}\mathbf{V}^{\mathrm{T}}\;0\,]\mathbf{T}^{\mathrm{T}}\mathbf{T}\begin{bmatrix}\mathbf{V}\mathbf{B}_k\\0\end{bmatrix}}{\left\|\,\dot{\mathbf{q}}_k^m\,\right\|^2}. \tag{102}$$

5.4.2. Recovering the Third Order Parameters. To recover the third-order surface parameters, we assume that we are able to estimate the second-order derivatives for the two reflected curves in the image plane, denoted by $\ddot{\mathbf{q}}_k^m (= [\ddot{u}_k^m \;\; \ddot{v}_k^m \;\; \ddot{w}_k^m])$ and $\ddot{\mathbf{q}}_j^m (= [\ddot{u}_j^m \;\; \ddot{v}_j^m \;\; \ddot{w}_j^m])$ (see Section 5.4.3 for details). In accordance with the decomposition of $\ddot{\mathbf{q}}$, we define

$$(\ddot{\mathbf{q}}_2)_k^m = \ddot{\mathbf{q}}_k^m - (\ddot{\mathbf{q}}_1)_k, \quad (\ddot{\mathbf{q}}_2)_j^m = \ddot{\mathbf{q}}_j^m - (\ddot{\mathbf{q}}_1)_j, \tag{103}$$

where $(\ddot{\mathbf{q}}_1)_k$ and $(\ddot{\mathbf{q}}_1)_j$ are known from Eq. (39), once we have recovered s, a, b, c. Let $\mathbf{T}_{22}$ denote the upper left 2×2 sub-matrix of $\mathbf{T}$, and let $\hat{\ddot{\mathbf{q}}}_2$ denote a vector consisting of the first two components of $\ddot{\mathbf{q}}_2$. It follows from Eq. (59) that

$$\hat{\ddot{\mathbf{q}}}_2 = \mathbf{T}_{22}\begin{bmatrix}\ddot{u}_2\\ \ddot{v}_2\end{bmatrix}. \tag{104}$$

Similar to the first-order analysis, we may re-express Eq. (41) as

$$\begin{bmatrix}\ddot{u}_2\\ \ddot{v}_2\end{bmatrix} = \frac{2\cos\theta}{r\left(h_1h_2 - h_3^2\right)}\begin{bmatrix}h_2 & h_3\\ h_3 & h_1\end{bmatrix} \times \begin{bmatrix}\dot{u}^2 & 2\dot{u}\dot{v} & \dot{v}^2 & 0\\ 0 & \dot{u}^2 & 2\dot{u}\dot{v} & \dot{v}^2\end{bmatrix}\begin{bmatrix}e\\f\\g\\h\end{bmatrix}. \tag{105}$$

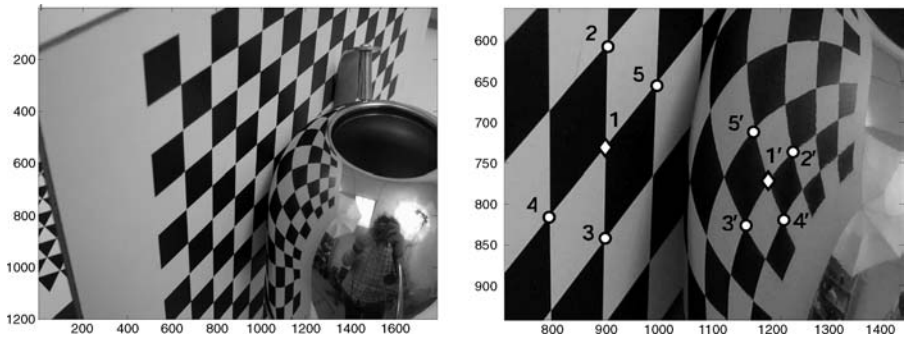

Figure 12. Data gathered from the image. In this example the measurements are the orientations and scale along two lines passing through $1'$ and may be estimated from the position of the points $2'$, $3'$, $4'$, $5'$.

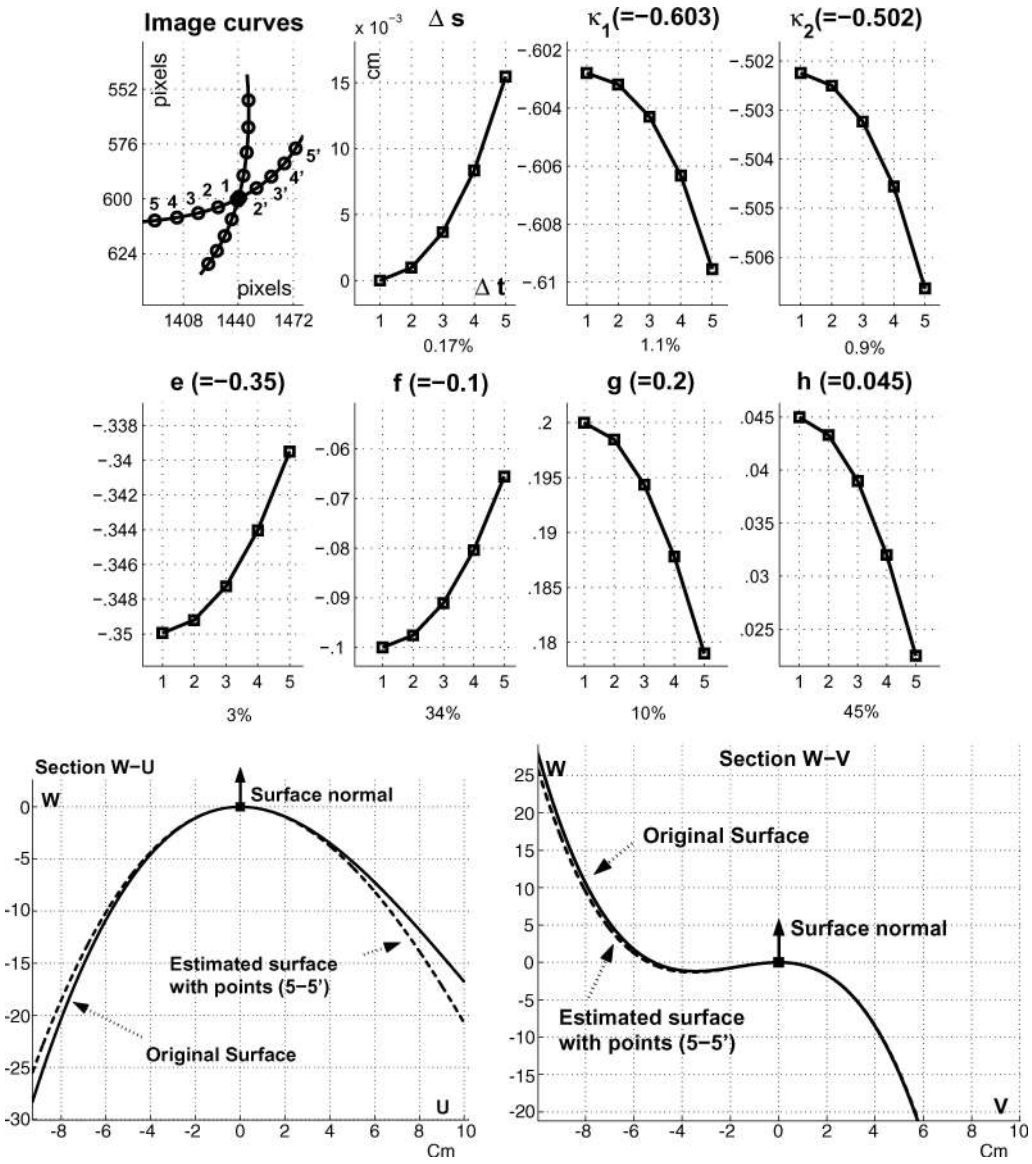

Figure 13. Reconstruction error. See Section 5.4.4 for details.

Let $(\hat{\ddot{\mathbf{q}}}_2)_k^m$ and $(\hat{\ddot{\mathbf{q}}}_2)_j^m$ denote vectors consisting of the first two components of $(\ddot{\mathbf{q}}_2)_k^m$ and $(\ddot{\mathbf{q}}_2)_j^m$. Using Eqs. (104) and (105), we obtain a constraint system for e, f, g, h by equating the estimates $(\hat{\ddot{\mathbf{q}}}_2)_k^m$ and $(\hat{\ddot{\mathbf{q}}}_2)_j^m$ with their real values, that is

$$\begin{bmatrix} (\hat{\ddot{\mathbf{q}}}_2)_k^m \\ (\hat{\ddot{\mathbf{q}}}_2)_j^m \end{bmatrix} = \frac{2\cos\theta}{r\left(h_1 h_2 - h_3^2\right)} \mathbf{M}_1 \; \mathbf{M}_2 \; \mathbf{M}_3 \begin{bmatrix} e \\ f \\ g \\ h \end{bmatrix}, \quad (106)$$

where $\mathbf{M}_1, \mathbf{M}_2, \mathbf{M}_3$ are defined as follows:

$$\mathbf{M}_1 = \begin{bmatrix} h_2 & h_3 & 0 & 0 \\ h_3 & h_1 & 0 & 0 \\ 0 & 0 & h_2 & h_3 \\ 0 & 0 & h_3 & h_1 \end{bmatrix}, \; \mathbf{M}_2 = \begin{bmatrix} \mathbf{T}_{22} & \mathbf{0} \\ \mathbf{0} & \mathbf{T}_{22} \end{bmatrix},$$

$$\mathbf{M}_3 = \begin{bmatrix} \dot{u}_k^2 & 2\dot{u}_k\dot{v}_k & \dot{v}_k^2 & 0 \\ 0 & \dot{u}_k^2 & 2\dot{u}_k\dot{v}_k & \dot{v}_k^2 \\ \dot{u}_j^2 & 2\dot{u}_j\dot{v}_j & \dot{v}_j^2 & 0 \\ 0 & \dot{u}_j^2 & 2\dot{u}_j\dot{v}_j & \dot{v}_j^2 \end{bmatrix}. \quad (107)$$

Equation (106) leads to the following closed-form solution for the third-order surface parameters, that is,

$$\begin{bmatrix} e \\ f \\ g \\ h \end{bmatrix} = \frac{r\left(h_1 h_2 - h_3^2\right)}{2\cos\theta}(\mathbf{M}_1 \ \mathbf{M}_2 \ \mathbf{M}_3)^{-1} \begin{bmatrix} (\hat{\ddot{\mathbf{q}}}_2)_k^m \\ (\hat{\ddot{\mathbf{q}}}_2)_j^m \end{bmatrix}, \tag{108}$$

where $(\hat{\ddot{\mathbf{q}}}_2)_k^m$, $(\hat{\ddot{\mathbf{q}}}_2)_j^m$ denote the first two components of $(\ddot{\mathbf{q}}_2)_k^m$, $(\ddot{\mathbf{q}}_2)_j^m$, which are defined in Eq. (103).

The existence of $(\mathbf{M}_1 \ \mathbf{M}_2 \ \mathbf{M}_3)^{-1}$ is based on the following proposition:

Proposition 20. *The matrix* $\mathbf{M}_1 \ \mathbf{M}_2 \ \mathbf{M}_3$ *is invertible.*

Proof: $\det(\mathbf{M}_1) \neq 0$ follows directly from $\Delta \neq 0$. Let $\mathbf{d} = (\mathbf{d}_x, \mathbf{d}_y, \mathbf{d}_z)$ in the reference system $[\mathbf{x} \ \mathbf{y} \ \mathbf{z}]$ centered at $\mathbf{c}$, with $\mathbf{v} = (0, 0, -1)$. We can express $\mathbf{T}$ in Eq. (30) as

$$\mathbf{T} = \frac{l}{s\mathbf{d}_z} \begin{bmatrix} 1 & 0 & -\mathbf{d}_x/\mathbf{d}_z \\ 0 & 1 & -\mathbf{d}_y/\mathbf{d}_z \\ 0 & 0 & 0 \end{bmatrix}, \tag{109}$$

which is singular, but obviously $\mathbf{T}_{22}$ is not. Hence $\det(\mathbf{M}_2) \neq 0$. Therefore, we only need to prove that $\mathbf{M}_3$ is invertible.

We first show that $\mathbf{M}_3$ is invertible when one of $\{\dot{u}_k, \dot{v}_k, \dot{u}_j, \dot{v}_j\}$ is zero. For example if $\dot{u}_k = 0$, then $\det(\mathbf{M}_3) = (\dot{v}_k \dot{u}_j)^4 \neq 0$. Otherwise, either $\dot{v}_k = 0$ or $\dot{u}_j = 0$ will contradict to our observation of two curves with different orientations. Next we shall consider the case where none of $\dot{u}_k, \dot{v}_k, \dot{u}_j, \dot{v}_j$ is zero. The proof is performed by contradiction. Under the assumption of observing two differently-oriented image curves, we should have

$$\dot{v}_k/\dot{u}_k \neq \dot{v}_j/\dot{u}_j, \quad \dot{v}_k/\dot{u}_k \neq -\dot{v}_j/\dot{u}_j. \tag{110}$$

Suppose that $\mathbf{M}_3$ is singular. Thus, its 4 row vectors U_1, U_2, U_3, U_4 are linearly dependent. Without loss of generality, we may assume that $U_4 = k_1 U_1 + k_2 U_2 + k_3 U_3$ (at least one k_i is nonzero), which can be expanded as

$$k_1 \dot{u}_k^2 + k_3 \dot{u}_j^2 = 0 \tag{111}$$

$$2k_1 \dot{u}_k \dot{v}_k + k_2 \dot{u}_k^2 + 2k_3 \dot{u}_j \dot{v}_j = \dot{u}_j^2 \tag{112}$$

$$k_1 \dot{v}_k^2 + 2k_2 \dot{u}_k \dot{v}_k + k_3 \dot{v}_j^2 = 2\dot{u}_j \dot{v}_j \tag{113}$$

$$k_2 \dot{v}_k^2 = \dot{v}_j^2 \tag{114}$$

By eliminating $\dot{u}_j^2, \dot{u}_j \dot{v}_j$ in Eq. (112) through substitutions from Eqs. (111), (113) and (114), we have

$$(k_1 + k_2 k_3)(k_3 \dot{v}_k + \dot{u}_k)^2 = 0. \tag{115}$$

Similarly, by eliminating $\dot{u}_k \dot{v}_k, \dot{v}_k^2$ in Eq. (113), we obtain

$$(k_1 + k_2 k_3)(k_1 \dot{v}_j - k_2 \dot{u}_j)^2 = 0. \tag{116}$$

If $k_1 + k_2 k_3 = 0$, then it follows from Eqs. (111) and (114) that $k_3[\dot{v}_j^2/\dot{v}_k^2 - \dot{u}_j^2/\dot{u}_k^2] = 0$. To satisfy Eq. (110), we must have $k_3 = 0$, which leads to $k_1 = 0$ and then $\dot{v}_k/\dot{u}_k = \dot{v}_j/\dot{u}_j$, contradictory to our assumption (110). Consequently, the two constraints (115) and (116) becomes

$$k_3 \dot{v}_k + \dot{u}_k = 0, \quad k_1 \dot{v}_j - k_2 \dot{u}_j = 0. \tag{117}$$

Equations (117), (111) and (114) present an over-constrained system for k_1, k_2, k_3. It follows that to satisfy all of them, we must have $\dot{v}_k/\dot{u}_k = \dot{v}_j/\dot{u}_j$, which is again contradictory to our assumption (110). Therefore, U_1, U_2, U_3, U_4 must be linearly independent, and $\mathbf{M}_3$ is invertible. □

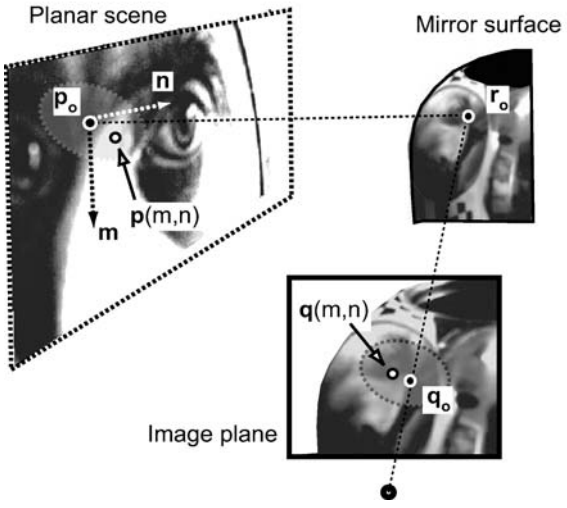

Figure 14. Example of generalized mapping. A set of points in the neighborhood of $\mathbf{p}_o$ (within a planar scene) are reflected off the mirror surface and observed in the image plane. By measuring the position of such reflected points in the image plane it is possible to estimate the local shape of the surface around $\mathbf{r}_o$.

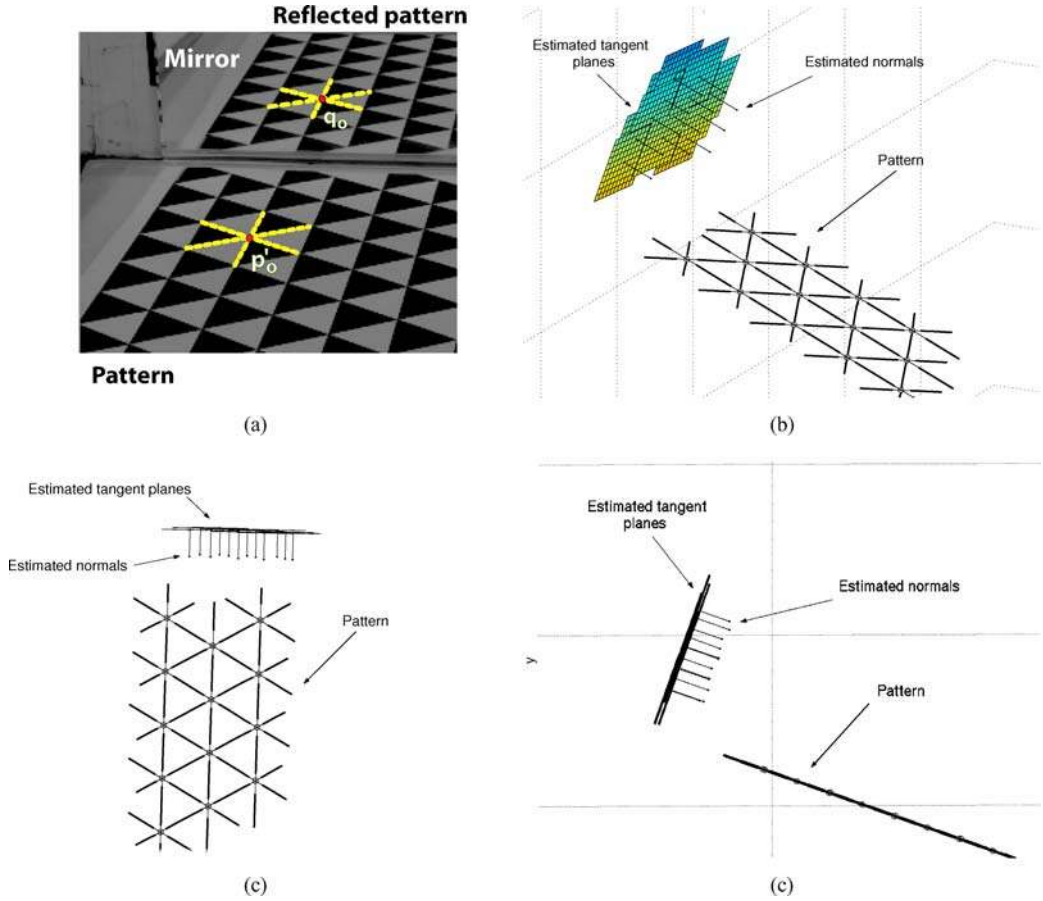

Figure 15. Reconstruction of a planar mirror. (a) A planar mirror placed orthogonal with respect to the ground plane. A triplet of pattern lines and the corresponding reflected triplet are highlighted with dashed lines. We reconstructed 12 surface points and normals on the mirror plane with algorithm A1 (see Table 5). The resulting mean position error (computed as average distance from the reconstructed points to the ground truth plane) was -0.48 mm with a standard deviation of 1.15 mm. The mean normal error (computed as the angle between ground truth plane normal and estimated normal) was 1.5×10^{-4} rad with a standard deviation of 6.5×10^{-4}rad. The reconstructed region was located at about 50 cm from the camera. (b) 3/4 view of the reconstruction; for each reconstructed point, tangent planes are plotted. (c) Top view. (d) Side view.

5.4.3. Reconstruction Procedure. To obtain two orientations at each examined point, we adopt a checkerboard pattern of 2 cm $\times$ 2 cm grid size. The edges of the pattern grids act as a pair of intersecting lines and corners serve as mark points (which provide scale information). See Fig. 11. In Sections 5.4.1 and 5.4.2, we have assumed that for a reflected curve $\mathbf{q}(t)$ observed on the image plane, we are able to measure its orientation $\tan\phi$, the first-order derivative $\dot{\mathbf{q}}^m$ and the second-order derivative $\ddot{\mathbf{q}}^m$ at $\mathbf{q}_0$. Next we shall describe how to compute these quantities numerically by finite difference approximation and/or B-spline interpolation.

To estimate $\dot{\mathbf{q}}$ (both direction and magnitude) and higher-order derivative $\ddot{\mathbf{q}}$, we may make use of mark points $\mathbf{p}_0 = \mathbf{p}(t_0)$, $\mathbf{p}_{-1} = \mathbf{p}(t_{-1})$, $\mathbf{p}_1 = \mathbf{p}(t_1)$, ... distributed along $\mathbf{p}(t)$ and use central finite difference approximation (see Fig. 11). Suppose that the mark points $\mathbf{p}(t_i)(i = \ldots, -1, 0, 1, \ldots)$ are mapped to the corresponding image points $\mathbf{q}(t_i)$. Define the step size $\Delta t = t_i - t_{i-1}$. We may approximate $\dot{\mathbf{q}}$ and $\ddot{\mathbf{q}}$ at $\mathbf{q}_0$ by using 2 points and 3 points respectively, that is

$$\dot{\mathbf{q}} \approx (\mathbf{q}(t_1) - \mathbf{q}(t_{-1}))/(2\Delta t) \tag{118}$$

$$\ddot{\mathbf{q}} \approx (\mathbf{q}(t_1) - 2\mathbf{q}(t_0) + \mathbf{q}(t_{-1}))/(\Delta t)^2. \tag{119}$$

See also Fig. 12. Notice that we may accurately measure the orientation of $\mathbf{q}(t)$ at $\mathbf{q}_0$ using B-spline interpolation. In fact, by constructing a B-spline that

Table 6. Algorithm A2.

1. Select a checkerboard intersection point and its reflected point (e.g. points 1 and $1'$ in Fig. 12).
2. Select four neighboring points from both checkerboard pattern (e.g. 2, 3, 4, 5) and corresponding reflected pattern (e.g. $2'$, $3'$, $4'$, $5'$).
3. From 1, 2, 3, 4, 5 compute $\mathbf{p}_0$ and the direction of two scene lines $\delta\mathbf{p}_1$ and $\delta\mathbf{p}_2$.
4. From $1'$, $2'$, $3'$, $4'$, $5'$ estimate $\mathbf{q}^m$, $\dot{\mathbf{q}}_1^m$, $\dot{\mathbf{q}}_2^m$ and $\ddot{\mathbf{q}}_1^m$, $\ddot{\mathbf{q}}_2^m$ using equations (118) and (119).
5. Recover the distance s by Eq. (101) from $\dot{\mathbf{q}}_1^m$, $\dot{\mathbf{q}}_2^m$.
6. Recover the parameter r (up to a sign) by Eq. (102) from $\dot{\mathbf{q}}_1^m$, $\dot{\mathbf{q}}_2^m$.
7. Recover curvature parameters (a,b,c) by Eq. (79).
8. Recover the third-order surface parameters (e, f, g, h) by Eq. (108) from $\ddot{\mathbf{q}}_1^m$, $\ddot{\mathbf{q}}_2^m$.

interpolates image points along the curve, the orientation of $\dot{\mathbf{q}}$ (i.e., $\tan\phi$) can be calculated by numerical differentiation of the resulting B-spline.

Using these numerical estimates, our local surface reconstruction algorithm at the intersection points of the reflected pattern can be summarized in Table 6.

5.4.4. Reconstruction Error. The reconstruction error of our algorithm comes mainly from the truncation error of the finite difference approximation (118). The truncation error decays when Δt decreases. To analyze how this numerical approximation affects the recovery of the distance, the curvature and the third-order parameters of the mirror surface, we simulated a synthetic mirror surface and implemented Eqs. (101), (102) and (108) in Matlab. Given the center of the camera $\mathbf{c}$ and 2 scene lines intersecting at $\mathbf{p}_0$, we observe two reflected image curves depicted in Fig. 13 (first panel). The synthetic mirror surface is positioned such that the distance s between the reflecting point $\mathbf{r}_0$ and $\mathbf{c}$ is 9 cm. The surface principal curvatures at $\mathbf{r}_0$ are $\kappa_1 = -0.603$ and $\kappa_2 = -0.502$, and the third-order surface parameters are $e = -0.35$, $f = -0.1$, $g = 0.2$, $h = -0.045$. By numerically measuring the first- and second-order derivatives at $\mathbf{q}_0$ (i.e. point 1) using pairs of mark points located at increasing distance Δt from $\mathbf{q}$ (i.e. mark point pair $(2, 2'), \ldots (5, 5')$), we recover the local surface at $\mathbf{r}_0$ as described in Sections 5.4.1 and 5.4.2. The remaining top and middle panels of Fig. 13 show each surface parameter that is computed as a function of the mark gap Δt, with the maximum percentage error reported at the bottom. Notice that the error of recovered distance s increases as a quadratic function of Δt, the curvature error is one order of magnitude bigger than the distance error, and the third-order parameter error is one order of magnitude bigger than the curvature error. In the bottom panel the reconstructed surface (estimated by using mark points $(5, 5')$) is qualitatively compared to the original one in both $\mathbf{w} - \mathbf{v}$ and $\mathbf{w} - \mathbf{u}$ sections of the **uvw** reference system. Numerical approximation (118) and (119) gives rise to reasonably good reconstruction results as long as the mark points are close enough to each other (i.e., Δt small enough).

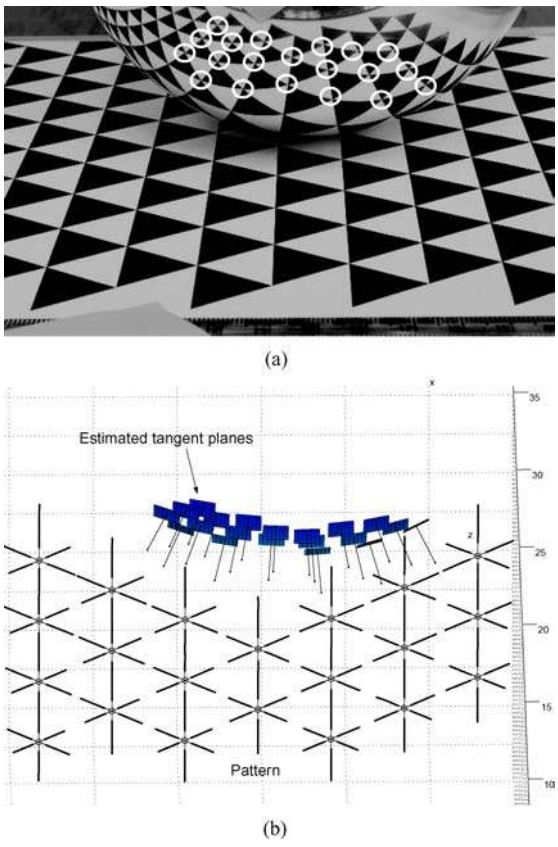

Figure 16. Reconstruction of the sphere. (a) A spherical mirror placed on the ground plane. We reconstructed 20 surface points and normals on the mirror sphere with algorithm A1 (see Table 5). The reconstructed points are highlighted with white circles. For each surface point we estimated the radius by means of Eq. (81). The ground truth radius was $r = 64.98\ \text{mm} \pm 0.013$. The mean reconstructed radius was 68.3 mm and the standard deviation was 7.0 mm. The reconstructed region was located at a distance about 30 cm to the camera. (b) Top view of the reconstruction.

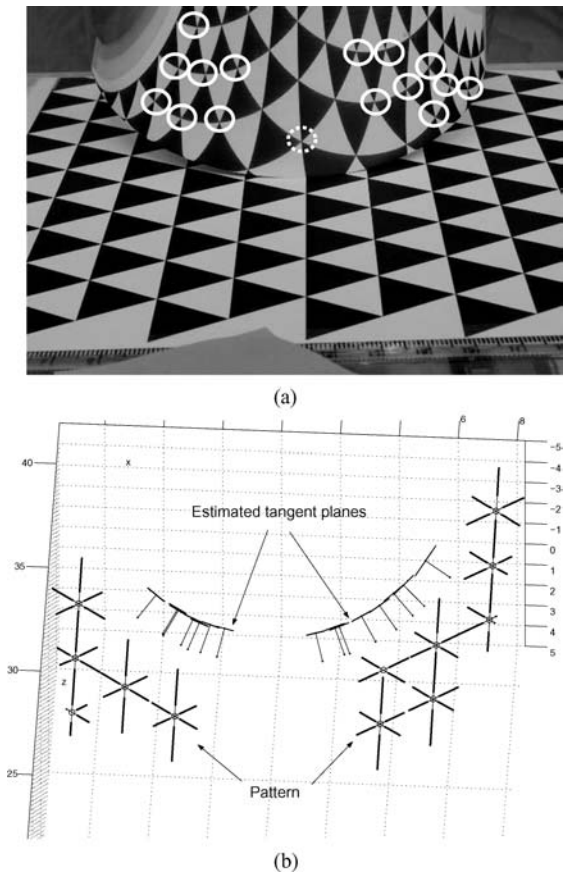

Figure 17. Reconstruction of the cylinder. (a) A cylinder placed with the main axis almost orthogonal to the ground plane. We reconstructed the surface (at the points highlighted with white circles) with algorithm A1. The dashed circle indicate an instance of point for which the reconstruction is highly inaccurate due to proximity to degenerate configuration (see Section 5.3.3 for details). (b) Top view of the reconstruction.

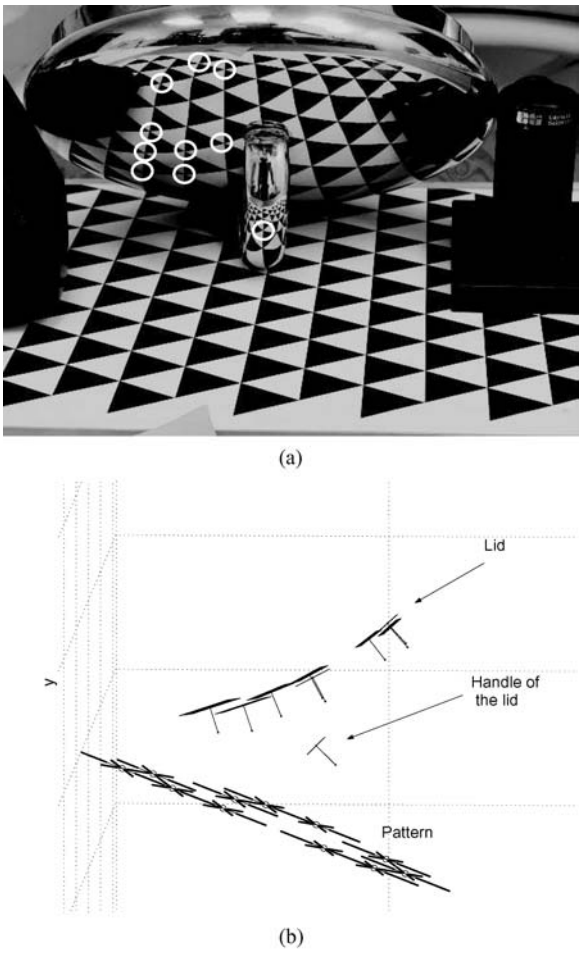

Figure 18. Reconstruction of the sauce pan's lid. (a) A sauce pan's lid placed with the handle touching the ground plane. We reconstructed the surface (at the points highlighted with white circles) with algorithm A1. Notice that one point belongs to the handle of the lid. (b) Side view of the reconstruction. Notice how the reconstructed point on the handle sticks out from the body of the lid.

5.4.5. Generalized Mapping. In this section we show that the hypothesis on the structure of the scene (i.e. scene composed of a grid of intersecting lines) is, in fact, not necessary. Information equivalent to scale and orientation measurements can be also extracted from the reflection of a planar scene patch of arbitrary geometry, provided that the reflections of distinctive points may be identified.

Let $\mathbf{p}_o$ be a scene point belonging to a planar scene patch. Let $\mathbf{r}_o$ be the corresponding reflection on the mirror and $\mathbf{q}_o$ be its observation. See Fig. 14. Set a reference system whose origin is located at $\mathbf{p}_o$ and whose orthogonal axis $\mathbf{m}$ and $\mathbf{n}$ belong to the scene patch and are arbitrarily orientated. Let m and n be the coordinates in the $[\mathbf{m}\ \ \mathbf{n}]$ reference system of a generic point $\mathbf{p}(m, n)$ belonging to the scene patch in a neighborhood of $\mathbf{p}_o$. Thus, we can define a mapping $\mathbf{Q}$: $(m, n) \in \Re^2 \rightarrow \mathbf{q}(m, n) \in \Re^2$ which maps a scene point of coordinates (m, n) into the corresponding reflected point $\mathbf{q}(m, n)$ in the image plane. In the following we show that if it is possible to identify $N \geq 6$ points $\mathbf{p}_1, \mathbf{p}_2, \ldots \mathbf{p}_N$ (as well as their corresponding image reflections $\mathbf{q}_1, \mathbf{q}_2, \ldots \mathbf{q}_N$) in a neighborhood of $\mathbf{p}_o$ then the mapping $\mathbf{Q}$ can be estimated up to second order and local shape around $\mathbf{r}_o$ can be recovered up to third order.

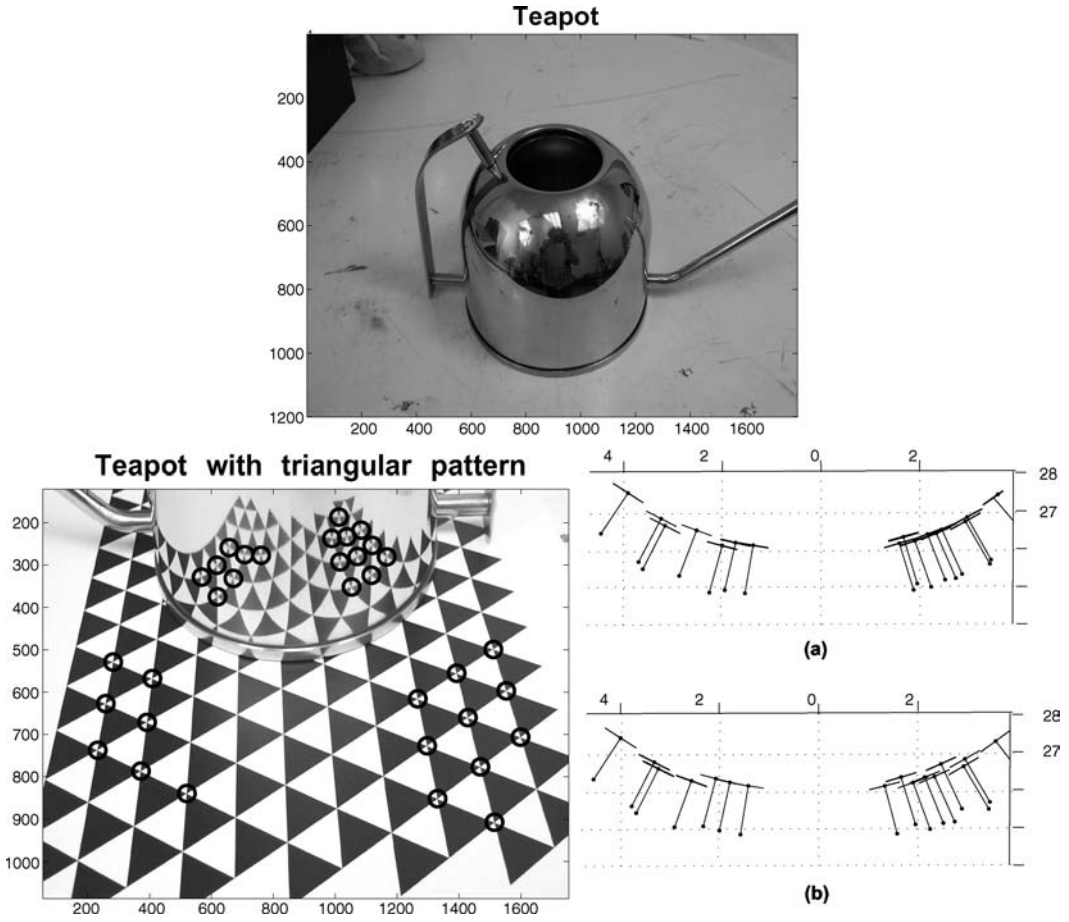

Figure 19. Comparison of the two proposed reconstruction methods. Top panel: a specular teapot. *Bottom left panel*: the two algorithms are tested at each point marked by circles. *Bottom right panel:* Reconstructed points and normal obtained by using 3 lines without scaling information obtained by mark points (a) and 2 lines with scaling information obtained by mark points (b). Notice that the performances of the two reconstructed points and normals are comparable. By means of algorithm A2 we recovered the principal curvatures of the cylinder. The diameter ground truth was 131.58 mm ±0.013. The estimated average principal curvatures were $\kappa_1 = -0.153 \pm 0.005$ and $\kappa_2 = 0.003 \pm 0.007$, which corresponds to an average estimated cylinder diameter of 130.72 mm ± 8.5 .

In fact, a point $\mathbf{q}(m, n)$ can be developed in Taylor expansion around $\mathbf{q}_o$ as follows:

$$\mathbf{q}(m,n) \approx \mathbf{q}_o + \dot{\mathbf{q}}_m m + \dot{\mathbf{q}}_n n + \frac{1}{2!}\ddot{\mathbf{q}}_{mm} m^2 + \frac{1}{2!}\ddot{\mathbf{q}}_{nn} n^2 + \ddot{\mathbf{q}}_{mn} mn, \quad (120)$$

where the vectors $\dot{\mathbf{q}}_m$ and $\dot{\mathbf{q}}_n$ are the components of the Jacobian (call it $\mathbf{J}_Q$) of the mapping; the vectors $\ddot{\mathbf{q}}_{mm}$, $\ddot{\mathbf{q}}_{nn}$ and $\ddot{\mathbf{q}}_{mn}$ are the components of the Hessian (call it $\mathbf{H}_Q$) of the mapping. It can be shown that $\mathbf{J}_Q$ and $\mathbf{H}_Q$ can be estimated from Eq. (120) if the measurement of $N \geq 6$ points in a neighborhood of $\mathbf{p}_o$ (i.e. $\mathbf{p}_1, \mathbf{p}_2, \ldots \mathbf{p}_N$) and their corresponding measurements ($\mathbf{q}_o, \mathbf{q}_1, \mathbf{q}_2, \ldots \mathbf{q}_N$) are available. From $\mathbf{J}_Q$, local shape of the mirror surface around $\mathbf{r}_o$ can be estimated up to second order (by means of Eqs. (101), (102), (79)). From $\mathbf{H}_Q$, third order surface parameters can be estimated (by means of Eq. (108)). $\mathbf{J}_Q$ and $\mathbf{H}_Q$ capture information equivalent to scale and orientation measurements around $\mathbf{q}_o$. Notice that the accuracy in estimating $\mathbf{J}_Q$ and $\mathbf{H}_Q$ depends on both the size of neighborhood around $\mathbf{p}_o$ and the curvature of the mirror surface around $\mathbf{r}_o$. Finally, notice that $\mathbf{J}_Q$ can be estimated from just three non-collinear points measured in the image plane. From $\mathbf{J}_Q$, local surface shape (up to second order) around $\mathbf{r}_o$ can be estimated.

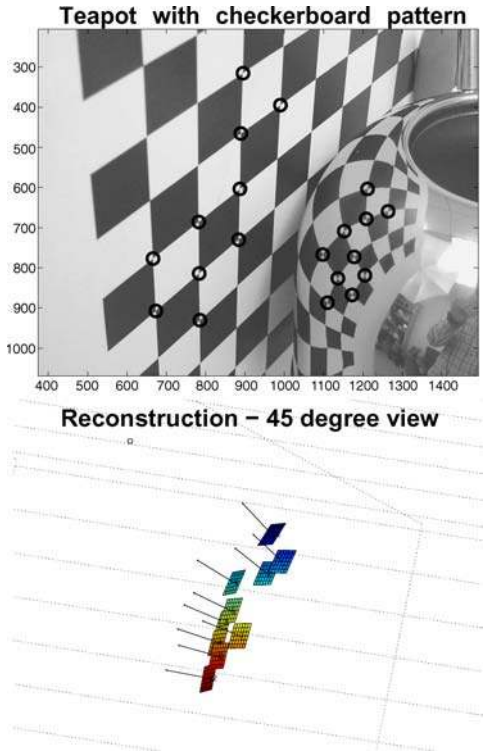

Figure 20. Teapot Experiment. Top panel: top part of a teapot. We reconstructed the surface at the points highlighted with black circles. *Bottom panel:* 45^o view of the reconstruction.

6. Experiments

We validated our theoretical results by recovering the local surface parameters of some real mirror objects. A Kodak DC290 digital camera with 1792×1200 pixel resolution was used to take the picture of a mirror surface reflecting a chosen ruled pattern. The mirror surface and camera were set $0.3 - 0.5$ meters apart. The pattern was placed such that both pattern and its specular reflection were visible from the camera (see Figs. 12 or 6). In order to test the reconstruction algorithms presented in Table 5 and Table 6 respectively, we experimented with two types of patterns: one is the triangular pattern introduced in Section 5.3.2, the other is a checkerboard pattern as in Section 5.4.3. The camera and pattern were calibrated by taking advantage of the visible portion of the pattern and by using the Bouguet calibration toolbox (Bouguet).

6.1. Results with Measurement of Orientations

We validated the algorithm A1 in Table 5 with four mirror surfaces: a plane (Fig. 15), a sphere (Fig. 16), a cylinder (Fig. 17) and a sauce pan's lid (Fig. 18). We reconstructed $10 - 20$ surface points and normals for the each of these mirror shapes. Correspondences between scene points and reflected points were established by hand. The curvature was recovered for the mirror sphere only. We tested the accuracy of the algorithm in estimating position and orientation of the mirror plane. We calculated the corresponding ground truth plane by attaching a calibrated pattern to the mirror plane and by recovering the position of 50 points on the pattern. The ground truth plane was then obtained as the least-square plane fitting such set of points. The least square error was 0.62 mm. Additionally, we tested the accuracy of the algorithm in estimating the curvature of the mirror sphere. The ground truth diameter of the sphere was measured with a caliper with accuracy 0.013 mm. Table 7 shows the statistics of the reconstruction error attached to these two experiments (see rows 1–3).

Table 7. Statistics of the reconstruction error for plane, sphere and cylinder.

Alg.	Surface	Fig.	Quantity	GT	Mean Error	Standard Dev.	N
A1	Plane	14	Point position	-	-0.48 mm	1.15 mm	12
A1	Plane	14	Normal orient.	-	1.5×10^{-4} rad	6.5×10^{-4} rad	12
A1	Sphere	15	Radius	64.9 mm	3.3 mm	7.0 mm	20
A2	Cylinder	18	Diameter	131.5 mm	0.86 mm	8.5 mm	17

The first column shows which algorithm was used. The second one shows which surface was tested. The third one shows the figure illustrating the corresponding quantitative reconstruction results. The 4th one shows the geometrical quantity whose reconstruction accuracy was evaluated. The 5th, 6th and 7th ones show the corresponding ground truth value, the mean error and its standard deviation, respectively. The last one shows the number of points reconstructed.

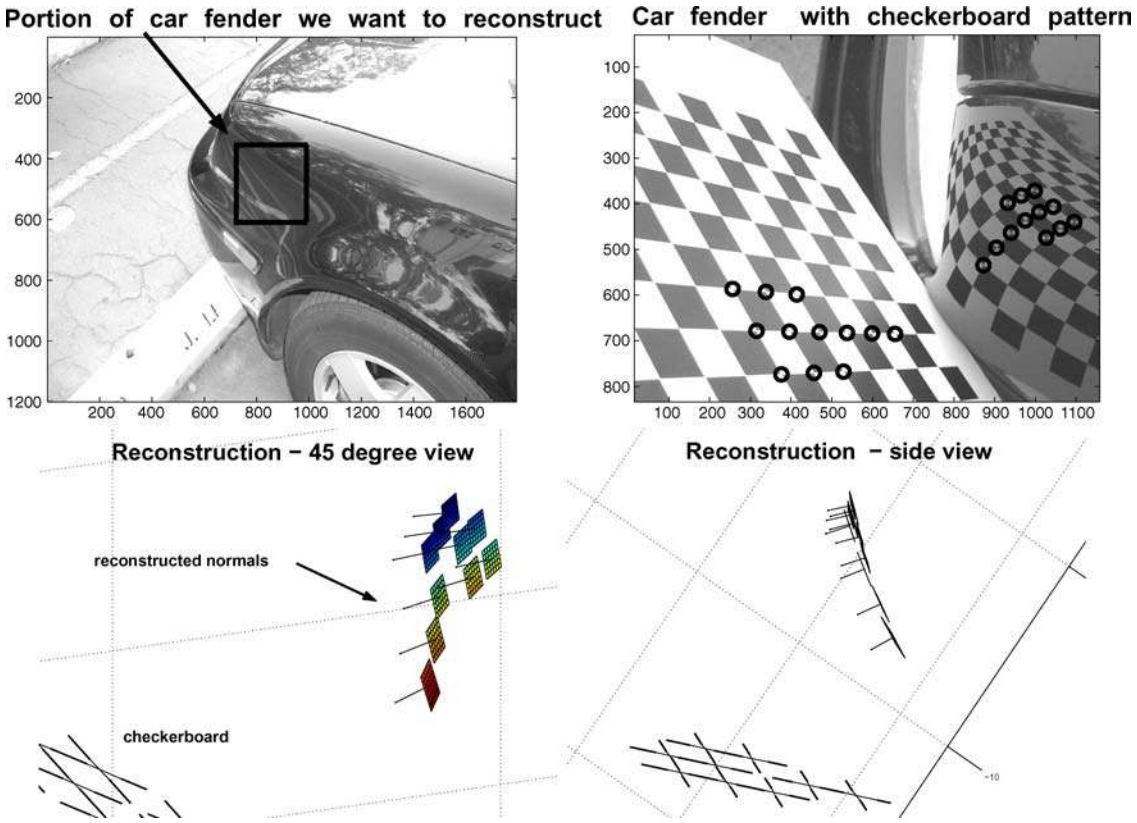

Figure 21. *Car Experiment. Top Left panel:* top portion of car fender we wanted to inspect. *Top Right panel:* we reconstructed the surface at the points highlighted with black circles. Notice that one image suffices to calibrate both camera and scene and recover the mirror's shape at the marked points. *Bottom left panel:* 45° view of the reconstruction. *Bottom right panel:* side view of the reconstruction.

6.2. *Results with Measurement of Orientations and Scale*

We validated the algorithm A2 in Table 6 with a specular teapot (see Fig. 20), and a portion of car fender (see Fig. 21). The recovery of the third-order surface parameters was validated in Fig. 13 using a synthetic mirror surface. We tested the accuracy of the algorithm in estimating the principal curvatures of the mirror cylinder (base of the teapot). The ground truth diameter of the cylinder was measured with a caliper with accuracy 0.013 mm. Table 7 shows the statistics of the reconstruction error (see rows $4-5$).

In Fig. 19 we qualitatively compared the cylinder's reconstruction results obtained with the 2 algorithms. Overall, the two methods exhibit similar performances in reconstructing position and surface normal at each intersecting point. However, the second approach is more advantageous than the 3-line approach in that it can also estimate curvature parameters and requires a simpler scene structure.

7. Conclusion and Future Work

We analyzed the geometry underlying specular reflections of a known planar scene. We first presented the differential relationship between a planar scene patch, the local shape of a mirror surface and its corresponding specular reflection in the image. We studied several properties attached to this mapping and its degeneracies.

We used this analysis as a starting point for the reconstruction problem: recover the shape of a specular surface from the reflections in one image. Under the assumption of an unknown mirror surface reflecting a known calibrated planar scene (e.g. a triangle-based pattern, a regular grid or an arbitrary drawing) onto

the image plane of a calibrated camera, we demonstrated that surface position and shape up to third order may be recovered. We started by assuming that the scene is composed of the simplest primary structure, namely lines intersecting at points. We assumed that measurements of orientation and curvature of each reflected curve are available. We proved that 3 orientation measurements are necessary and sufficient to recover the surface shape up to first order (position and orientation). Second order surface parameters may be recovered only up to an unknown parameter. Curvature measurements may be used as a further constraint. In a second step, we assumed that the scene is a grid of intersecting lines and that the measurements are both orientations and local scale of the reflected lines at the grid point. We proved that if orientation and local scale measurements along (at least) 2 reflected curves are available, local surface shape can be fully recovered up to third order accuracy. Finally, we generalized these results to the case of arbitrary planar scenes. We proved that local shape up to third order can be extracted from the reflection of a planar scene patch observed in the image plane.

We validated our theoretical results with both numerical simulations and experiments with real surfaces and found that the method is practical and yields good quality reconstruction. Since our reconstruction scheme allows local shape recovery around each reflected point, we obtain a "piece-wise" parabolic reconstruction. A robust estimation of the surface's shape may be ultimately obtained by integrating such information.

These results can be considered as an ideal observer theory for local shape reconstruction from specular reflection and may be used as a complementary tool to investigate the abilities and limitations of the human visual system (Savarese et al., 2004) (Fleming et al., 2003).

Future work is needed to (i) calculate automatically the correspondence between pattern points and their reflected image points; (ii) calculate the shape from uncalibrated scenes. This effort will most likely require integrating additional cues, such as occluding boundaries, and some form of prior knowledge on the likely statistics of the scene geometry.

Acknowledgments

This work is supported by the NSF Engineering Research Center for Neuromorphic Systems Engineering (CNSE) at Caltech (EEC-9402726). We wish to thank Gabriel Taubin, Jean Ponce, Marzia Polito, Jerry Marsden and Jim Arvo for helpful feedback as well as Matthew Cook, Fei-Fei Li and Massimo Franceschetti for many fruitful discussions.

Notes

1. Notice that we use the same notation for points and vectors. This is done to improve the readability of the paper.
2. $\lambda_0 = 2\cos\theta_0$ is obtained by dot product Eq. (15) with $\nabla g(\mathbf{r}_0)$.
3. The hypothesis of coplanar scene lines is necessary for the ensuing development. See in particular Proposition 13.
4. Each column of these matrix-format tensors is another matrix.

References

Binford T. 1981. Inferring surfaces from images. *Artificial Intelligence*, 17:205–244.

Blake, A. 1985. Specular stereo. In *IJCAI*, pp. 973–976.

Blake, A. and Brelstaff, G. 1988. Geometry from specularities. In *Proc. of Int. Conf. of Computer Vision*, pp. 394–403.

Bonfort T. and Sturm, P. 2003. Voxel carving for specular surfaces. In *Proc. of Int. Conf. of Computer Vision*, pp. 394–403.

Born, M. and Wolf, E. 1965. *Principle of Optics—Electromagnetic Theory and Propagation*. OPergamon Press.

Bouguet, J. *http://www.vision.caltech.edu/bouguetj/*.

Carmo, M.D. 1976. *Differential Geometry of Curves and Surfaces*. Prentice-Hall.

Chen, M. and Arvo, J. 2000. Theory and application of specular path perturbation. *ACM Transactions on Graphics*, 19:246–278

Cipolla, R. and Giblin, P. 2000. *Visual Motion of Curves and Surfaces*. Cambridge University Press,

Dörrie, M. 1989. *100 Great Problems of Elementary Mathematics: Their history and Solution*. Dover Publications.

Fleming, R. Torralba, A., and Adelson, E.H. 2003. How image statistics drive shape-from-texture and shape-from-specularities. In *Proc. of Third Annual Meeting of the VVS*.

Halsead, M., Barsky, A., Klein, S., and Mandell, R. 1996. Reconstructing curved surfaces from reflection patterns using spline surface fitting normals. In *SIGGRAPH*.

Healey, G. and Binford, T. 1988. Local shape from specularity. *Computer Vision, Graphics, and Image Processing*, 42:62–86.

Ikeuchi, K. 1981. Determining surface orientation of specular surfaces by using the photometric stereo method. *IEEE Journal of Pattern Analysis and Machine Intelligence*, 3:661–669.

Koenderink, J. and van Doorn, A. 1980. Photometric invariants related to solid shape. *Optica Apta*, 27:981–996.

Goesele, M., Tarini, M., Lensch, H., and Seidel, H.P. 2002. Shape from distortion: 3d range scanning of mirroring objects. In *Proc. of SIGGRAPH, Sketches & Applications*, pp. 248.

Neumann, P. 1998. Reflections on reflection in a spherical mirror. In *The American Mathematical Monthly*.

Oren, M. and Nayar, S.K. 1997. A theory of specular surface geometry. *Trans. International Journal of Computer Vision*, pp. 105–124.

Perard, D. 2001. "Automated Visual Inspection of Specular Surfaces with Structured-lighting Reflection Techiniques." PhD thesis, VDI Verlag (Nr. 869).

Savarese, S., Chen, M., and Perona, P. 2002. Second order local analysis for 3d reconstruction of specular surfaces. In *Proc. of 3D Data Processing Visualization and Trasmission*.

Savarese, S., Chen, M., and Perona, P. 2004. Recovering local shape of a mirror surface from reflection of a regular grid. In *Proc. of European Conference of Computer Vision*.

Savarese, S., Fei-Fei, L., and Perona, P. 2004. What do reflections tell us about the shape of a mirror? In *ACM SIGGRAPH—Applied Perception in Graphics and Visualization*.

Savarese, S. and Perona, P. 2001. Local analysis for 3d reconstruction of specular surfaces. In *Proc. of IEEE Conference of Computer Vision and Pattern Recognition*.

Savarese, S. and Perona, P. 2002. Local analysis for 3d reconstruction of specular surfaces—part ii. In *Proc. of European Conference of Computer Vision*.

Smith, J. 1992. The remarkable Ibn al-Haytham. *Math. Gazette*, 76:189–198.

Solem, J., Aans, H., and Heyden, A. 2003. A variational analysis of shape from specularities using sparse data. In *International Symposium on 3D Data Processing Visualization and Transmission*.

Swaminathan, R., Grossberg, M.D., and Nayar, S.K. 2001. Caustics of catadioptric cameras. In *Proc. International Conference on Computer Vision*.

Swaminathan, R., Nayar, S.K., and Grossberg, M.D. 2004. Designing mirrors for catadioptric systems that minimize image errors. In *Proc. of the Fifth Workshop on Omnidirectional Vision*.

Wang, J. and Dana, K.L. 2003. A novel approach for texture shape recovery. In *Proc. International Conference on Computer Vision*.

Zheng, J. and Murata, A. 2000. Acquiring a complete 3d model from specular motion under the illumination of circular-shaped light sources. *IEEE Journal of Pattern Analysis and Machine Intelligence*, Vol. 8.

Zisserman, A., Giblin, P., and Blake, A. 1989. The information available to a moving observer from specularities. *Image and Video Computing*, 7:38–42.